TNO report

TNO-060-UT-2011-01184/C | 2

Property prediction of Plio-Pleistocene sediments in the A15 shallow gas systems

Oil and Gas
Princetonlaan 6
3584 CB Utrecht
P.O. Box 80015
3508 TA Utrecht
The Netherlands

www.tno.nl

T +31 88 866 42 56
F +31 88 866 44 75
infodesk@tno.nl

Date	10 June 2011
Author(s)	Dr. J. H. ten Veen, Drs. C.R. Geel G. Kunakbayeva MSc. Dr. T.H. Donders Dr. R.M.C.H. Verreusel
Copy no	
No. of copies	
Number of pages	(incl. appendices)
Number of appendices	7
Sponsor	EBN
Project name	Shallow Gas A15
Project number	034.24292

All rights reserved.
No part of this publication may be reproduced and/or published by print, photoprint, microfilm or any other means without the previous written consent of TNO.

In case this report was drafted on instructions, the rights and obligations of contracting parties are subject to either the General Terms and Conditions for commissions to TNO, or the relevant agreement concluded between the contracting parties. Submitting the report for inspection to parties who have a direct interest is permitted.

© 2011 TNO

CONFIDENTIAL

Summary

This report describes a best-practise workflow for assessment of the distribution and properties of both bright-spot occurrences and their hosting sediments, i.e. the shallow gas plays, in the Southern North Sea. The A15 block was selected as the best area to conduct this pilot study, since it contains several types of bright spots at different stratigraphic levels and has exploration wells through both normal- and gas-bearing sediments.

The project includes 3 main work packages that involve: 1) refinement of the 3D geological model built on sequence-stratigraphic principles, using high resolution seismic interpretation and automated horizon tracking techniques, 2) finding a temporal and/or spatial relationship between the occurrence of shallow gas and depositional elements (paleoenvironments) of the Tertiary Eridanos delta sediments, and 3) finding a good method to distribute the most relevant model properties (Phi, S_w, V_{shale}) through the obtained geological model. The research was conducted in collaboration with de Groot-Bril (dGB).

The geological models consist of 15 horizons that delineate the main depositional sequences The sequences are deposited in a pro-delta, turbiditic setting at the base of the studied interval. A general, coarsening upward trend reflects shallowing towards an upper shelf setting, resulting form the westward progradation of the delta system. Higher-order trends in grain size are super-imposed. The sequences are age-constrained by a chronostratigraphic framework and it appears that a strong coupling exists between paleoclimate and sediment properties. The warmest intervals (interglacials) are coupled to the coarsest-grained sediments, and the coldest intervals or glacials are linked to the finer-grained sediments. Furthermore it shows that high TOC contents in the silts (low gamma ray) are coupled to high SST (based on dinoflagellate cysts), and relatively warm climate (increased forest cover based on pollen analyses). Thus the high gamma-ray values, corresponding to finer-grained clayey intervals, represent the glacial periods, i.e. periods of relative low sea-level. This gamma-ray signal is a-typical compared to the standard used.

A petrophysical evaluation of the Tertiary sediments of four wells drilled in the A15 block has been performed that aimed at calculating effective porosity, shale volume, and water saturation. Both multi-mineral models and simpe shaly-sand models were used. Result of the first method work well in sandy interval, but are less applicable to shaly intervals in which simple shaly sand models perform better produce less residual errors. In order to calculate permeability, a relationship was derived from NMR permeability and effective porosity. This relationship agreed very well with core plug measurements. Effective porosities in the sandy intervals range from 15% to 35%, total porosities are in the range 30-45%. Wells A15-01 and A15-04 were dry, but wells A15-02 and A15-03 were gas-bearing. Gas saturations are in general low. Most of the bright spots identified on seismic contain less than 30% gas. Only a few thin reservoirs contain gas saturations higher than 50%. Sands with a high gas saturation are probably at irreducible conditions and are therefore likely to produce water-free gas. On the other hand, low gas-saturated sands produce also water, and are therefore not at irreducible saturations. This means that their top seals are probably leaking, and the gas in these sands is residual gas.

Seismic horizons and well log data were the main input for the subsequent seismic inversion workflow (performed by dGB) aimed at determining reservoir properties for bright spots and their surrounding rocks. First an accurate initial model was created using a HorizonCube that traces the seismic reflectivity over the entire interval of interest. This cube was generated through subdivision of the 15 interpreted sequences into multiple horizons using seismic horizon auto-tracking. The

horizon cube was used to guide the amplitude-to-impedance inversion process. The good quality of the inversion results is demonstrated by the low overall synthetic seismic error derived from the impedance volume. The good match between synthetic seismic impedance traces from the wells and the inverted impedance shows the reliability of the impedance results. Like any deterministic inversion the output resolution is bound to the bandwidth of the seismic and sampling rate, thus lower than the log resolution (up to 500Hz). The prediction of porosity from lithological/depositional information alone is not feasible, because the training set is too small to establish proper relations (only 4 wells in a non-layer cake depositional geometry). Therefore, porosity prediction and localization of gas-saturated areas were trained by the impedance cube using neural network modelling; the results, however, are of low quality. The match of the porosity volume with the modelled logs is of medium quality, mainly because of the resolution differences between properties based on the impedance cube and those derived from the actual well-logs. Also, doubts remain on the distinction between gas-related and porosity-related anomalies in the low impedance areas. No reliable relation between seismic, impedance, volume of clay and water saturation was found when training the neural networks.

Main recommendation for future studies aiming at property distribution in shallow gas systems is to construct a detailed geometrical model (geobody model) at a desired resolution. The maximum resolution would be that of the well-log data. Such models should act as the main steering in Neural Network property distribution, rather than using any type of seismic data. If seismic data was to be used it is recommended to perform new acquisition or to reprocess existing data. Both methods should in all aspects focus on shallower targets.

Contents

1 Introduction

1.1 Shallow gas system in the Netherlands

Shallow gas in the Dutch subsurface is defined as gas occurrences in unconsolidated sediments of Cenozoic age. It mainly occurs in shallow marine to continental (deltaic) deposits of the Plio-Pleistocene Eridanos delta (Overeem et al., 2001), in Pleistocene tunnel-valley fill deposits and in volcanoclastics at the base of the Paleocene (e.g. Basal Dongen Tuffite). Shallow gas is either structurally trapped in anticlines associated with rising salt domes or occurs in stratigraphic or depositional traps. Exploration of shallow gas is mainly focused on the identification of Direct Hydrocarbon Indicators (DHI's) such as bright spots, which might indicate trapped and sealed hydrocarbon accumulations. The Netherlands has good potential for offshore shallow gas fields in the northern offshore sector (A/B/F blocks). The first shallow gas field is in production by Chevron (A12 block), and a second field (block F02) is now developed by PetroCanada/DANA (De Haan, 2010).

1.2 Rationale for the project

- A pilot study by EBN (2010) suggests a systematic, though insufficiently understood relation between the occurrence of shallow gas (bright spots) and depositional environment.
- Other studies, e.g. Kuhlmann and Wong (2008), suggest the bright spots to be related to specific stratigraphic intervals related to the inception of large-scale glacials.
- DHI's for Tunnel valleys include bright spots and several other types of velocity anomalies, which are well known by offshore operators as they may strongly affect the correct imaging of deeper subsurface (energy absorption, ray distortion, etc). Their study and characterization has therefore important industry application (geo-hazards, exploration of deeper levels)

Thus, effective exploration and production may clearly benefit from an increased understanding of how the distribution of depositional environments is related to external (climate, tectonics, sea-level) and internal (delta lobe switching, avulsion) processes. A sequence-stratigraphic framework for the evolution of the Eridanos delta and other potential reservoirs (tunnel valleys) should give critical knowledge of the architecture and reservoir properties of these, yet not-well understood reservoirs and the continuity of sealing clays. A reservoir model based on such framework should further be combined with information on origin of the gas and charging, preservation and pressure conditions. As such, it forms a crucial database that enables assessment of economic profitable or hazardous shallow gas occurrences in offshore Netherlands.

1.3 Objectives & Methods of the current study

This study aims to develop a 3D reservoir model of the shallow gas systems in the A15 block (Figure 1-1 Locality map of the A15 block with indication of production and exploration licenses and wells (source: www.nlog.nl).), which are contained in the Cenozoic Eridanos delta. The reservoir model forms the basis for the prediction of petrophysical properties (V_{shale}, Phi, S_w) by using Neural Network distribution techniques. Key elements in the reservoir model are depositional sequences that are uniquely linked to external controls and which are temporarily and spatially constrained by extensive well data, including bio/chrono- stratigraphic, geochemical, and paleoenvironmental information. The main objectives of this pilot study are 1) to set up a best-practice work-flow for property prediction, 2) to use this workflow to both qualitatively and quantitatively assess the potential of seismic bright spots as indicators for shallow gas occurrences and 3) to make recommendations for follow-up studies. The reservoir model also forms the basis for a future migration/charging model for shallow gas based on present-day fluid dynamic data and basin modeling to predict (economically profitable or hazardous) shallow gas occurrences.

Outside the scope of the current project are accurate prospect evaluations, including POS estimates, heights of hydrocarbon columns, and well productivities. It is our intention to predict properties, on the basis of which oil companies can make their own evaluations.

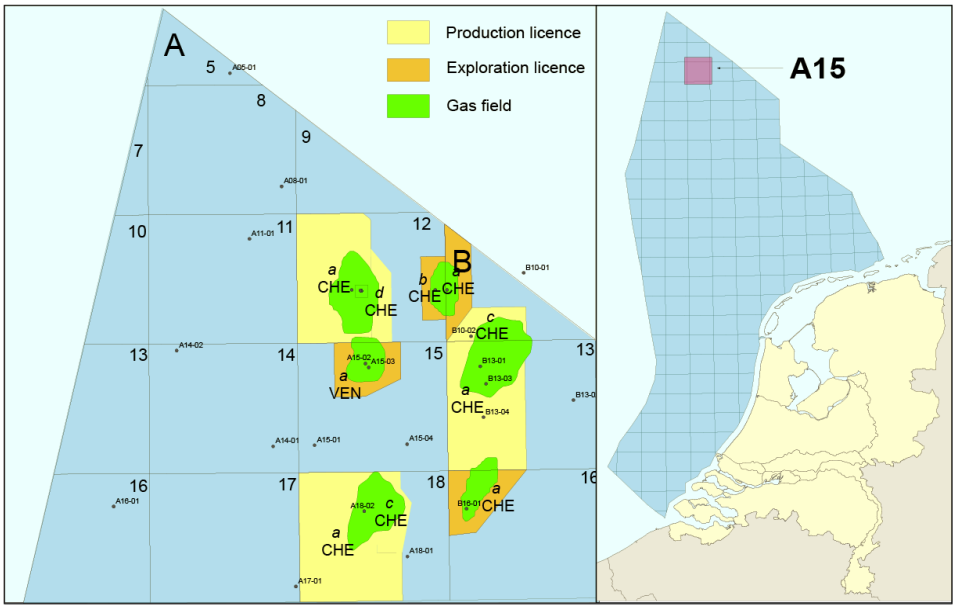

Figure 1-1 Locality map of the A15 block with indication of production and exploration licenses and wells (source: www.nlog.nl). Right window shows coverage of 3D seismic data in the A15 block.

The project consists of 4 components that join the main activities and expertise of TNO and dGB:

Component		Activities
C1	**Reservoir architecture and bright spots distribution and analysis** (in collaboration with dGB)	a. Detailed seismic interpretation of depositional sequences within shallow gas reservoir systems. b. Seismic-well tie c. Petrophyisical analysis d. Creation of a predictive conceptual model of the depositional sequences in a timeframe that also combines sediment- and geochemical properties (based on C2), using dGB's OpendTect SSIS functionality to perform sequence-stratigraphic interpretations, which enable improved seismic facies and lithofacies predictions and identification of potential stratigraphic traps.
C2	**Bio/chronostratigraphy & sedimentary data**	a. Identify omissions in data coverage, with particular reference to known bright spots and E&P interest. b. Carry out selected biogeological analyses (pollen/spore and dinoflagellate data, combined with micropaleon-tological data and geochemical analyses to refine and extent the stratigraphic model. c. Gather available bio/chronostratigraphic data from all wells and compile ages in relation to mapped seismic sequences (C1). d. Paleotemperature data for input in maturation history. e. Characterization of delta environment, facies typing.
C3	**3D seismic inversion and rock property prediction** (in collaboration with dGB)	a. Seismic data enhancement to increase the seismic resolution (noise removal, edge sharpening) to facilitate the interpretation process (integrated with C1a). b. Horizon cube generation, constrained stratigraphically by mapped seismic horizons and reservoirs defined in C1a. c. Acoustic Impedance Inversion, using a detailed low frequency model of the multi-horizon cube generated under b. d. Trained Neural Network Rock analysis to find (non-linear) relationships between acoustic impedance and/or seismic attributes. Using these meaningful relationships, the trained neural network will be applied to the reservoir interval to create rock property volumes (porosity, V_{shale} and saturation).
C4	**Integration & reporting**	

2 Seismic Interpretation (C1a)

2.1 Seismic data availability

Thirteen seismic units (S1 to S13) were identified in the 3D Z3WIN2000A survey (block A15; Figure 1-1) through a study by Kuhlmann & Wong (2004). All seismic horizons were available for the current study, except the S4 and S2 units which were newly interpreted by TNO. For this study, the same Z3WIN2000A survey was available, which is publically available since 2010. The survey data consisted of 16 small files, which were compiled into one composite file. The SEGY settings are displayed in Figure 2-1. To optimize the processing and interpretation time, the 3D seismic cube was cropped and only includes the interval above the Mid Miocene Unconformity, I.e. base NU (see

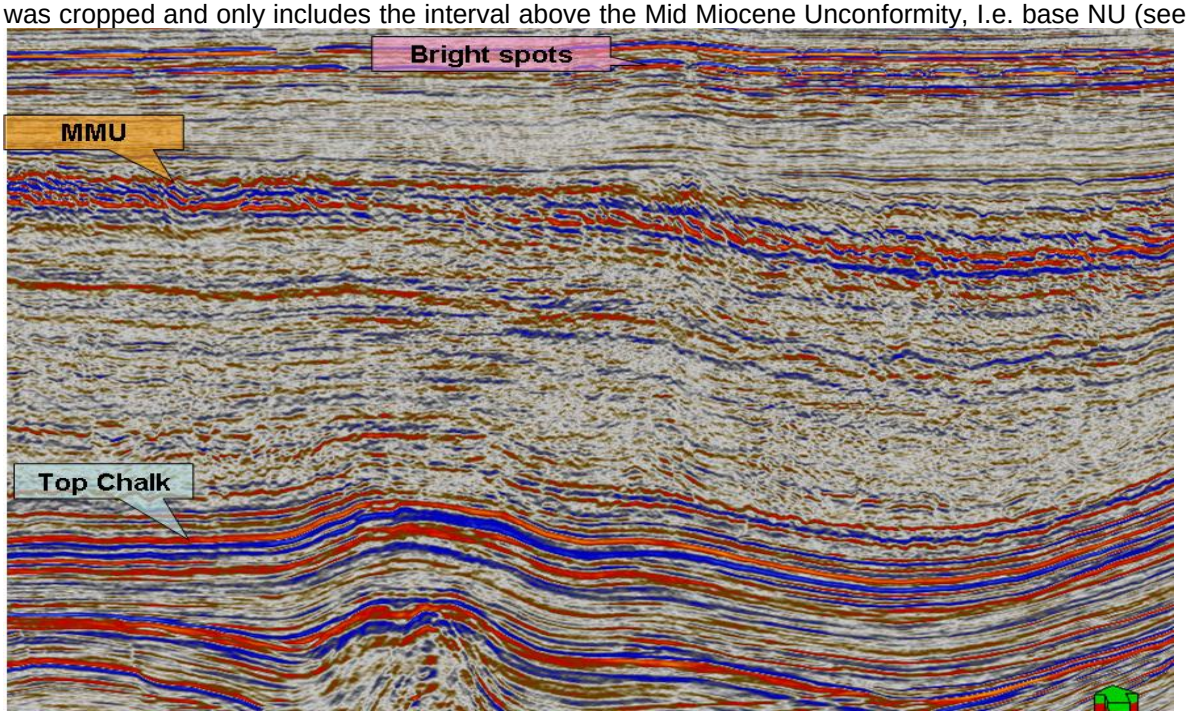

Figure 2-2) and was realized and saved in ZGY format.

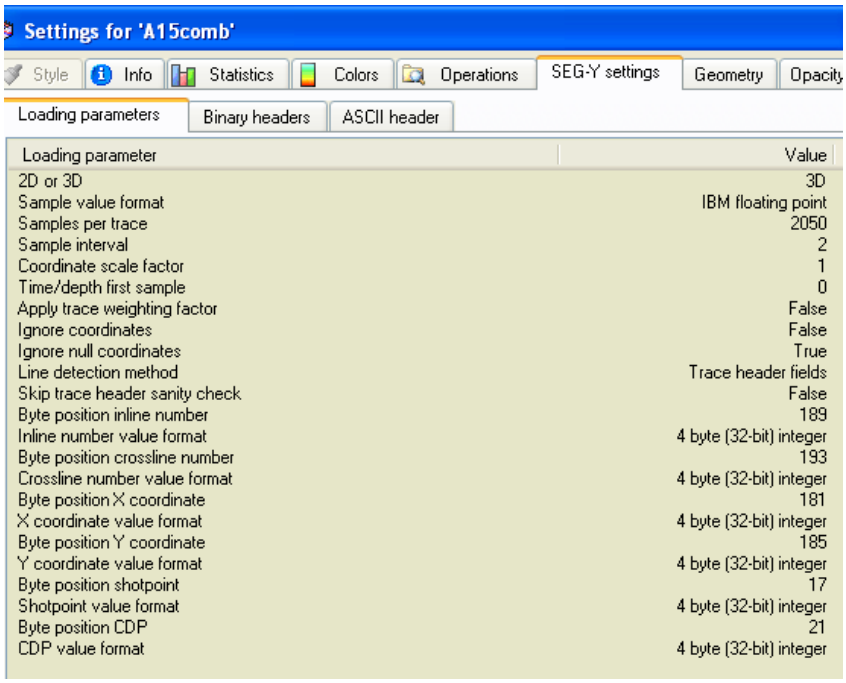

Figure 2-1 SEGY settings of the A15 3D survey

2.1.1 *Seismic cube polarity*

The polarity of 3D seismic cube appeared to be SEG normal, i.e. opposite to the North Sea convention. For a zero phase wavelet, a positive reflection coefficient is represented by a central peak. An example is illustrated on the seismic line shown in Figure 2-2, here an increase in acoustic impedance results in a peak, e.g. the transition from unconsolidated siliciclastic sediments of the North Sea Group to tight limestones of the Chalk Group. The standard colour convention of Petrel© is used: blue is negative amplitude (trough) and red is positive amplitude (peak).

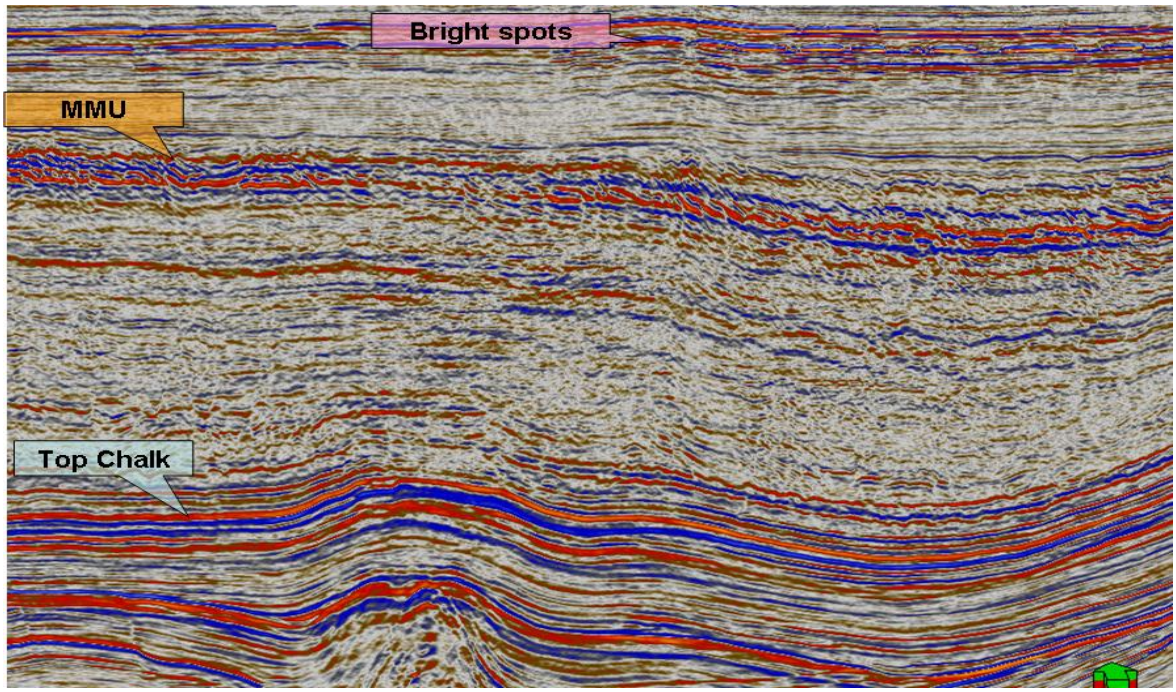

Figure 2-2 Example showing that the A15 seismic cube is SEG normal polarity, because the Top Chalk shows up as an amplitude peak due to positive AI contrast.

2.1.2 *Seismic interpretation*

The seismic reflectors at the tops of units S2 and S4 were interpreted throughout the seismic volume. The seismic horizons are picked as high-amplitude troughs. The seismic units S2 and S4 show a westward decrease in thickness, respectively 170-0 ms and 70-0 ms; unit S2 downlaps on the S1 horizon. The seismic units are characterized by low-amplitude, continuous parallel reflections. The thickness maps are presented in Figure 2-3.

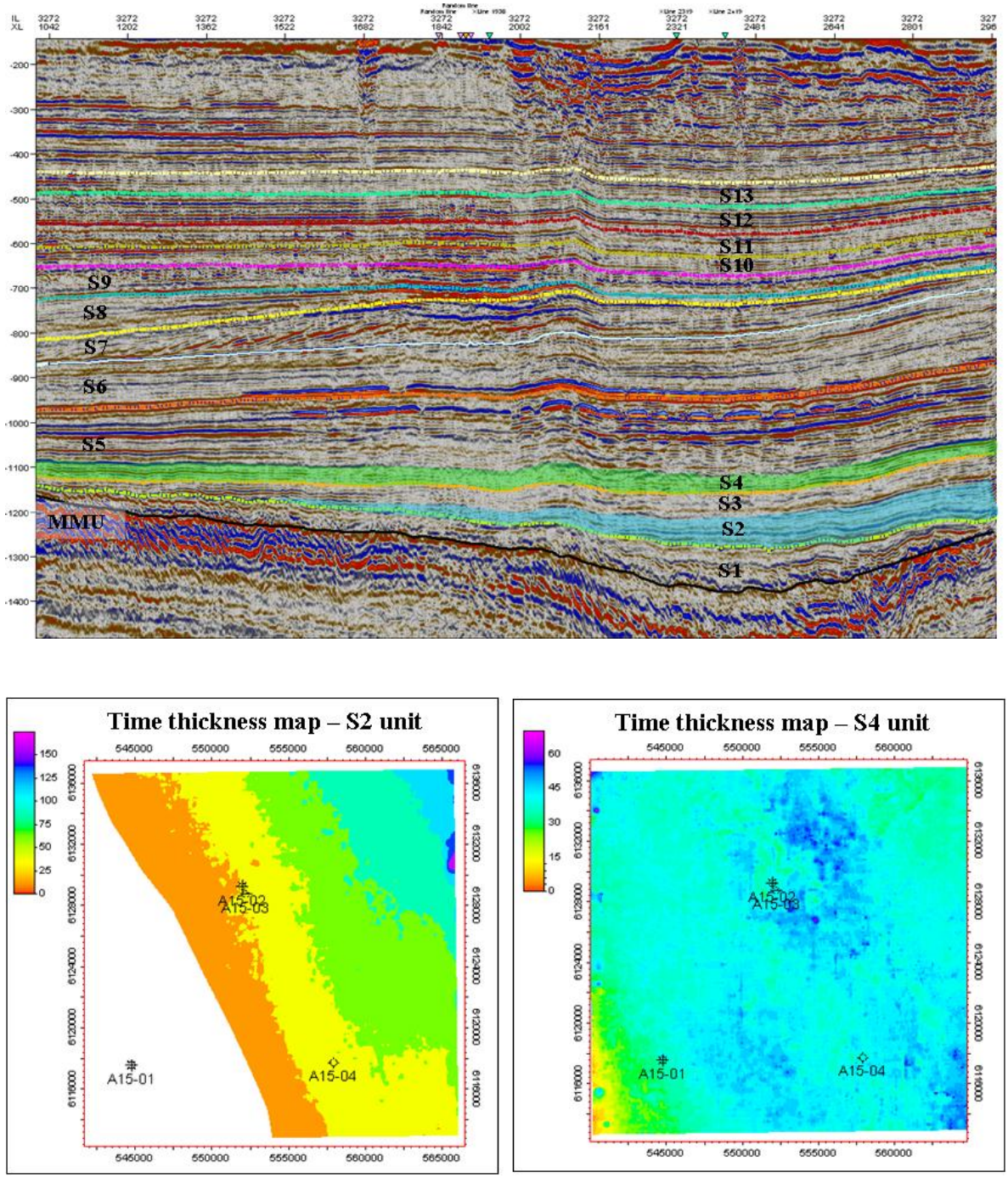

Figure 2-3 Thickness maps of seismic units S2 and S4

The seismic quality is strongly reduced in the intervals below bright spots, in particular around well A15-03 (for the well location see Figure 2-3). Several seismic attributes, e.g. TGS, Relative Acoustic Impedance were tried out in order to improve the continuity of the reflectors. However, the seismic attributes did not add to the result and the horizon interpretations were interpolated in the low-quality intervals.

2.1.3 *Seismic anomalies and problems*

The following anomalies were encountered during seismic interpretation:

- Bright spots, i.e. high amplitude reflectors often associated with shallow gas accumulations;
- Phase changes in bright spot intervals (Figure 2-5).
- Local decrease of the reflection amplitude (dimming effects) below bright spot intervals. The horizon interpretation in those areas contains some uncertainty;
- Pull up effect due to pronounced Pleistocene glacial channels (or rather their fills) in the shallowest intervals (Figure 2-6). A proper velocity model should correct for those effects.
- Sedimentary features: Low-perm streaks were recognized at the level of the bright spots within unit S5, where polarity contrast was observed. The features were characterized by normal polarity, whereas the bright spots show reverse polarity. The sedimentary bodies were aligned north-south, i.e. parallel to the paleo-coastline.

Similar elongated bodies were recorded on the present-day sea floor of the Gulf of Mexico (Figure 2-7), which also contains sand ridges more or less parallel to the slope. Another possible analogue is provided by Knutz & Cartwright (2004), who describe a system of sand ridges and grooves west of the Shetland Islands in Pliocene/Pleistocene times (Figure 2-8). These sand ridges are thought to be deposited by contour currents, which gradually migrate upslope.

Figure 2-4 (opposite page) All other seismic horizons were previously interpreted by Kuhlmann and were imported into Petrel as data points, and converted into interpretation lines The surface of the Mid Miocene unconformity (MMU) has been obtained from the NCP2 mapping project (available through www.nlog.nl).

If the features outlined in Figure 2-5 are indeed sand ridges created by contour currents, it is likely that the reservoir properties will be better than when these sediments were deposited by turbidity currents or delta slope sedimentation. According to Bouma (1973), the prolonged winnowing due to contour currents produces well-sorted sands which presumably have a high porosity.

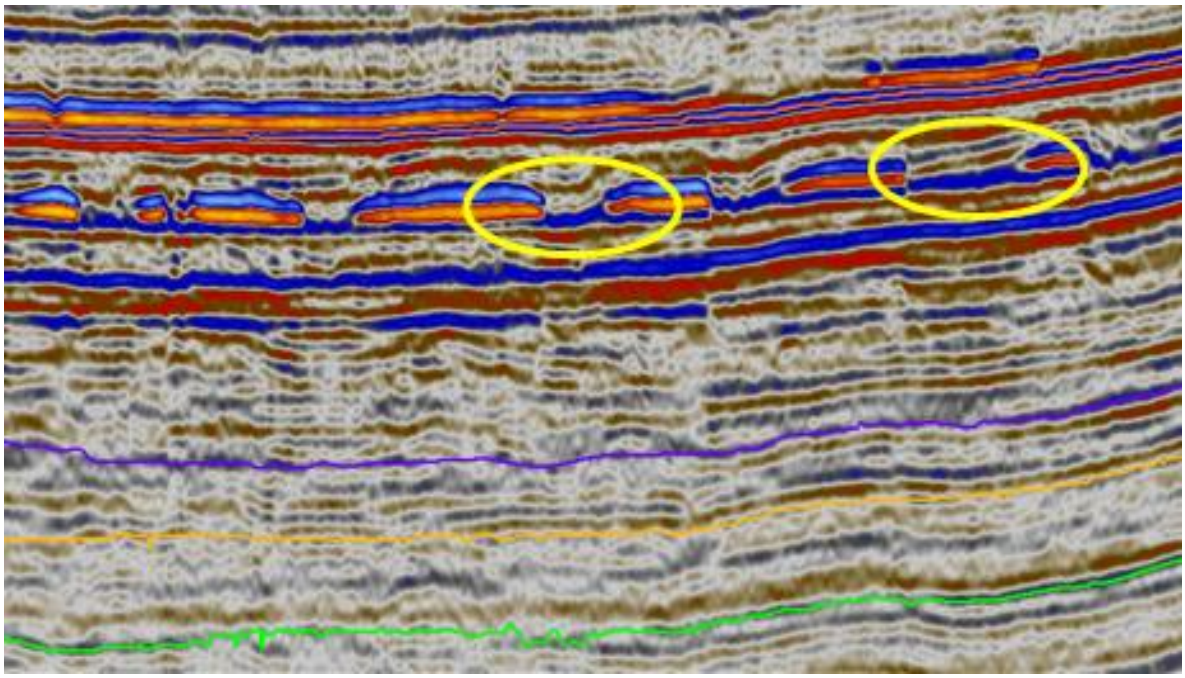

Figure 2-5 Phase reversal at the bright spots and reduction of reflection amplitudes below bright spots.

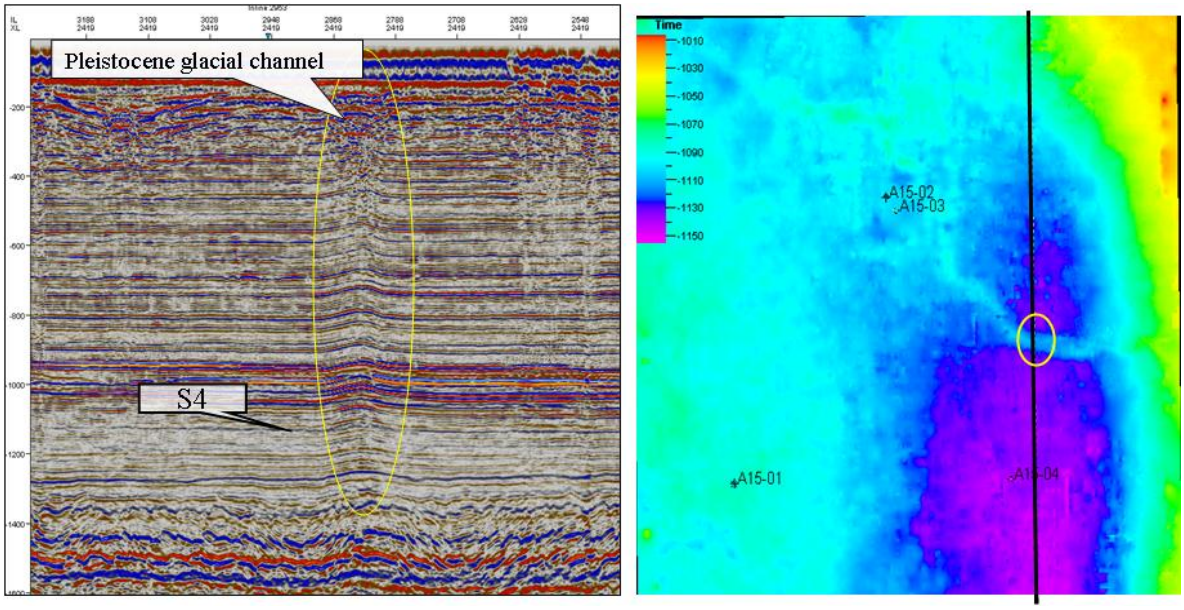

Figure 2-6 Left: X-line 2419. Pull-up effect due to presence of glacial valleys at shallower depth. Right: The curved/sinuous channel-like features are clearly expresses on the time slice (-1100ms). Here the TGS attribute Trace Amplitude Gain control is displayed.

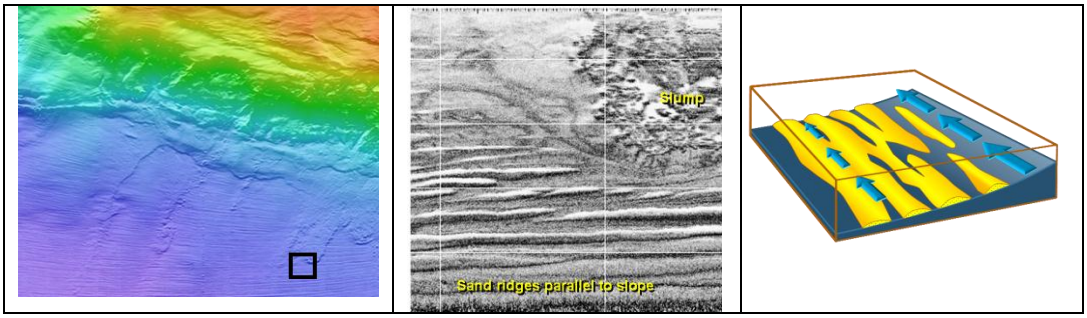

Figure 2-7 Left: Multibeam bathymetry showing elongated sand bodies formed by contour bottom currents. Middle: side-scan sonar image of the continental slope, Gulf of Mexico (www.cctechnol.com), Right: Cartoon illustrating the relaton between current direction and sand ridge geometry.

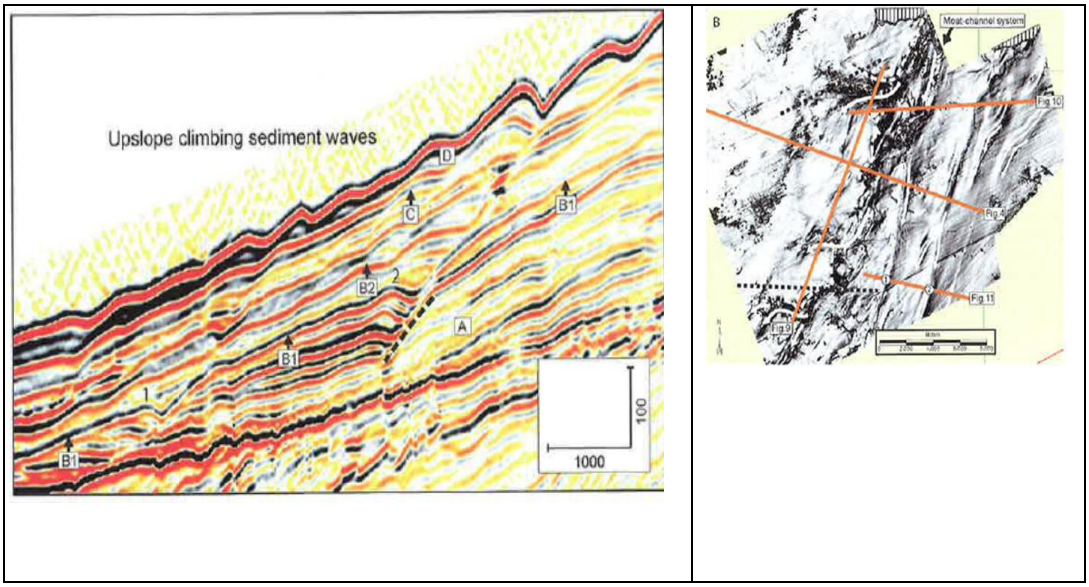

Figure 2-8 Seismic cross-section illustrating the succession of upslope climbing waves (Knutz & Cartwright (2004). Bold numbers refer to ridge-channel systems shown on the dipmap. The top bounding reflector of contourite drift units A, B1, B2, C and D are indicated. Scale bar in meters. B) Dipmap of B1 surface. Bold numbers refer to prograding ridges profiled in the left image.

2.2 Seismic well tie (C1b)

2.2.1 *Well data availability and quality issues*

Here we present a brief review of log quality issues that are relevant for the seismic well tie process. For a more detailed log analysis see Chapter 3 on Petrophysical log analysis. The conventional logs, such as gamma-ray (GR), sonic (DT), density (RHOB), were used for the seismic-well tie process. Spikes in the DT and RHOB logs were discarded where necessary. In case of missing log values over certain intervals, a constant value was assigned. A list of available well-logs per well is presented in Table 2-1.

Well A15-01

Aberrant values were recognized in the composite log of well A15-01, probably because logging was run through the casing. The DT log has very high values, while GR is less pronounced. To obtain reasonable log values, the GR log was edited in the Petrel calculator, using the following algorithm:

GR= GR original + 20 API

A corrected DT log was available from the public website nlog.nl. A detailed checkshot survey had been conducted on A15-03, which resulted in a corrected velocity log. The documented log file was digitized into las.format.

Well A15-02
This well is located in near proximity to well A15-03. The well logs were deemed to be OK, however. the depth values in the composite log (from www.nlog.nl) was not adjusted for KB elevation. This depth reference was updated.

Well A15-03
The sonic log shows noise spikes in some intervals, which were replaced by values derived from different log correlations. The corrected log is named “Patched_DT”. For further details on the correlations used, see the section on Petrophysical log analysis. Well A15-03 is used as reference well in the well-log correlation and seismic- well tie process, because most horizons in this well were previously calibrated with bio-, magneto, and isotopestratigraphy.

Well A15-04
The density log was corrected for “bad-hole” conditions. A DT log correlation was used to obtain reasonable log values for those intervals. The corrected density log was named “Patched_RHOB”. For further details on log computation, see Chapter 3 on Petrophysical log analysis.

Table 2-1 – Well data availability. Depth is in mAH.

Well data	A15-01	A15-02	A15-03	A15-04
GR	0-3910m	410-1190m	7-1243m	70-1100m
DT	320-1299m	410-1190m	122-1229m	457-1084m
RHOB	1516-3910m	410-1190m	411-1243m	457-1100m
Checkshot data	250-2450m	410-1190m	229-1329m	NA
Well markers	NA	NA	17 log units	NA

2.2.2 *Well correlation*

Based on previously defined log units in A15-03 (Kuhlmann & Wong, 2004), a well correlation was carried out between available A15 wells. Due to lateral log unit variation, the well correlation process was guided by seismic data as well. Integration of seismic- and log data based on calibrated TZ relation in A15-03 required the previously interpreted 17 log units to be modified. The original well markers had to be revised, shifted and additional markers were created, in order to have proper correspondence of seismic to log units. To avoid any confusion, a new TNO nomenclature was introduced, where 24 log units were defined in total (
Table 2-2). Once the log units were interpreted in reference well A15-03, they were further correlated to the other A15 wells. The TNO well markers defined in all the A15 wells are presented in Appendix B.

The well marker correlation from A15-03 to A15-01 is not straightforward due to rapid lithology and thickness variations and was therefore guided by seismic data. Well A15-02 is located nearby the reference well A15-03, thus the log units are easy correlatable. Well A15-04 is located along the depositional strike of the structure, so the log units are well correlatable. The top of the log unit X_S13 has different log responses in the wells. The log response in well A15-03 is uncertain, as it is affected by the casing shoe set at a depth of 430m MD. The log responses in wells A15-01 and A15-04 are attributed to lithological variations. The optimum well correlation panel and table with assigned well markers are enclosed as Appendix A and B.

Table 2-2 – Well log markers defined in well A15-03

A15-03	X coordinate	Y coordinate	TVDSS, m	MD, m
X_S13	552409.2	6128759.3	-389.5	430.1
W	552400.8	6128760.3	-429.5	470.9
V_S12	552398.5	6128760.6	-440.3	482.0
U_S11	552388.4	6128762.3	-489.9	532.6
T	552387.2	6128762.6	-496.1	539.0
S_S10	552378.5	6128764.3	-539.5	583.3
R	552375.8	6128764.8	-553.0	597.0
Q_S9	552368.6	6128766.3	-589.1	633.9
P	552366.8	6128766.7	-598.0	643.0
O	552363.4	6128767.5	-614.7	660.0
N_S8	552359.5	6128768.3	-634.3	680.0
M_S7	552355.1	6128769.3	-655.9	702.1
L	552341.5	6128772.3	-721.4	769.0
K_S6	552334.8	6128773.8	-753.6	802.0
J	552326.1	6128775.6	-795.4	844.7
I_S5	552311.1	6128779.0	-867.0	918.0
H	552301.6	6128783.4	-914.9	967.0
G	552294.5	6128786.0	-950.1	1003.0
F	552289.3	6128787.2	-974.5	1028.0
E	552280.7	6128789.3	-1015.6	1070.0
D_S4	552274.5	6128790.6	-1044.9	1100.0
C_S3	552265.8	6128791.2	-1086.0	1142.0
B_S2	552255.7	6128792.2	-1134.3	1191.4
A_S1	552249.1	6128793.5	-1166.5	1224.3
MMU	552243.6	6128794.7	-1192.8	1251.2

2.2.3 *Synthetic Seismogram*

The input data used for this process are: the 3D seismic survey, well logs, well markers and checkshot data.

The sonic (DT) log was edited to remove any spikes or anomalous values and, over the range of depths without log recovery, a constant sonic value was assigned. For example, in well A15-03 the interval 478-509 m MD had no values in the original DT log. The log was edited to eliminate the spikes and assigned a constant value for that particular interval, such that the log could be used for the generation of synthetic seismograms.

The synthetic seismograms were constructed by calculating the acoustic impedance from the sonic log, which was calibrated with checkshot data to improve time-depth conversion. The impedance curve was convolved with a theoretical zero phase seismic wavelet (Figure 2-9) to produce a synthetic seismogram. By comparing the synthetic seismogram to an original seismic section, the seismic units were identified in the well logs. The procedure was carried out using the “Synthetics” module in Petrel©.

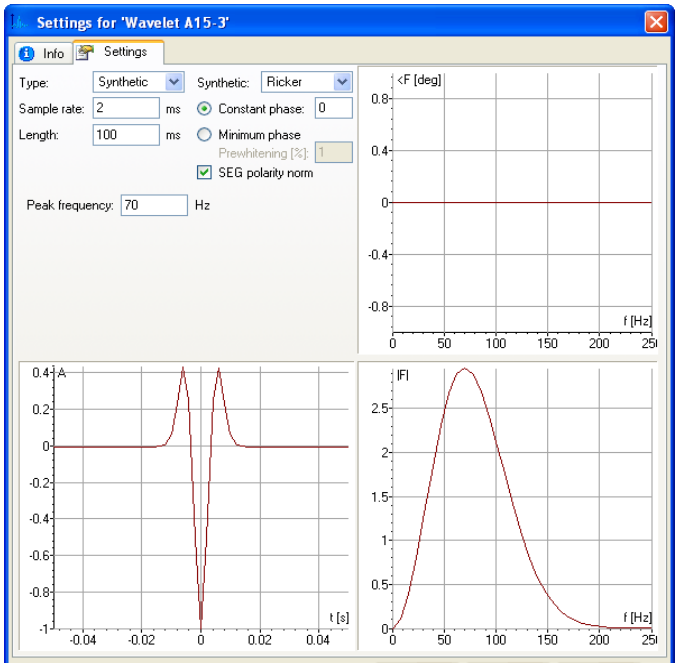

Figure 2-9 Theoretical seismic wavelet settings

Usually, both sonic and density logs are used to generate synthetic seismograms. Here we only used the sonic, because there is no density log recorded in the shallowest interval of well A15-01. This is approach is validated by the fact that almost no difference was observed between the synthetics based on the sonic log alone or those based on a sonic-density combination. This can be explained by the good correlation between the sonic and density logs. Both logs have small radius of investigation, which means that both tools read mostly into the invaded zone, where most of the gas has been replaced by mud filtrate. Thus, the sonic log does not record the gas effect and therefore, synthetic seismograms based on the sonic log do not capture the phase change observed in the bright spot intervals in the actual seismic data.

2.2.4 *Seismic well tie*

A previous time-depth conversion by Kuhlmann & Wong (2004) assumed a simple 1m = 1ms conversion to be valid at a regional scale. This conversion did not seem appropriate at the reservoir scale, thus check shots were used to calibrate the time curve derived from sonic log alone (Figure 2-10). The correspondence of seismic-log units is presented in Appendix C.

The correspondence between seismic and log unit is given in Table 2-3 - Seismic to log correspondence. Note that the well markers correspond to the top of the seismic units.

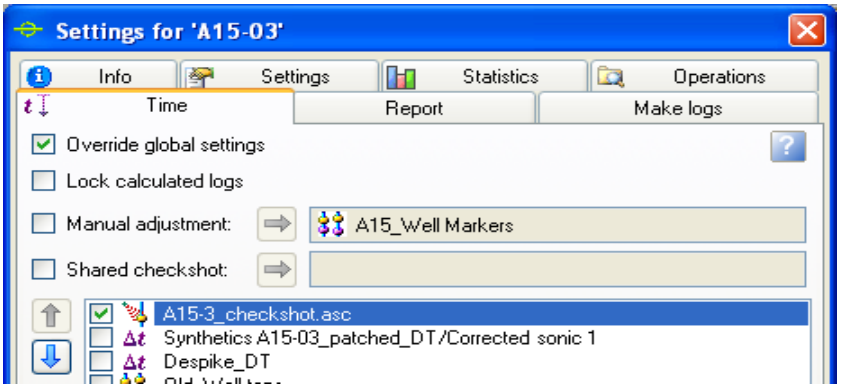

Figure 2-10 - Time-depth calibration in well A15-03, based on checkshot data

Well **A15-03** with its defined log units was a reference well in the seismic well tie process, where a good match between seismic and well log units was obtained (see Appendix D). The result of the A15-03 seismic-well tie is displayed in the well section of Appendix A.

In well **A15-01** the seismic well tie was good (
Figure 2-13).

In well **A15-04** no checkshot data was available. A bulk shift of 29ms OWT was applied, in order to tie the log units to the seismic horizons (Figure 2-14).

Well **A15-02** showed discrepancies in the checkshot data and the TZ relation was not straightforward. The time log based on the checkshot data showed a mismatch between seismic and log units.To obtain a reasonable match, the time log was replaced by the TZ log received from dGB. They applied a shift up to +5 ms, i.e. added to OWT values. As a result, most of the seismic units became matched, except unit S13, see Figure 2-15.

Table 2-3 - Seismic to log correspondence

Kuhlmann & Wong, Log Unit	Kuhlmann & Wong, 2004 Seismic Unit	TNO, 2010 Log Unit	Notes
18	S13	X_S13	**Top seimic unit S13 corresponds to the well marker X, etc.**
		W	
17	S12	V_S12	
16	S11	U_S11	
		T	
15	S10	S_S10	
		R	
14	S9	Q_S9	
		P	**Note, that TNO seismic to well relation was different from Kuhlmann approach and the well markers were adjusted in some cases, therefore do not tie two nomenclatures to each other**
		O	
13	S8	N_S8	
12	S7	M_S7	
		L	
11	S6	K_S6	
10		J	
9	S5	I_S5	
8		H	**The nomenclatures are given for general comparison**
7		G	
6		F	
		E	
5	S4	D_S4	
4			
3	S3	C_S3	
2	S2	B_S2	
1	S1	A_S1	

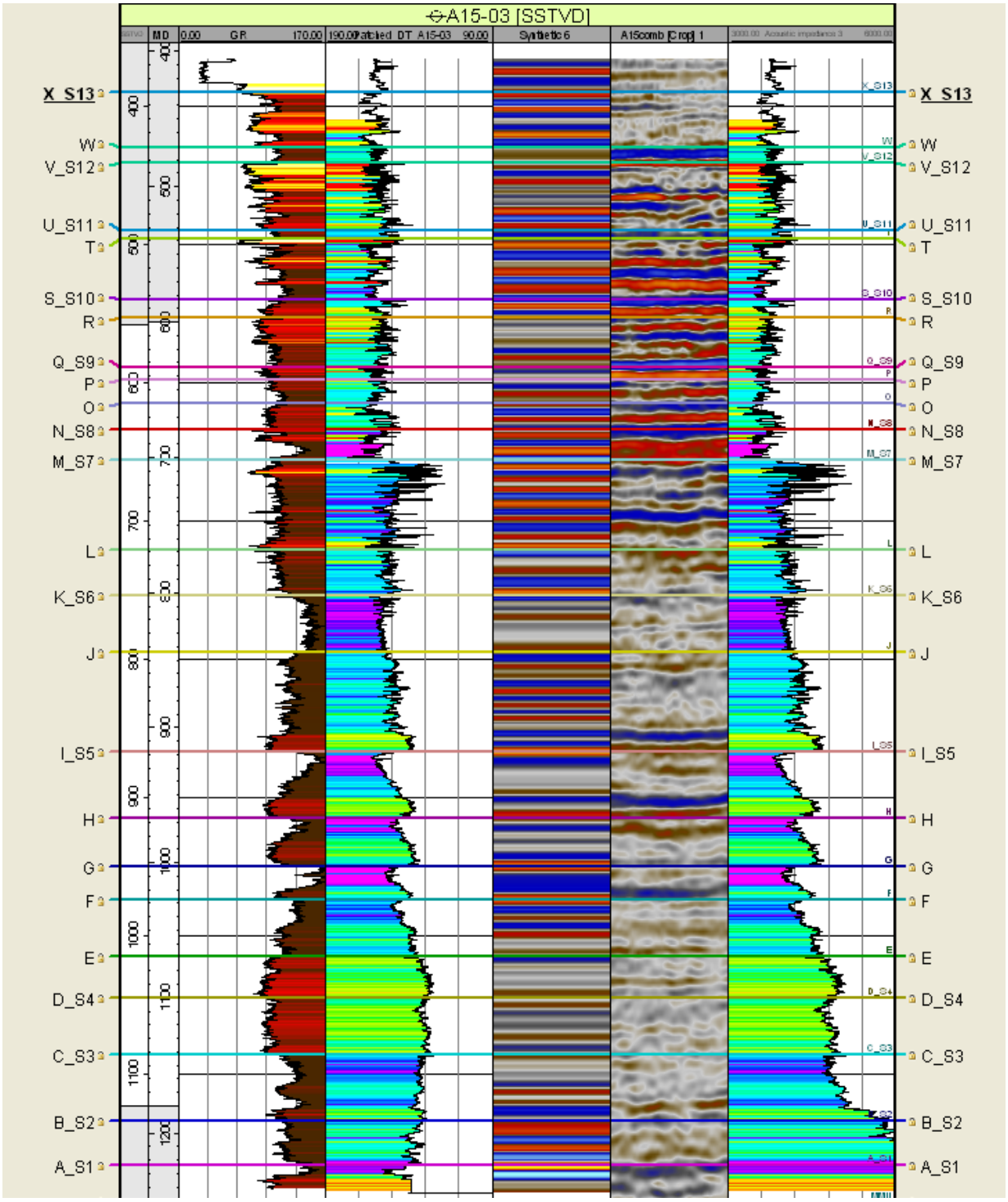

Figure 2-11 Seismic well tie of well A15-03. Shown are: GR log (0-170 API), DT_Patched (240-100ms/ft), Well Synthetic, Seismic section, Acoustic Impedance log.

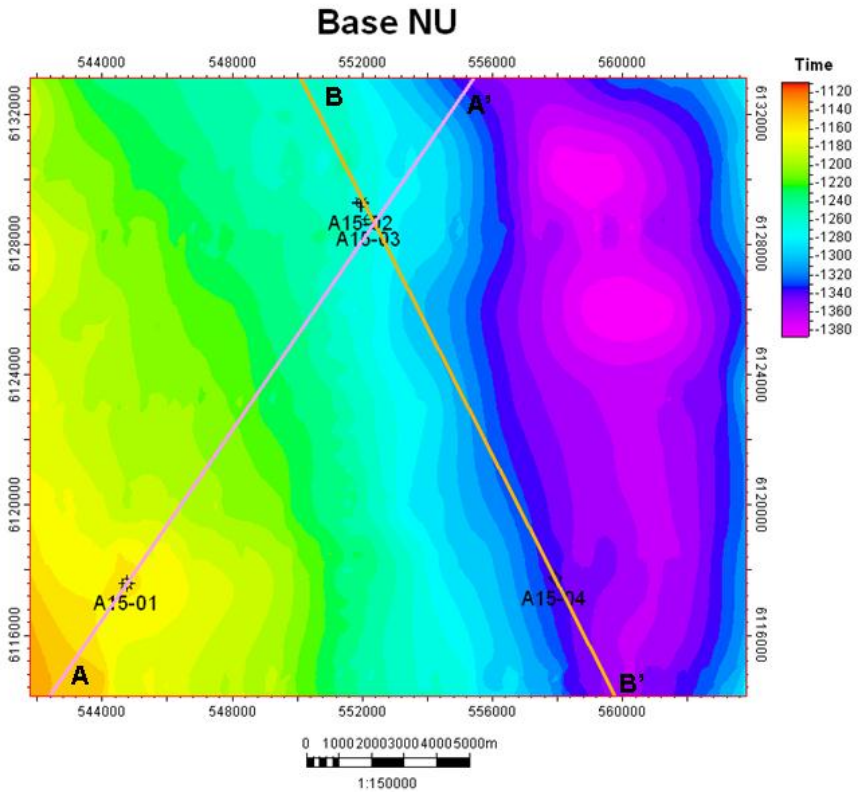

Figure 2-12: Overview map of the well locations and seismic intersection lines.

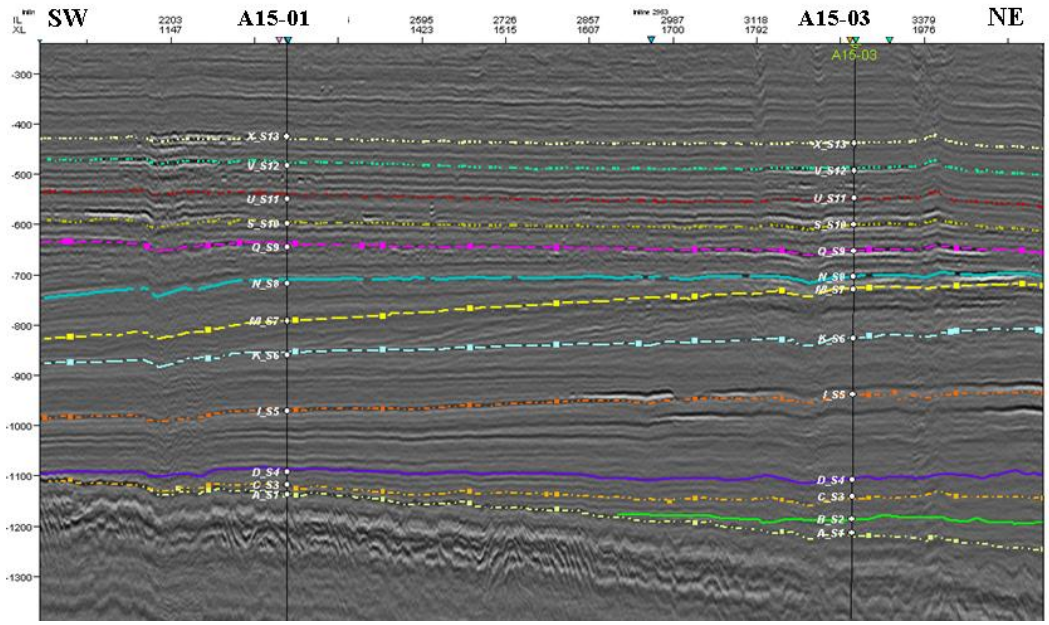

Figure 2-13: Seismic cross section AA' along wells A15-01 and A15-03. See Figure 2-12 for location.

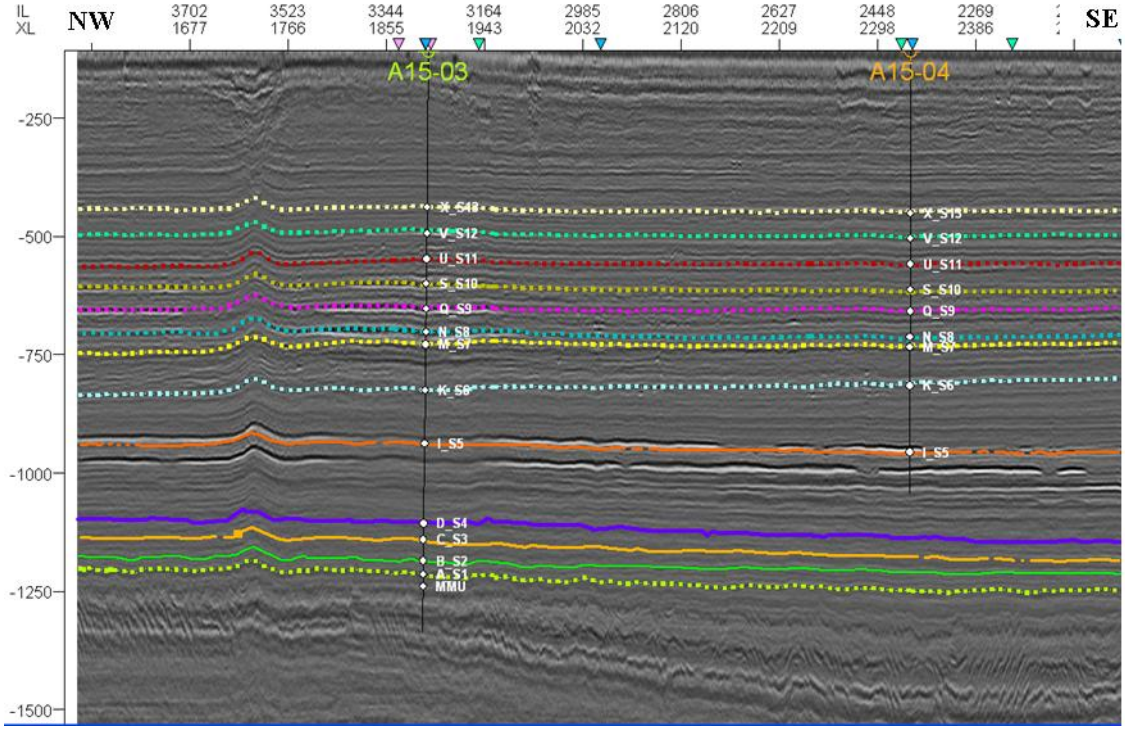

Figure 2-14: Seismic cross section BB' along wells A15-03 and A15-04. See Figure 2-12 for location.

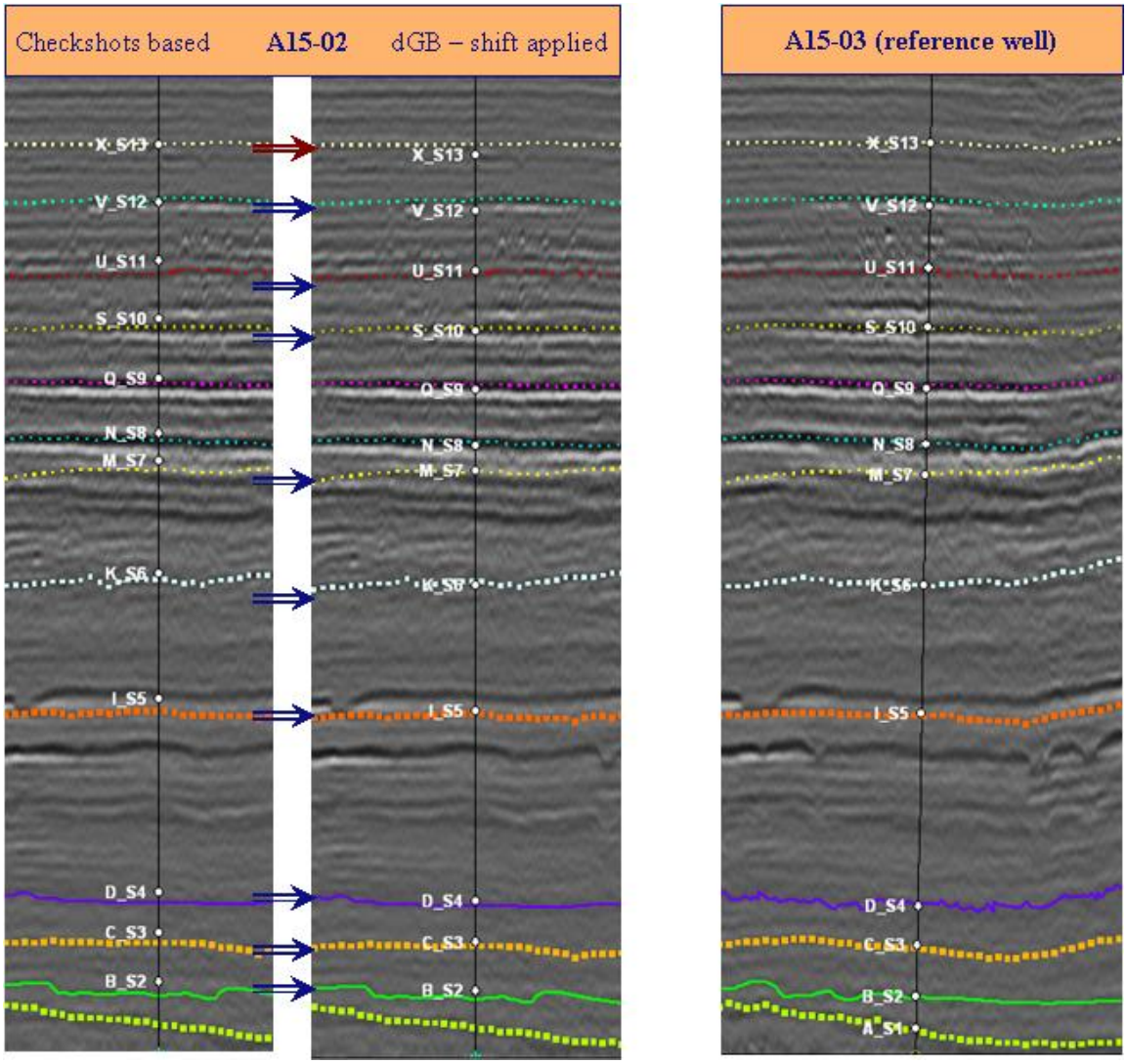

Figure 2-15: Seismic well tie in A15-02, shift 5ms applied in TZ log.

3 Petrophysical analysis (C1c)

3.1 Introduction

One of the lines of research in this pilot study was to see whether it was possible to invert porosity, water saturation, shale volume, and permeability from the A15 3D seismic cube. The inversion process requires known values of these properties at the wells. Thus, a full petrophysical analysis was done on the four wells of A15 (Figure 3-1).

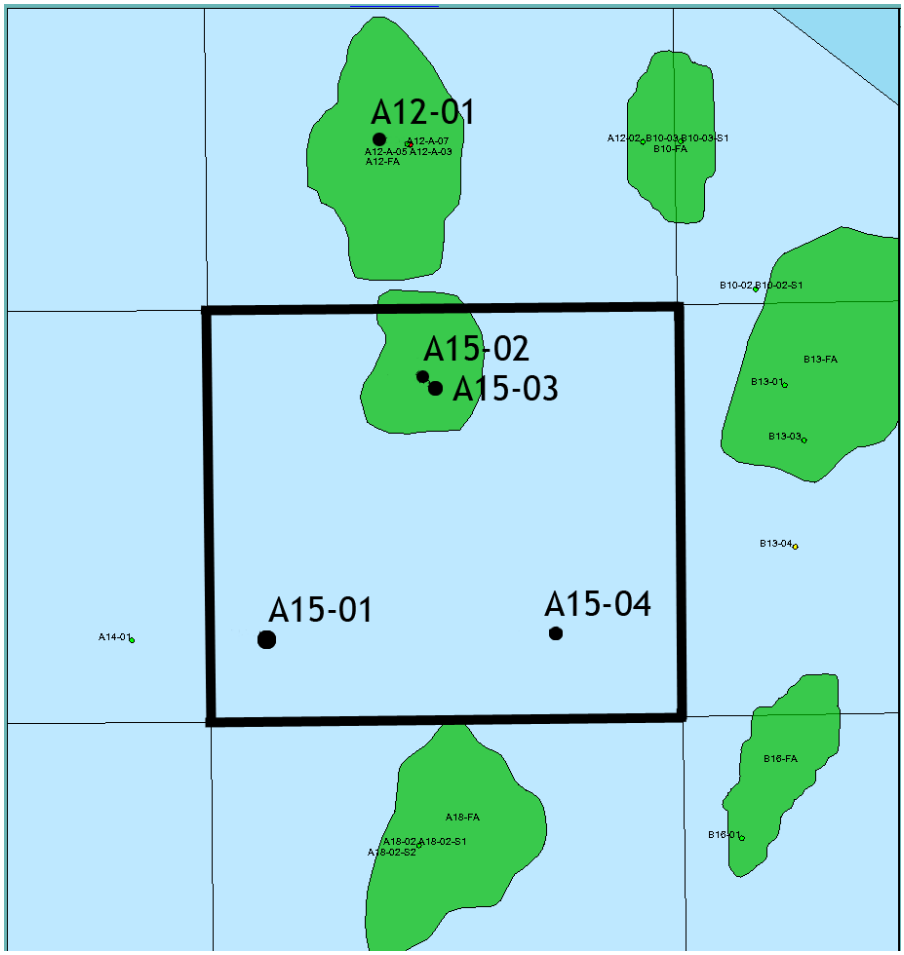

Figure 3-1: Location map of the four wells drilled in the A15 block plus well A12-01. Indicated in green are the shallow gas fields in A15 and its surrounding blocks.

3.2 Data and methods

Well log data for the A15 wells were retrieved from the NLOG website, except well A15-04 which although located in open area was not yet released at the time of the study. For this well we received permission from the A15a Production License applicant (a consortium led by Centrica, among which EBN) to use the well data. Unfortunately at the time of the study only a basic set of composite (spliced) logs was available. Furthermore, the A15-04 logs were in LAS format, hence without information on logging and borehole conditions.
Table 3.1 shows the available data for the A15 wells.

Table 3.1 – Overview of available well logs and core data from A15.

	A15-01	A15-02	A15-03	A15-04
GR Gamma ray	•	•	•	•
SGR Spectral gamma-ray		•	•	
DT Sonic	•	•	•	•
DSI Shear sonic			•	
NPHI Neutron porosity		•	•	
RHOB Bulk density		•	•	•
PEF Photo-electric effect		•	•	
LLD Resistivity		•	•	•
NMR Nuclear Magnetic Res.			•	
FBST Borehole image logs			•	
Core Photos			•	•
Core analysis			•	•
XRD			•	
Thin sections / Petrography			•	
ELAN interpretation available		•	•	

It will be clear from Table 3.1 that well A15-03 is the well that will act as a reference well on which various petrophysical models can be tested. From the petrography and the XRD measurements a good overview of the mineralogy can be obtained. The spectral gamma-ray log provides enough information to distinguish between the most common clay minerals, and the NMR log provides an independent measurement of water saturation (mobile, capillary, and clay-bound), plus a good estimate of permeability. The image logs of the Full Bore Scanner (FBST) tool may provide further support to distinguish pay sands from non-pay silts and clays. Furthermore, the Neutron-Density-PEF, DSI, and resistivity logs were logged with a high-resolution, non-standard 2” sampling interval.

TNO does not have extensive experience in these types of reservoirs, especially not in petrophysical evaluation. It was therefore decided to spend sufficient time to experiment with different petrophysical models and parameters.
The approach taken was as follows. Well A15-03 provides a plethora of information so a multi-mineral model was set up to include the most frequent occurring matrix and clay minerals according to the point countings from the thin sections and XRD analyses. Since this approach involves two or more clay minerals with different Cation Exchange Capacities, it was decided to use the values for dry clay minerals. A Dual Water approach for water saturation calculation is then a logical next step. As wells A15-01 and A15-04 only have a basic log suite they were evaluated using a conventional shaly sand model. The parameters were derived from a shaly sand model run on A15-03. The absence of resistivity logs in well A15-01 excludes the calculation of water saturation in this well. Well A15-02 has an extensive log suite, although not as comprehensive as A15-03. It lacks NMR, DSI, and FMI. Similar to A15-03, this well was evaluated using both a multi-mineral/Dual Water model and a shaly sand model.
All evaluations were done with the program Interactive Petrophysics.

3.3 Well A15-03 evaluation

3.3.1 *Mineralogy and petrography from core data*

A comprehensive sedimentological and petrographic study on A15-03 was done in 1999 by Panterra Geoconsultants. The results of combined whole-rock analysis and XRD analysis, plus a petrographic point counting of a few tens of samples are presented in Appendix A. From this analysis it follows that the most important matrix minerals are Quartz, K-Feldspars, and Mica. Heavy minerals (unspecified) and carbonaceous fragments (mostly coal) are present as accessory minerals, sometimes up to 10%. Trace amounts of pyrite, calcite, and siderite were recorded occasionally.
The volumetrically most important clay minerals are Illite and Smectite, and to a lesser degree Kaolinite and Chlorite.

In Panterra's analysis no distinction was made between Biotite and Muscovite. For log analysis however, this distinction is important as the two minerals differ considerably in specific density (2.82 g/cc for Muscovite, 2.99 for Biotite) and in Pef-value (2.40 vs. 6.27 barns/cc). Choosing one or the other mineral in the mineral model for log analysis may have an important impact on the calculated porosity.

Not included in Table A1, but quite conspicuous from thin section descriptions is the occurrence of heavy minerals (See Table A2). They are volumetrically not very important (typically 1-2%) but they may influence the log readings as they are heavy and usually radioactive. Ignoring them may result in too low porosities. Typically, ignoring 2% heavy minerals with a specific density of 4.0 g/cc results in a 1.7 percent point too low porosity. One sample (SWS 21, 687 m depth) is reported to have 10% heavy minerals. Ignoring this would result in a 7.6 percent point too low calculated porosity.
On the other hand, the thin section descriptions also report the occurrence of substantial amounts of tiny char-coal fragments. Substantial means here 1-2%. Coal has a very low density (about 1.0), so even an amount of 2% coal fragments will result in a calculated porosity which is 2 percent point too high.
When the results (heavy minerals and carbonaceous material) from Table A-3 are cross plotted, an inverse relationship becomes apparent (Figure 3-2). Although the amount of data is not very high, it appears that heavy minerals and carbonaceous material are mutually exclusive. The relationship can be tentatively described as a hyperbola, of which the envelope is depicted in Figure 3-2.

Recently, cuttings from the Pliocene of well F02-06 were investigated by TNO. Almost all samples that were inspected showed both char coal fragments and heavy minerals to be present in the fine-grained sands. Biotite was only rarely seen, but Muscovite was abundantly present. Well F02-06 is quite a distance apart from well A15-03, and was paleogeographically speaking deposited in a more proximal deltaic setting. It is therefore uncertain whether these observations can be directly applied to Block A15, but they give at least a clue as to what minerals might be expected.

Figure 3-3 and Figure 3-4 show photomicrographs of two A15-03 samples. These thin sections give a fair overview of the complex mineralogy present in the A15 sands.

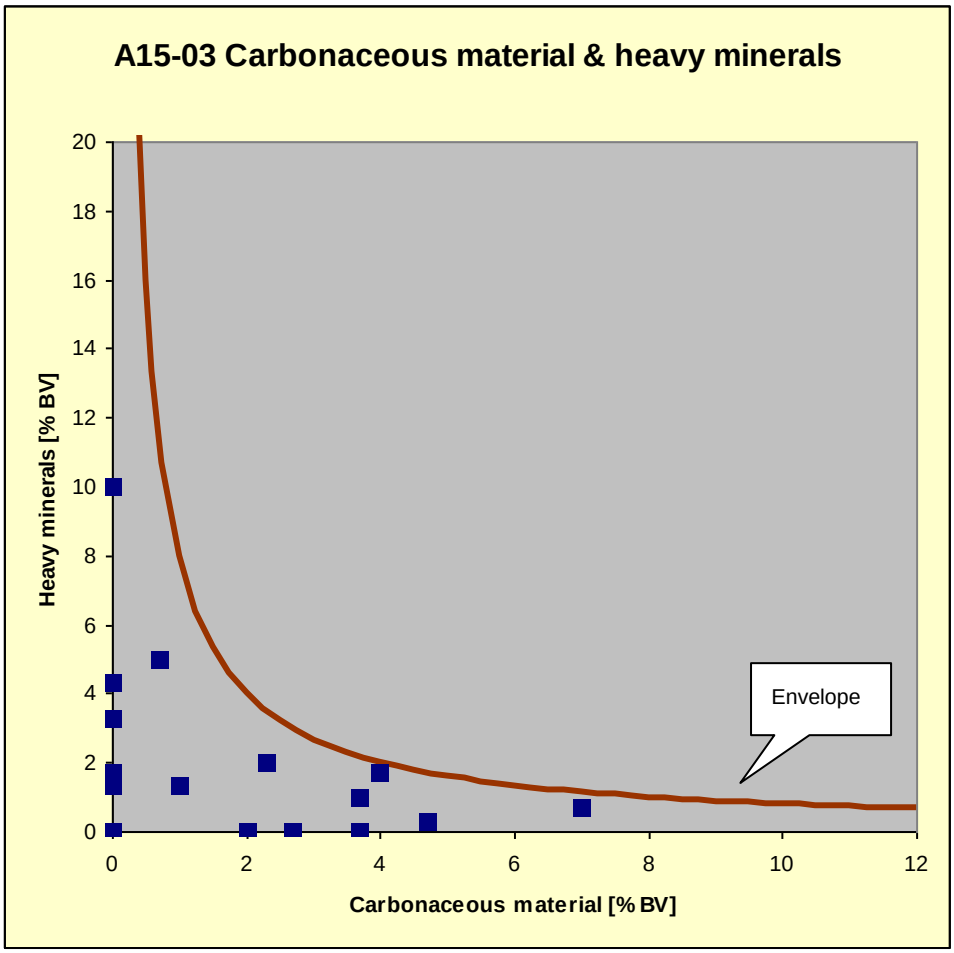

Figure 3-2: Relationship between heavy minerals and carbonaceous material in well A15-03.

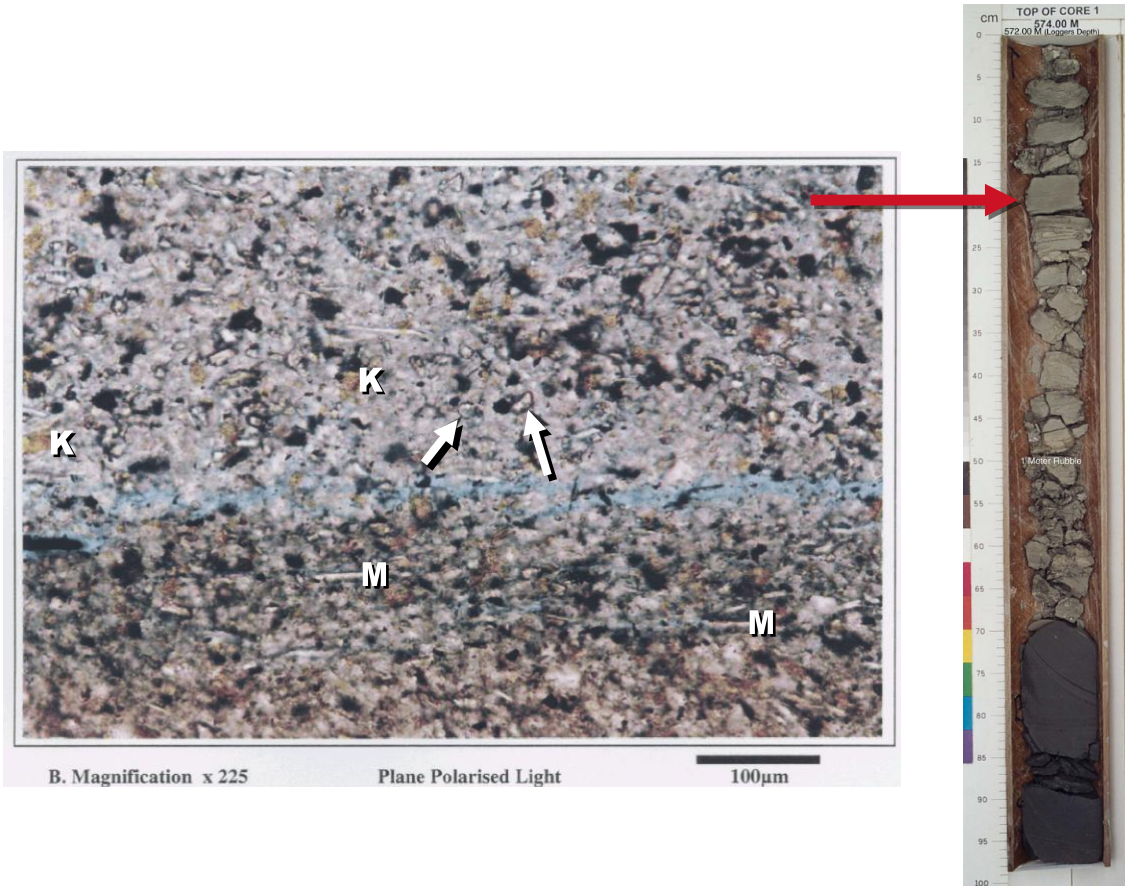

Figure 3-3: Fine-grained sandstone showing the complex mineralogy of the Eridanos sediments. Mineralogy consists mostly of Quartz, K-feldspar (K; yellow stain), heavy minerals (arrows), Mica (M). Right side of the picture shows core photograph and approximate position of the thin section. Well 15-03, log depth 572.18m, A40 sand.

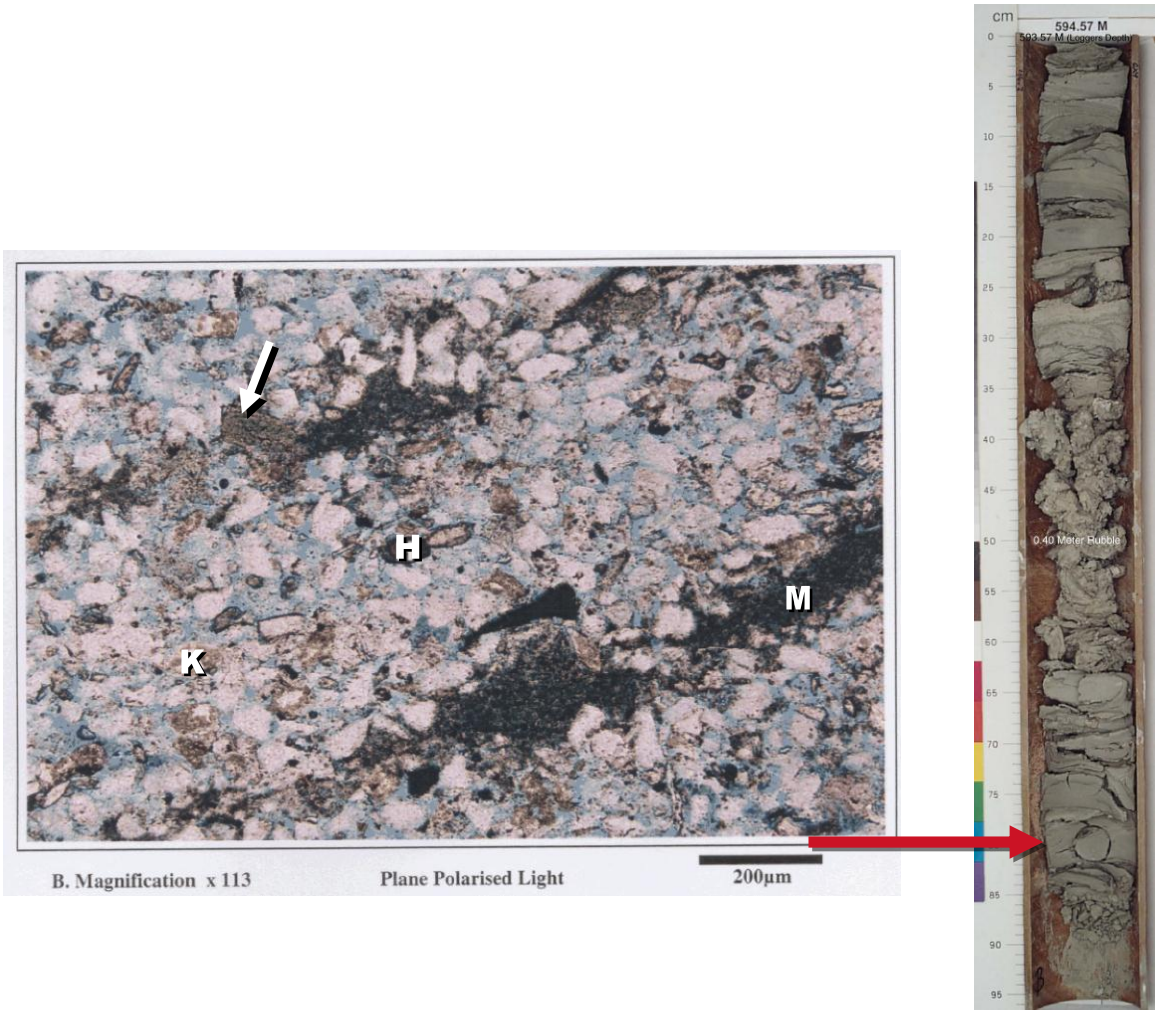

Figure 3-4: Alternation of clean siltstone laminae and argillaceous laminae (M). K-feldspar (K) and heavy minerals (H) are common while glauconite (arrowed) is rare in the siltstone laminae. Right side of the picture shows core photograph and approximate position of the thin section. Well 15-03, log depth 594.32m, plug number 23.

3.3.2 *Log quality*

Various DLIS files for A15-03 were downloaded from the NLOG website. The quality of most logs was good, but several porosity logs were adversely affected by the borehole conditions. For example, the DSI tool had several intervals where both P-wave and S-wave sonic logs read much too low travel times (Figure 3-5). The combination of a short sonic tool, a slow formation, and a wide borehole can cause signals travelling through the drilling mud to arrive earlier than those through the formation (Ellis & Singer, 2008).

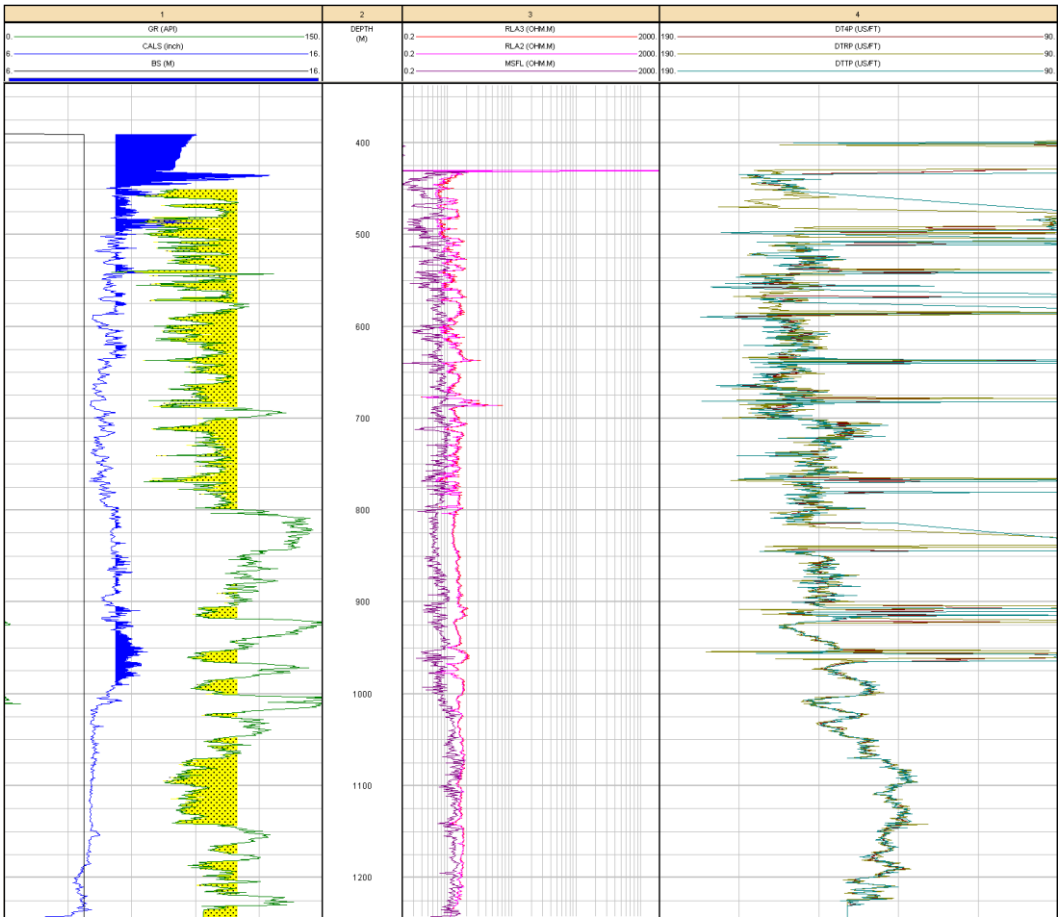

Figure 3-5: Well A15-03 showing P- and S-sonic (rightmost track) to have anomalously low values in several depth intervals. The probable cause is the acoustic signal travelling through the drilling mud.

Despite the borehole enlargement due to washout in the entire well down to a depth of 1200 m (Figure 3-5), the neutron and density logs were of good quality, as exemplified by Figure 3-6. The density corrections (DRH, black line, track 4) that were applied down hole were only minor. Therefore, a good estimate of porosity from neutron and density logs was to be expected.
The drilling mud used in the borehole interval 400-1250 m contained KCl which has a serious impact on both gamma ray log and spectral gamma ray log. This is clearly demonstrated in Figure 3-6 where the interval 400-800 m shows GR values around 80 API units, whereas the lithological description from cores and cuttings indicate relatively clean quartz sandstone which should have a value of 30-40 API, similar to the one recorded in well A12-01 which was drilled with sea water.

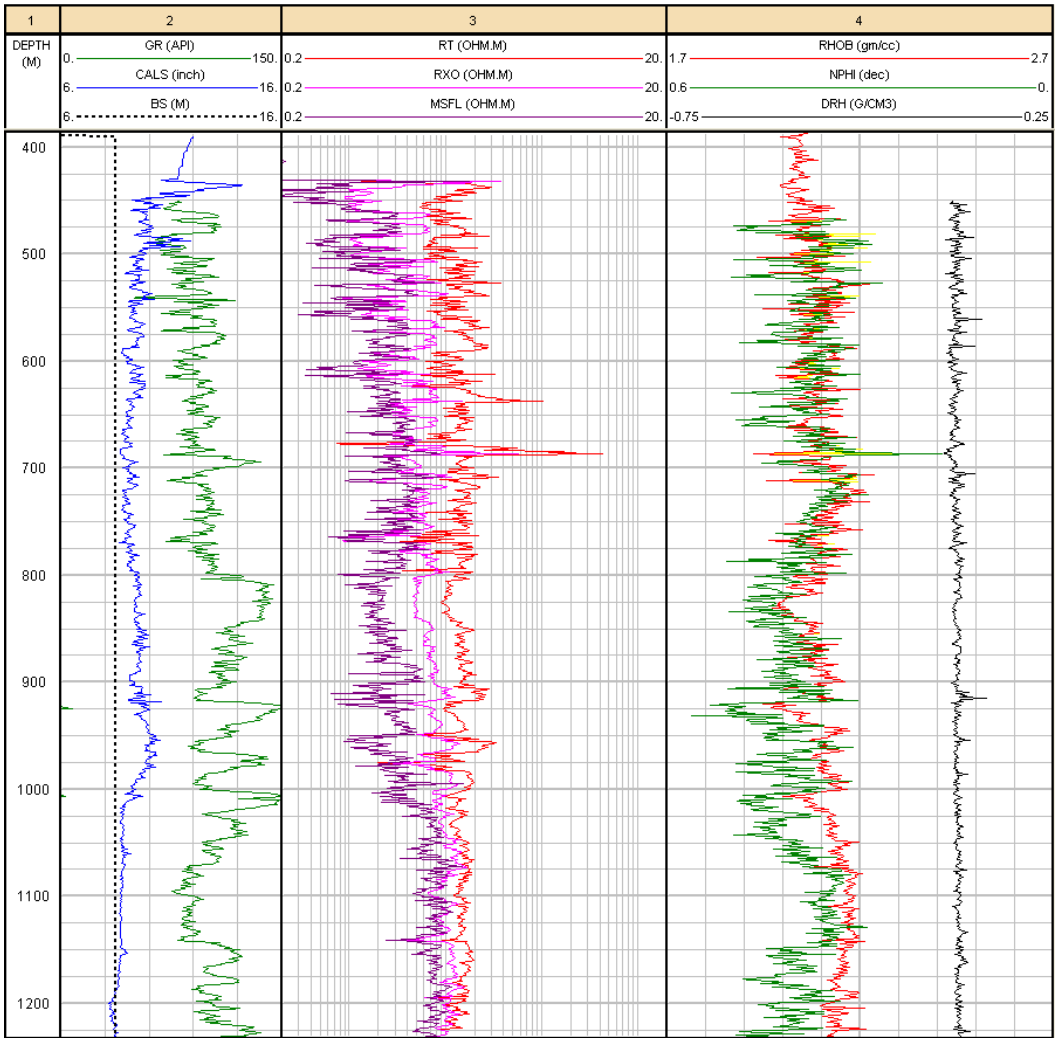

Figure 3-6: Triple-combo plot of well A15-03 showing 1) borehole enlargement due to washouts when comparing the caliper log (CALS) to bit size (BS); 2) the effect of KCl drilling mud on the gamma-ray log, and 3) the good quality of the neutron and density logs.

The electrical logs were of good quality. Schlumberger's High Resolution Laterolog Array (HRLT-B) was run with in-place calculated RT and RXO which after inspection were deemed to be ok. Special logs, like NMR and FBST logs were not loaded. Instead, the scanned playbacks of these logs were retrieved from www.nlog.nl and used as reference material.

3.3.3 *Log corrections*

3.3.3.1 Gamma ray

As the project progressed, it became apparent that almost all wells in the North Sea area are drilled in the Tertiary section with KCL/Polymer drilling mud. The potassium ions in the KCl solution prevents the -mostly smectitic- clays from swelling (Reid & Minton, 1992). The high salt levels used in many of these muds also promote clay flocculation by collapsing extended electrical double layers. This helps limit shale dispersion. High-molecular-weight linear polymers, such as PHPA, adsorb on mineral surfaces to form a slick, robust coating that provides a degree of mechanical integrity to shale softened by the ingress of mud filtrate.

The Potassium ions in the borehole and in the mud filtrate in the formation affect both gamma-ray and Potassium logs. The amount of additional radiation depends on the concentration of KCl, on the borehole size, and on the invasion diameter.
Correction charts for the gamma-ray log have been published by e.g. Weatherford (2007) but these charts require the concentration of KCl in the drilling mud, which in general is not available in most log headers. When daily drilling reports or the End-of-Well Report is available the concentration of KCl in the drilling mud might be reconstructed. However, these reports are often not available.
An easier method is to normalize the gamma-ray logs against a standard well. This can be be done in Interactive Petrophysics or in Petrel. The method is described in Van Hooff & Geel (2010). It basically matches the mean and the standard deviation of the gamma-ray log to the GR log of a selected standard well. It requires two conditions: Firstly, the statistical properties of the wells need to be calculated over the same stratigraphic interval, and secondly, a regional trend in shaliness should not be present in the wells. It remains to be seen whether this second condition holds for the Pliocene delta over the width of the Dutch offshore.

In this pilot study we adopted a much simpler approach. The GR of A15-03 was compared to the GR of the nearby well A12-01 (
Figure 3-1), which was drilled without KCl mud. The shift amount was added to the GR response of each mineral (see Section 3.3.4.2). Based on this shift, an estimate was made for the correction of the Potassium (POTA) log.

3.3.3.2 Sonic

A DSI was run in A15-03 but recorded very low travel times in several depth intervals (Figure 3-5). Both P and S sonic were affected. Leaving the shear-wave sonic for the moment, we tried to repair only the P-sonic. The approach taken here to correct these faulty intervals was first to blank out these intervals, then to find a correlation between the sonic and some other log in the depth interval around the faulty sections, and then apply this correlation.
It soon became apparent that a single solution did not exist for the entire stratigraphic interval. In total four different stratigraphic intervals were repaired, each one with its own correlation/substitution log. Appendix B shows the efforts to derive the corrections for the various intervals. The end result is shown in Figure 3-7.

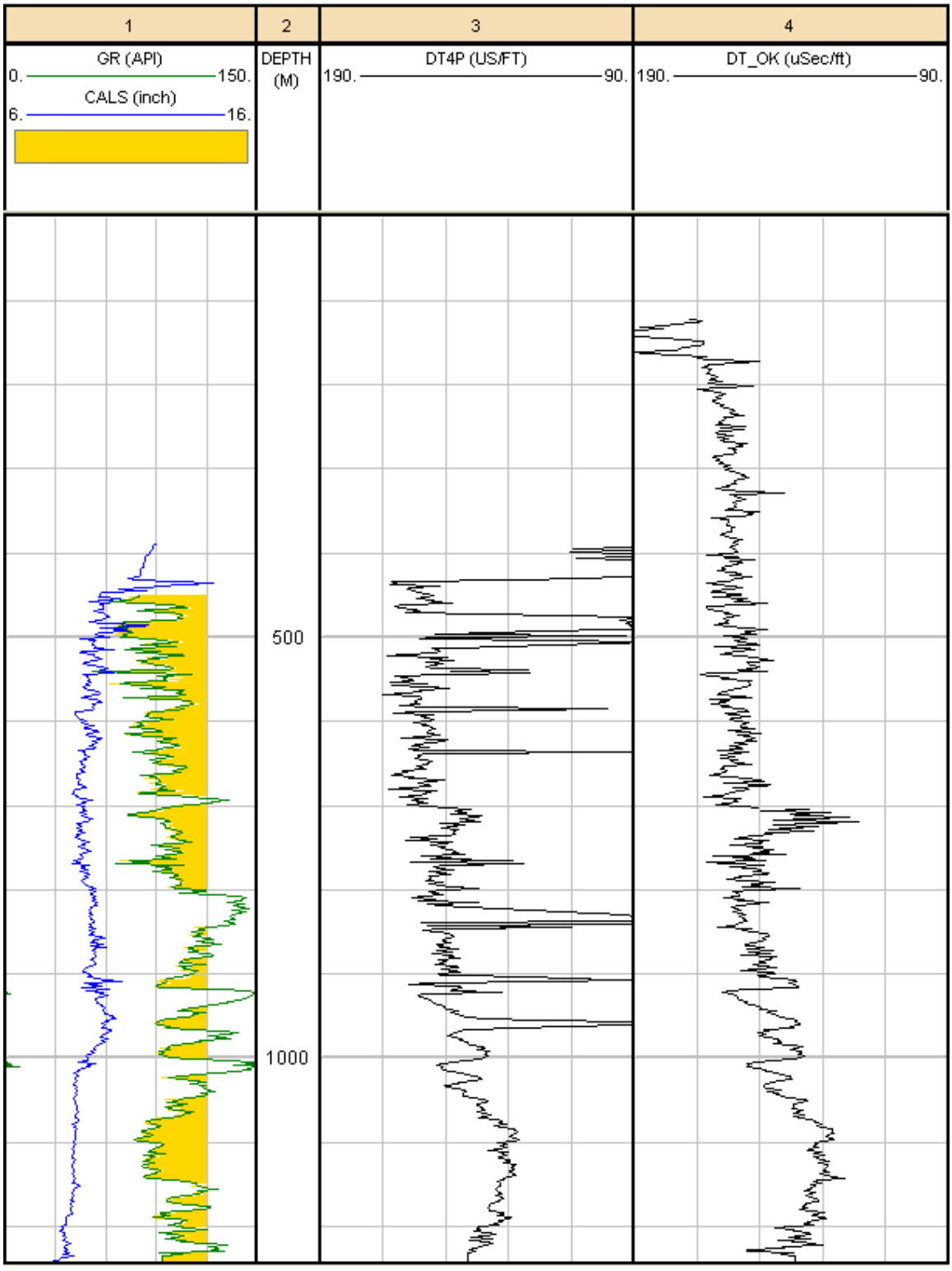

Figure 3-7: End result of the repair process of the P-wave sonic log of well A15-03. Track 3 shows the recorded sonic log with many anomalously low travel times, Track 4 shows the repaired sonic.

3.3.4 *Formation evaluation using a multi-mineral & Dual Water model*

3.3.4.1 Mineral inventory

In section 3.3.1 an inventory was made of the mineralogy of the Tertiary of A15-03. It will be obvious that not all minerals listed in Appendix A can be included in a petrophysical mineral model, simply because 1) some of these minerals give very similar tool responses, and 2) the number of minerals is far more than the number of logs that were recorded. This means that a selection of minerals has to be made, based on their expected impact (on Vclay, Phie, Sw) and on whether or not they can be detected at all by the logs. Figure 3-8 to Figure 3-12 show a number of cross plots of logs (both raw and derived logs) that are sensitive to mineralogy.

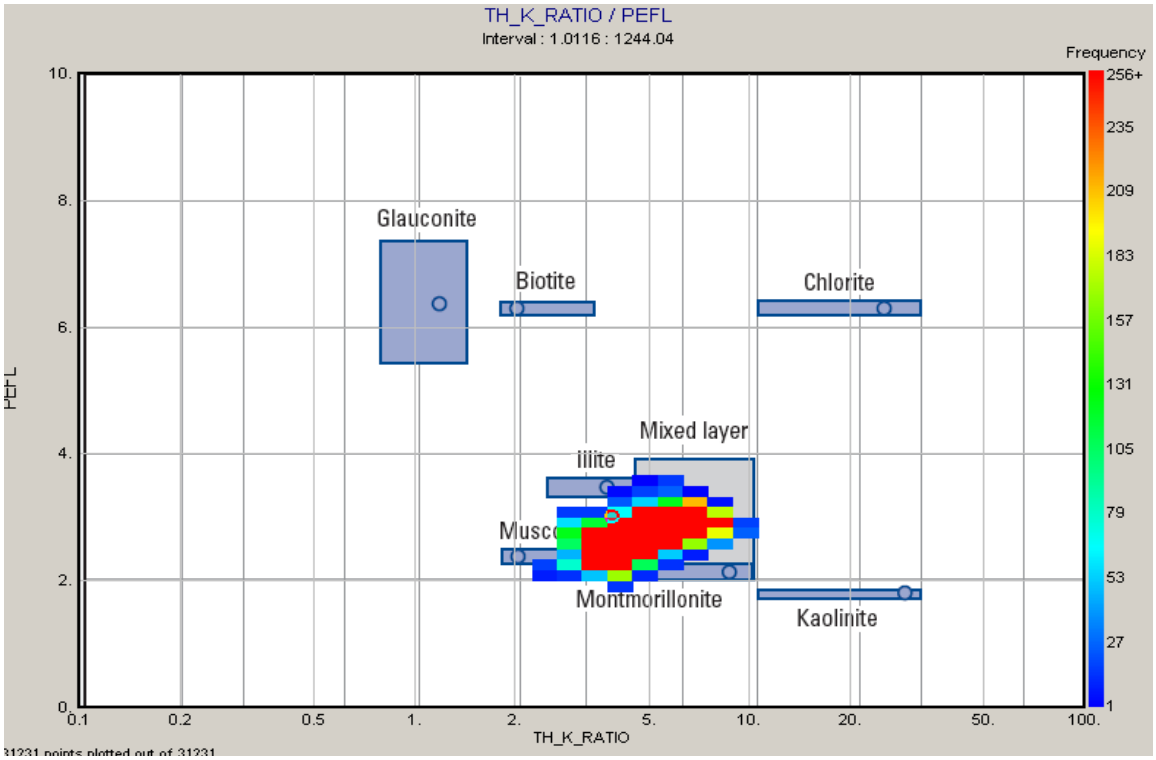

Figure 3-8: Mineral identification in A15-03: TH:K ratio – Pef xplot. The bulk of the minerals fall into Muscovite-Smectite-Illite fields.

Most of these cross plots are based on the Thorium and Potassium logs from the spectral gamma ray tool, the Photoelectric Effect (PEF) log from the lithodensity tool, and the density log also from the lithodensity tool.

The responses to these tools in A15-03 are dominated by clay minerals, most notably Smectite and Illite. Also Muscovite can be detected (Figure 3-8).

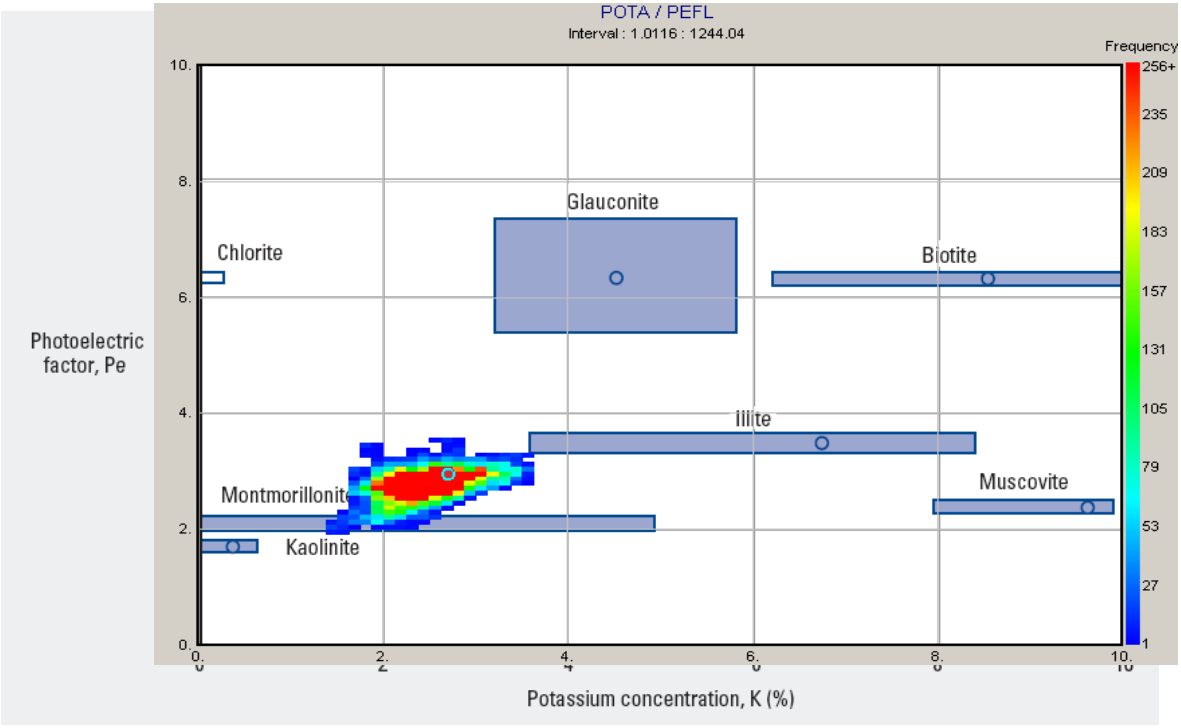

Figure 3-9: Mineral identification in A15-03: Pota – Pef xplot. The bulk of the minerals fall into Smectite-Illite fields.

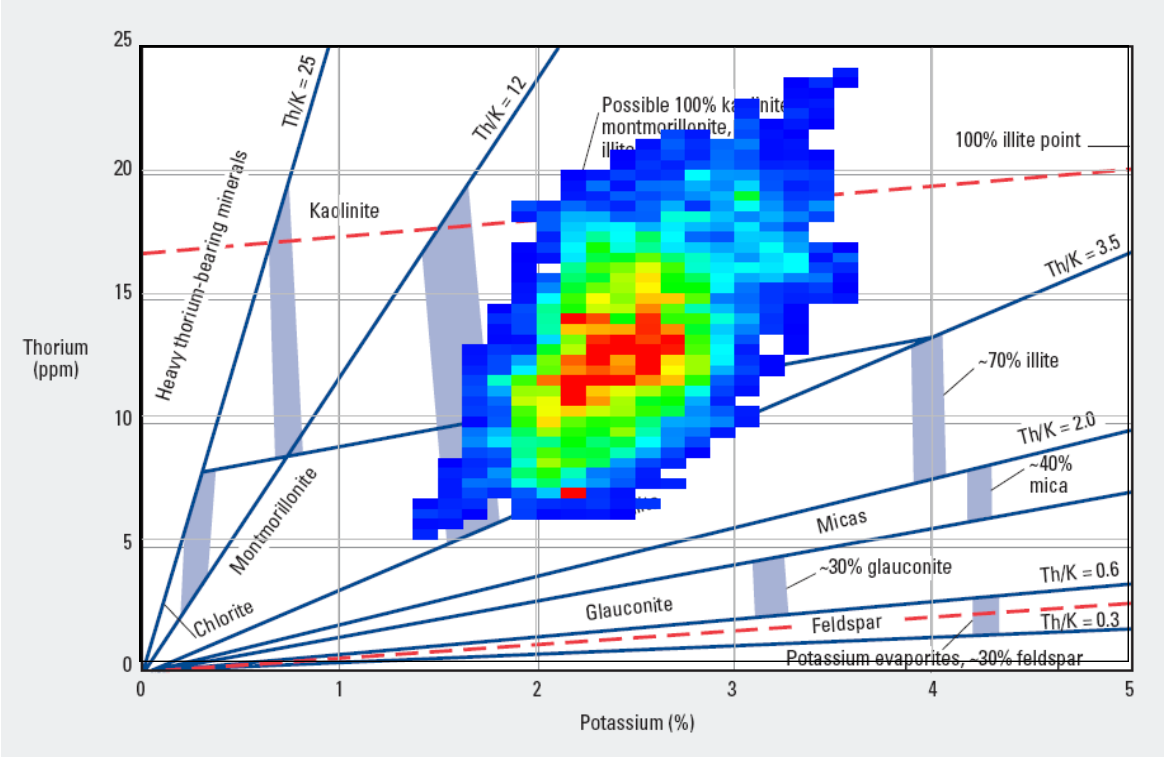

Figure 3-10: Mineral identification in A15-03: Pota – Thor xplot. The bulk of the minerals fall into Smectite-Illite fields.

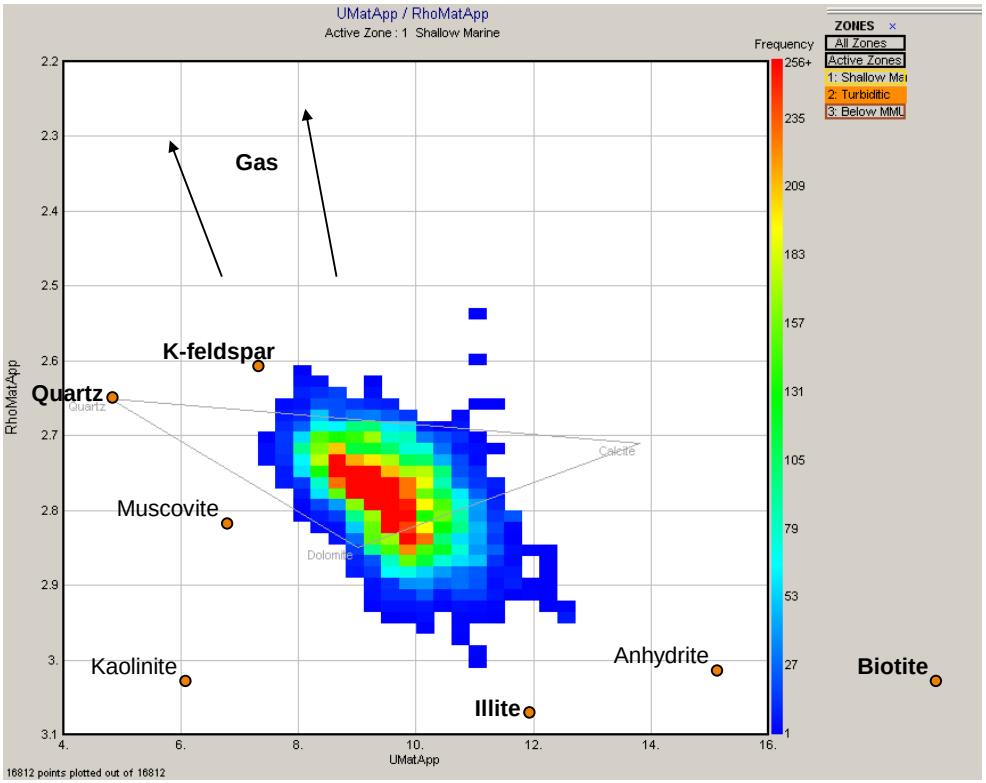

Figure 3-11: Matrix identification in A15-03: Rhomaa-Umaa xplot, lower (turbiditic) interval.

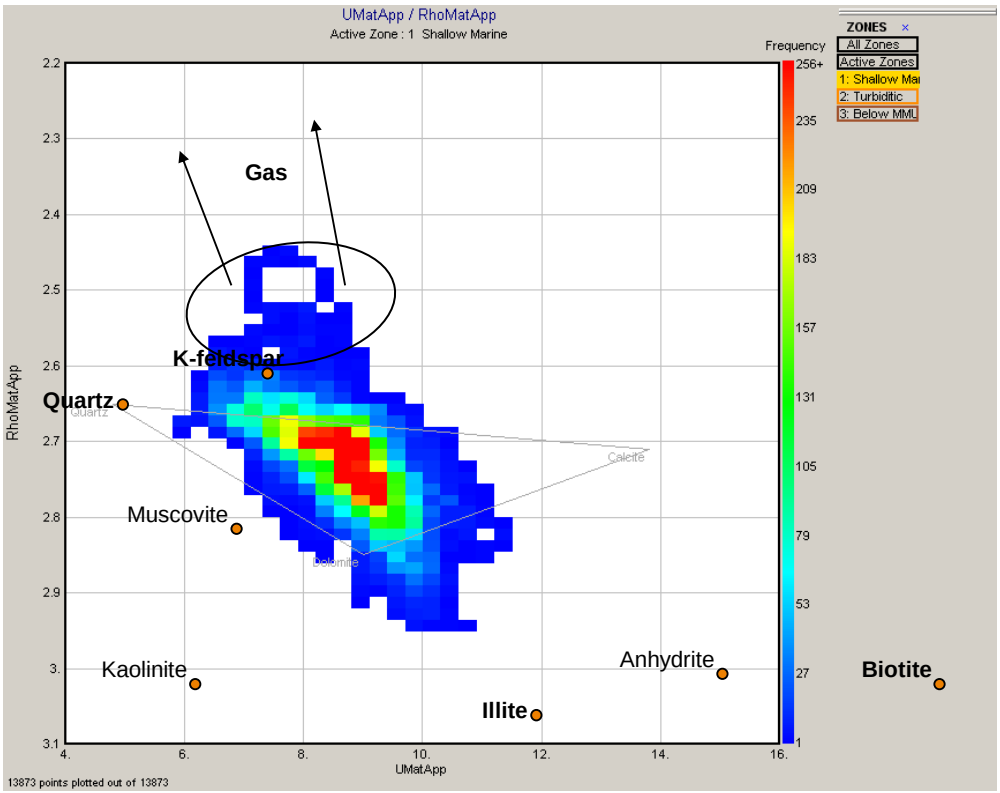

Figure 3-12: Matrix identification in A15-03: Rhomaa-Umaa xplot, upper (shallow marine) interval. Ellipse marks the effect of high gas saturations

3.3.4.2 Mineral model

Using the 'Mineral Solver' option of Interactive Petrophysics a multi-mineral model was set up. A number of boundary conditions were used to evaluate the results:
1) The residual error for each log should be minimized. This is the squared difference between the actual recorded log (e.g. Rhob) and the log that is produced by the calculated volumes of each of the constituting minerals. If the choice of minerals and their end point values for each log are perfect, the residual error should be zero. If however, the wrong minerals are chosen, or their log responses are out of range, the residual errors will be large.
2) The total porosities (Phit) produced by the model should be close to the measured core porosities.
3) Matrix densities (RHOMA) produced by the model should be close to the measured core grain densities.
4) The effective porosities (PHIE) produced by the model should be comparable to the ones produced by an ELAN evaluation done by Schlumberger in 2000 (document available from www.nlog.nl).

It soon became apparent that the inclusion of either coal or heavy minerals, or both resulted in non-realistic results. The inclusion of coal for example yielded a volumetric composition where all porosity was replaced by coal. Including a heavy, radioactive mineral resulted in much too high porosities, and up to 20% heavy minerals.

After some trial and error, the eventual mineral model included the following minerals: Quartz, Orthoclase, Mica, Montmorillonite, and Illite. Logs involved included: GR, Rhob, Nphi, U (density-corrected PEF), Pota, and Thor. Log values for each of these minerals are shown in Figure 3-13. These values are partly based on literature values (Schlumberger, 2009) and partly on estimates made on cross plots (Figure 3-14 to Figure 3-17).

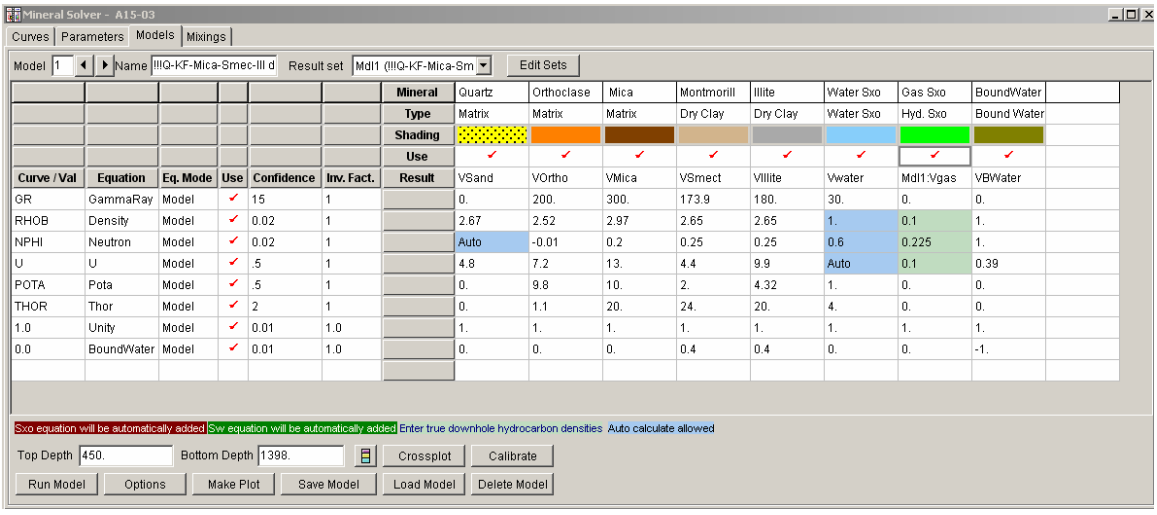

Figure 3-13: Overview of the final multi-mineral model used in A15-03. Screen dump of the 'Mineral Solver' option of the 'Interactive Petrophysics' software.

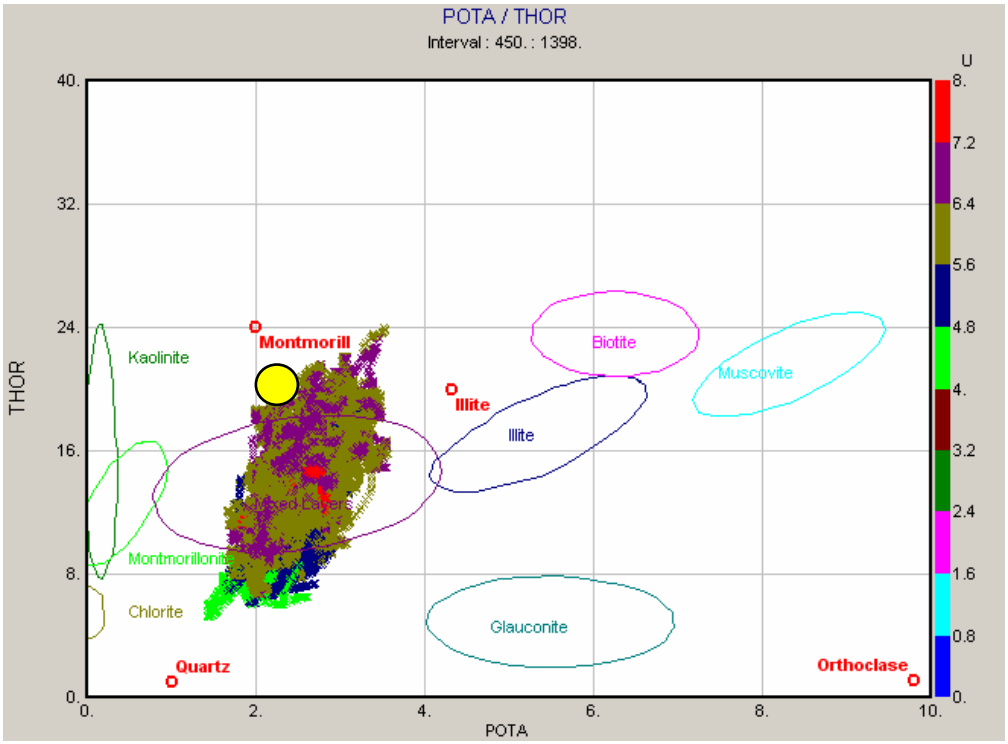

Figure 3-14: Cross plot of Thorium vs. Potassium with U on the Z-axis. Mineral fields (coloured ellipses) are according to 'Interactive Petrophysics'. Minerals used in the multi-mineral model are indicated in red. Yellow circle represents the 'cold shales' (see text below).

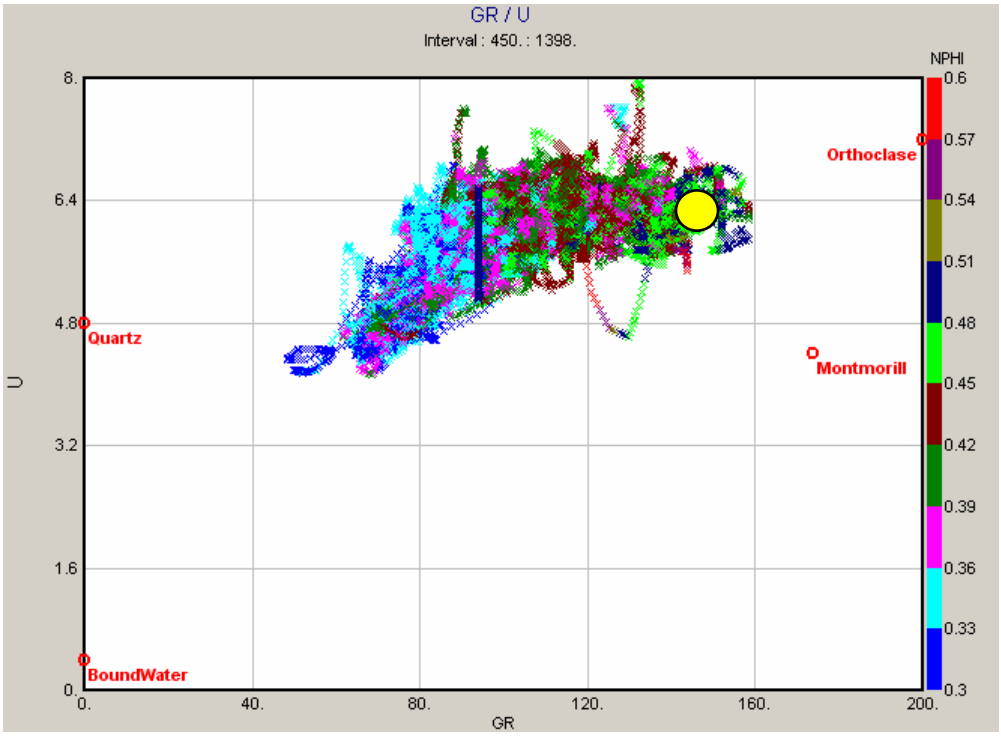

Figure 3-15: Cross plot of U vs. Gamma Ray with NPHI on the Z-axis. Legend as in Figure 3-14.

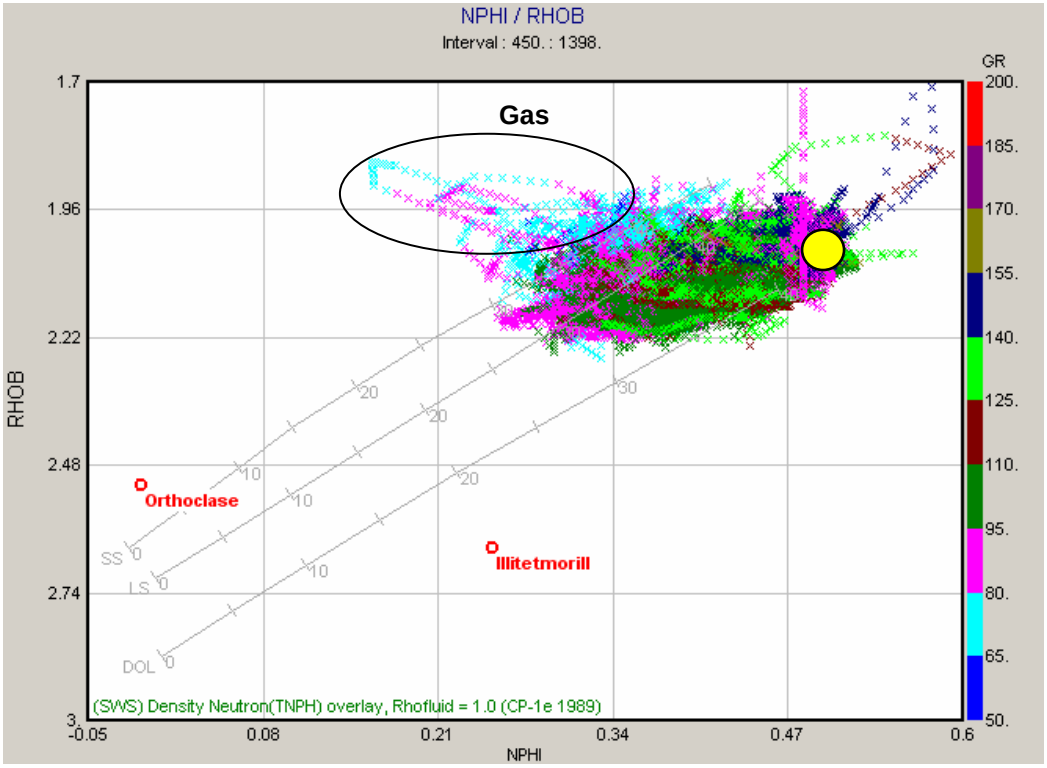

Figure 3-16: Cross plot of RHOB vs. NPHI with GR on the Z-axis. Ellipse marks the effect of high gas saturations on the neutron and density logs. Legend as in Figure 3-14.

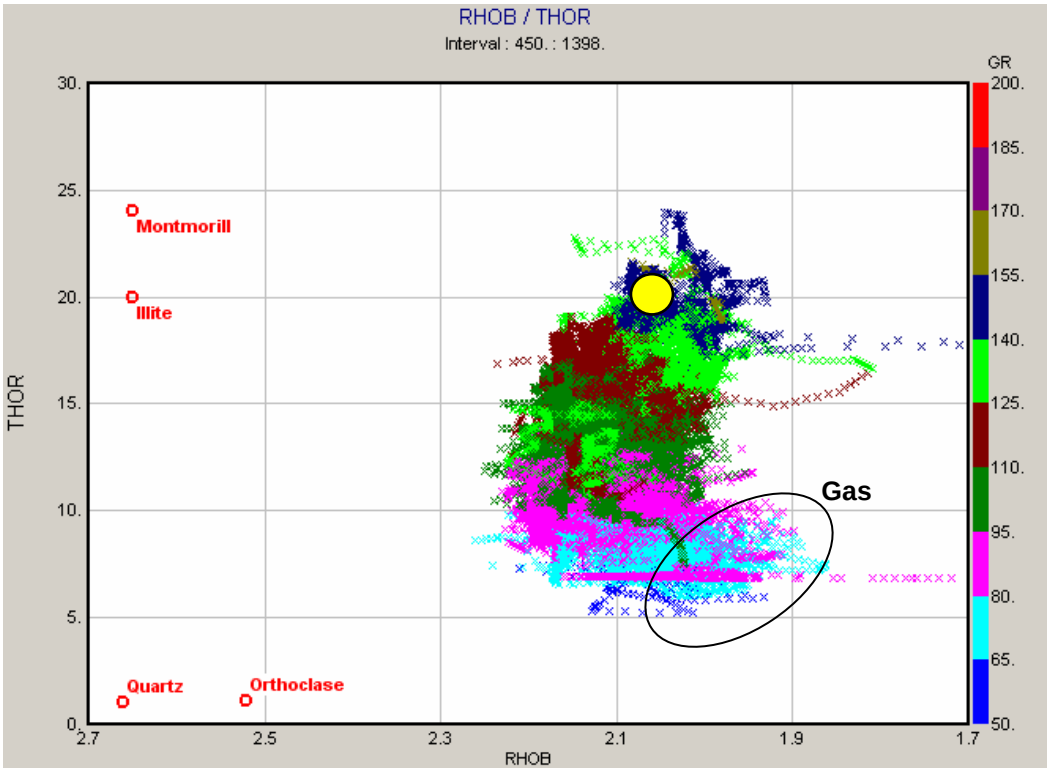

Figure 3-17: Cross plot of Thorium vs. RHOB with GR on the Z-axis. Legend as in Figure 3-14.

The multi-mineral model was run together with a water saturation module for which the Dual Water model was chosen. In view of the large amounts of smectitic clays that are present (and even Kaolinite) a saturation model that adequately accounts for the Cation Exchange Capacities of these type of clay minerals seems appropriate. This of course requires the clay mineral values to be specified as Dry Clay values (Figure 3-13).
Figure 3-18 shows the settings for the water saturation module. Mud filtrate resitivity (Rmf) values were adapted from the log headers of the well site log playbacks, the formation water resistivity value (Rw) was calculated from the salinity values of formation water produced during drill stem tests.

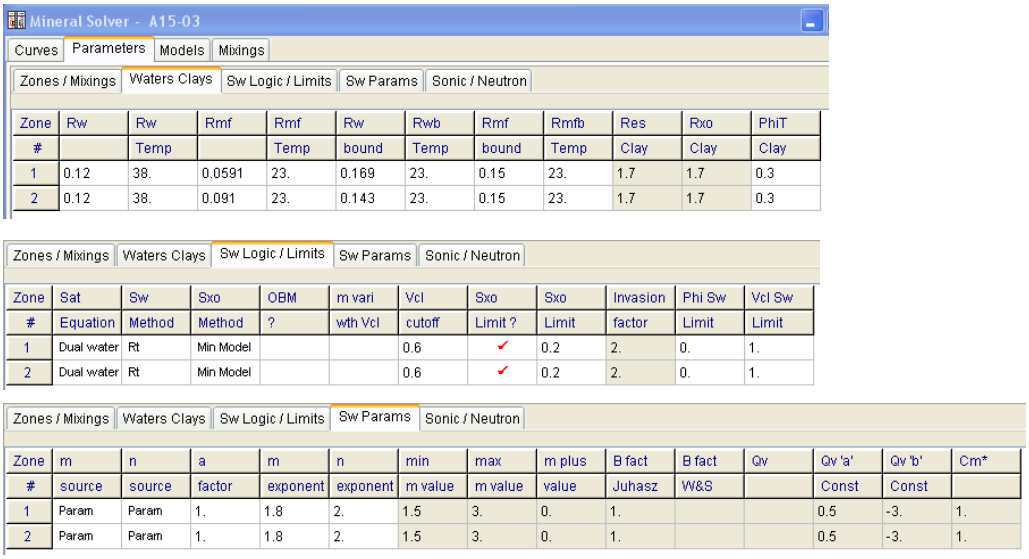

Zone	Rw	Rw	Rmf	Rmf	Rw	Rwb	Rmf	Rmfb	Res	Rxo	PhiT
#		Temp		Temp	bound	Temp	bound	Temp	Clay	Clay	Clay
1	0.12	38.	0.0591	23.	0.169	23.	0.15	23.	1.7	1.7	0.3
2	0.12	38.	0.091	23.	0.143	23.	0.15	23.	1.7	1.7	0.3

Zone	Sat	Sw	Sxo	OBM	m vari	Vcl	Sxo	Sxo	Invasion	Phi Sw	Vcl Sw
#	Equation	Method	Method	?	wth Vcl	cutoff	Limit ?	Limit	factor	Limit	Limit
1	Dual water	Rt	Min Model			0.6	✓	0.2	2.	0.	1.
2	Dual water	Rt	Min Model			0.6	✓	0.2	2.	0.	1.

Zone	m	n	a	m	n	min	max	m plus	B fact	B fact	Qv	Qv 'a'	Qv 'b'	Cm*
#	source	source	factor	exponent	exponent	m value	m value	value	Juhasz	W&S		Const	Const	
1	Param	Param	1.	1.8	2.	1.5	3.	0.	1.			0.5	-3.	1.
2	Param	Param	1.	1.8	2.	1.5	3.	0.	1.			0.5	-3.	1.

Figure 3-18: Parameters used in the Dual Water model.

To our knowledge no Formation Factor measurements were made, so an estimate for 'm' was made from a Pickett plot (Figure 3-19). The main problem in the A15-03 sands is that most of the gas-bearing sands have low gas saturations. It is therefore difficult in a Pickett plot to unequivocally determine the 100% water line. Figure 3-19 shows our best estimate, which, when 'a' is assumed to be 1.0, and 'n' to be 2.0, results in a value for 'm' of 1.8.
The results of this model are shown in Figure 3-20 and Figure 3-21. As can be seen in track 8 of both figures, the residual error is quite small, except for very shaly intervals in the lower, turbiditic part of the stratigraphic sequence. The sediments in these intervals were deposited during glacial periods (see Chapter 4 on Biostratigraphy) and are nick-named 'cold shales' here. Inspection of the reconstructed logs and crossplots of the original logs (Figure 3-14 to Figure 3-17) show that the multi-mineral model in these intervals underestimates GR, POTA, and especially THOR. This means that the mineral model fails for the cold shales, and that the most likely cause is that a specific mineral is lacking from the model. It can be speculated that the weathering conditions during glacials yielded more Thorium-rich minerals, like Kaolinite or pure Montmorillonite. Kaolinite is less likely, as it is known to be produced mainly in warm, humid tropic areas. The low density of these 'cold clays' (Figure 3-16) rather suggests pure Montmorillonite.

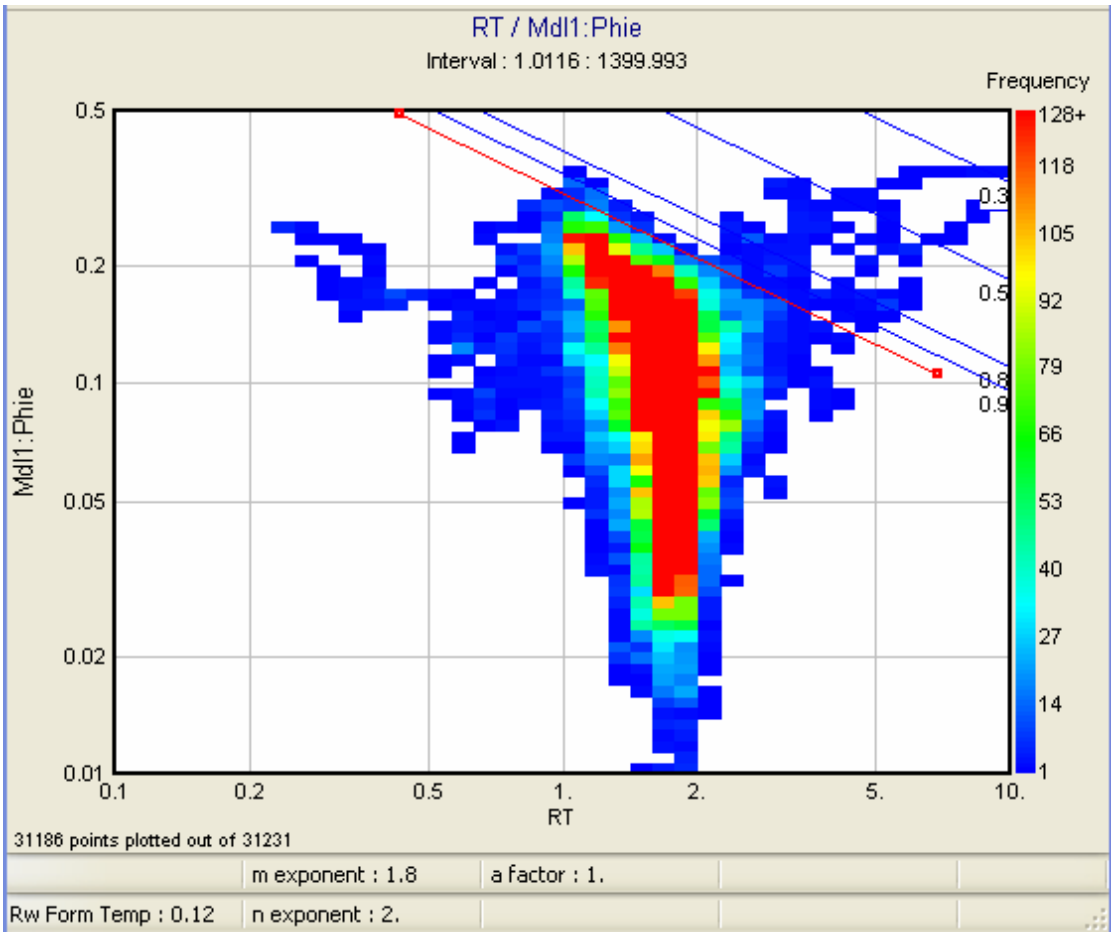

Figure 3-19: Determination of cementation exponent ‘m’ from a Pickett plot. The best estimate for the slope of the 100% water saturation line results in a value for ‘m’ of 1.8. The various parallel lines represent water saturation values given the current set of a, m, and n values.

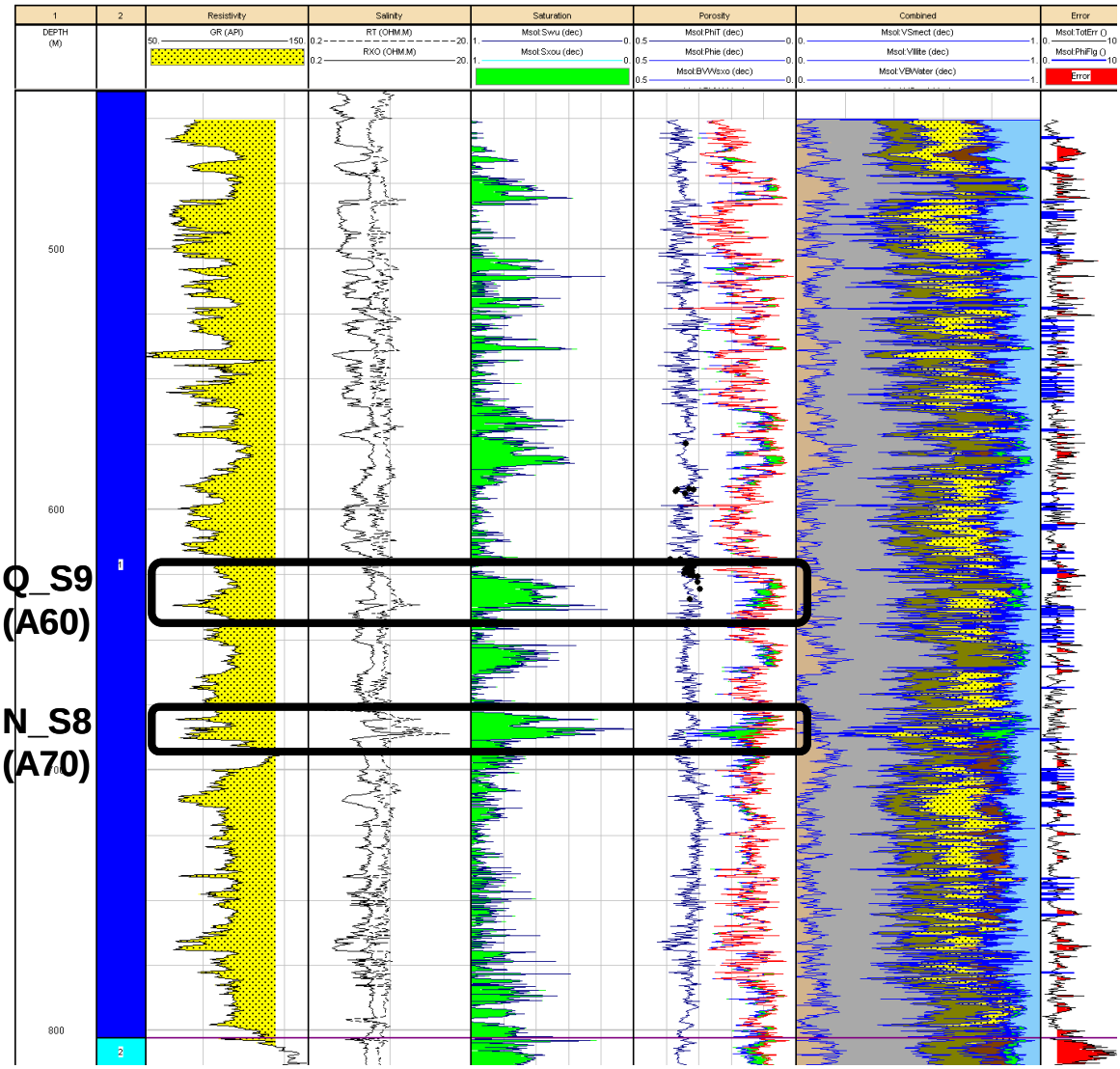

Figure 3-20: A15-03 Results multi-mineral model, upper part of the stratigraphy. Two gas-bearing sands (Q_S9 and N_S8) are indicated. Note the excellent match between core porosities (dots) and PHIT (blue line, track 6).

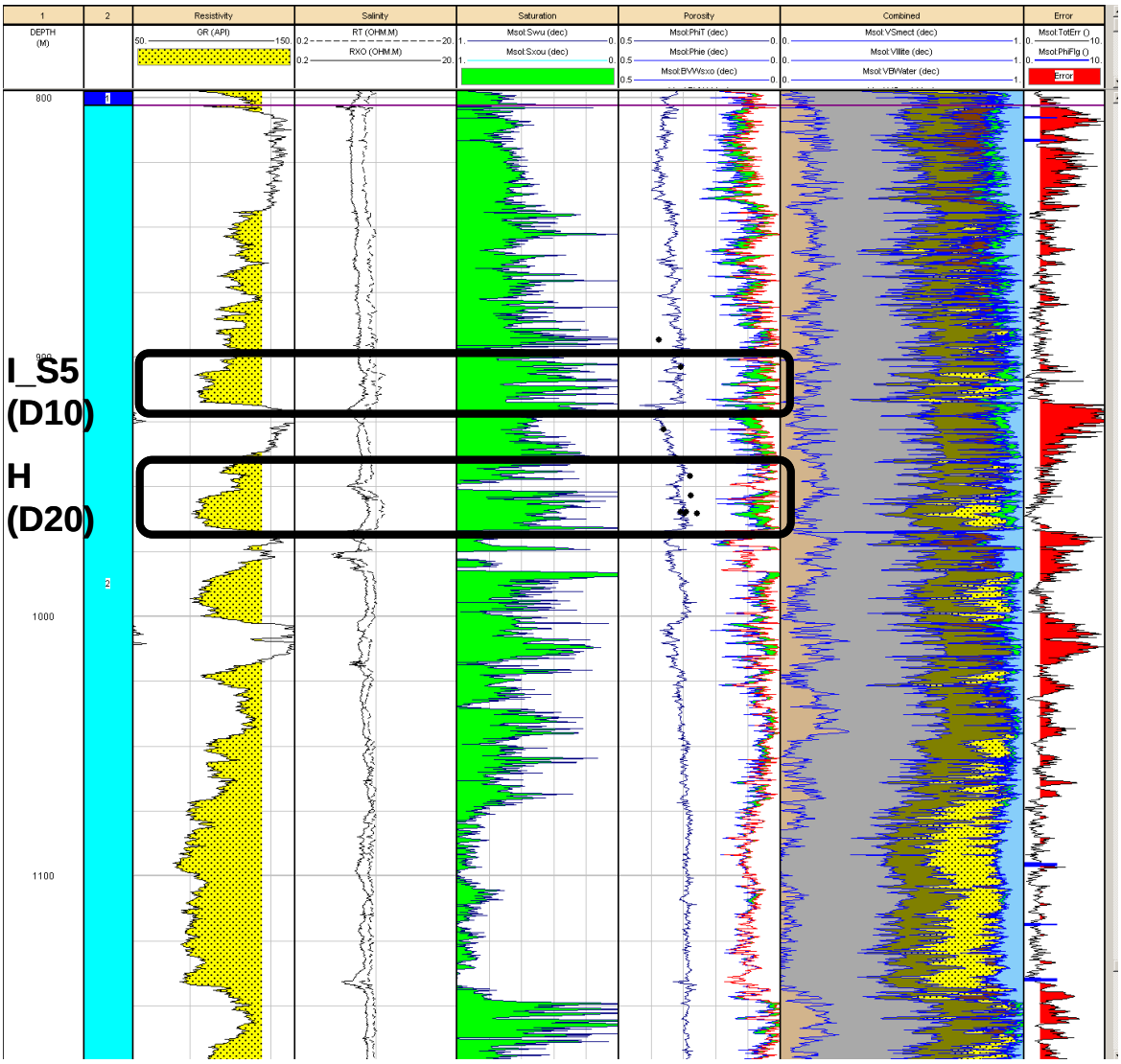

Figure 3-21: A15-03 Results multi-mineral model, lower part of the stratigraphy. Two gas-bearing sands (I_S5 and H) are indicated. Note the good match between core porosities (dots) and PHIT (blue line, track 6).

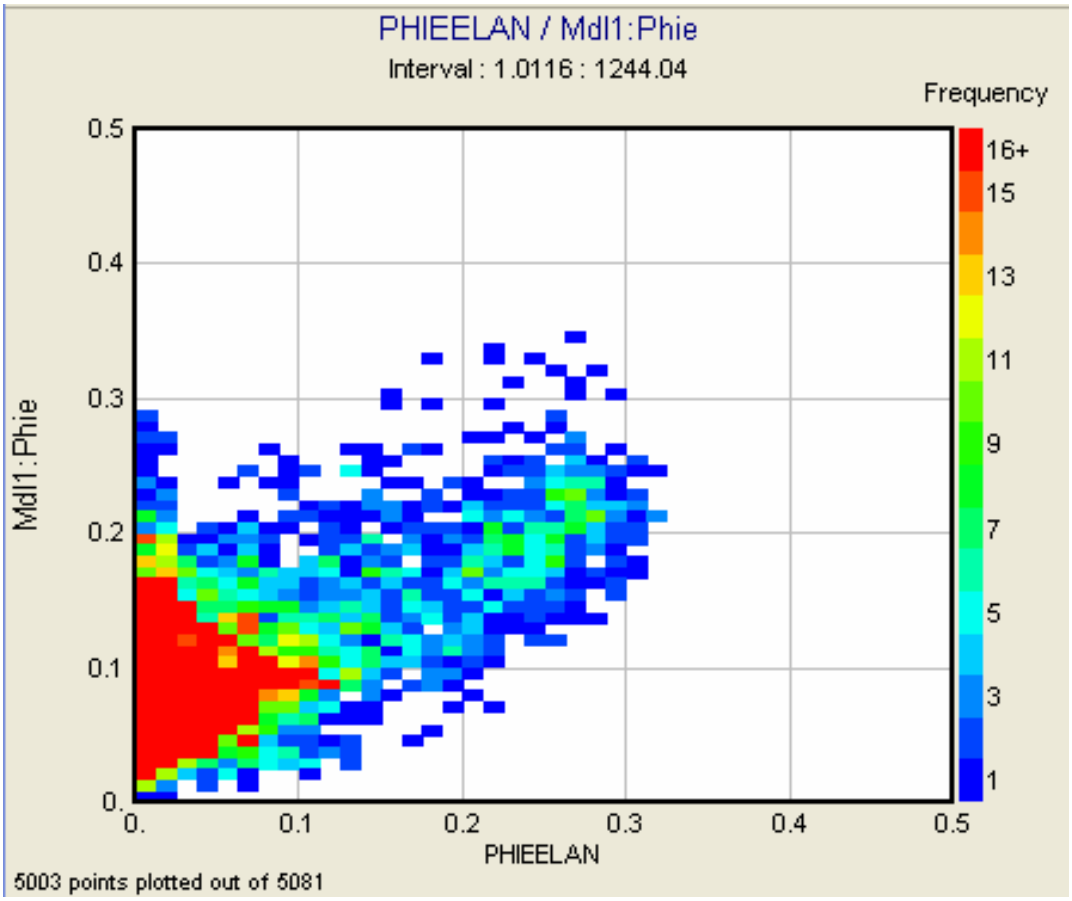

Figure 3-22: Comparison of TNO's Phie vs. Schlumberger's ELAN Phie. In the higher porosities, TNO's Phie is about 5 percent point lower than the ELAN version.

Figure 3-22 compares the results of the effective porosity (Phie) of the multi-mineral model to the effective porosities calculated by Schlumberger using their ELAN software package. It can be seen that TNO's porosities are generally higher than Schlumberger's in the low porosity range, and lower in the high-porosity range. In the low porosity range the scatter is large.

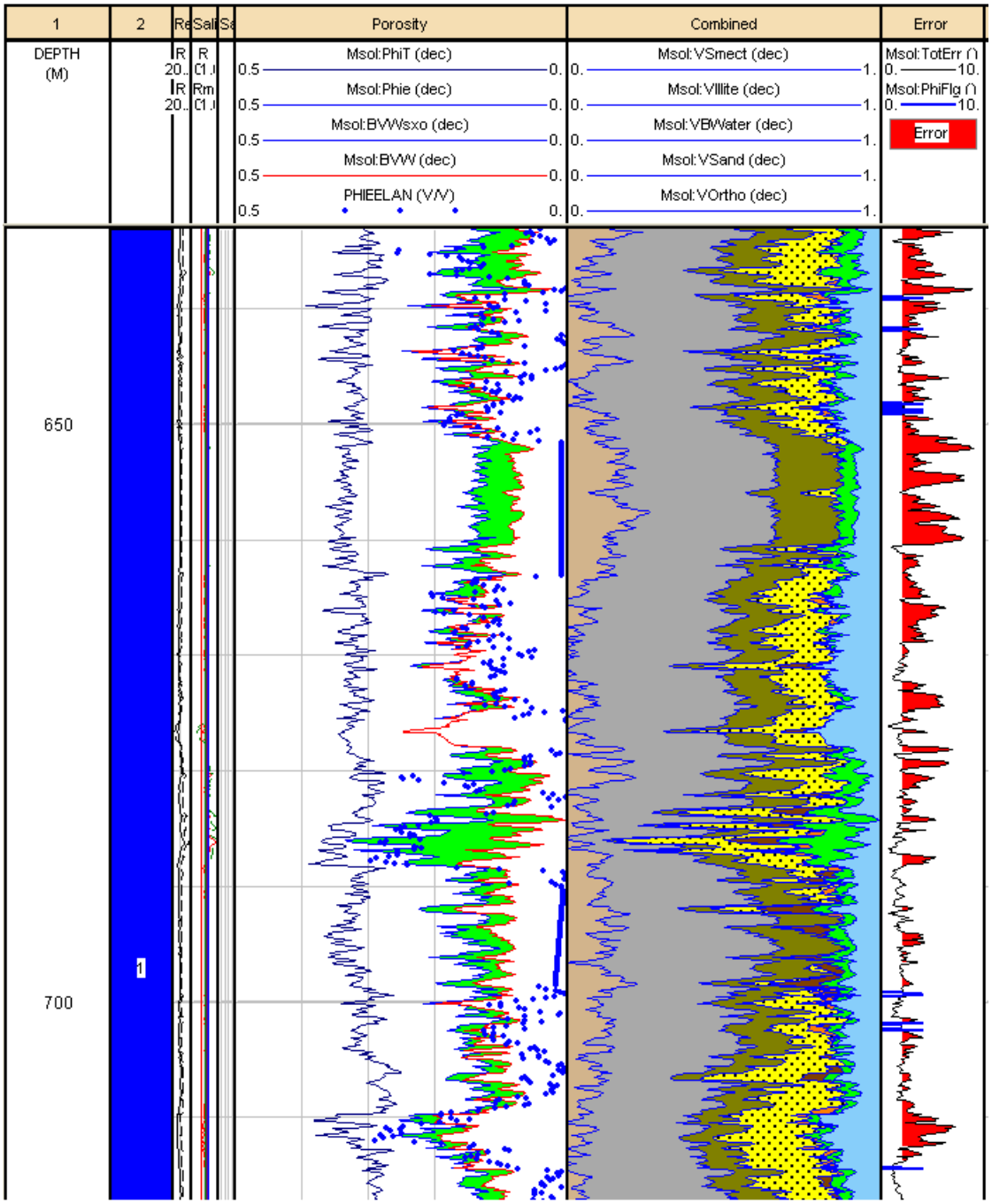

Figure 3-23: Comparison of TNO's Phie (blue line) and Schlumberger's ELAN Phie (blue dots). See text for explanation.

Comparison of the two porosities in a log playback may provide an explanation for these large differences (Figure 3-23). The high porosities in the sands, either gas or water bearing, are quite comparable. The main difference is in the low porosity intervals, mostly shaly, (e.g. 650-660 m) where TNO's model predicts some 10% porosity, and Schlumberger's model 0%.
On the one hand, effective porosities of 0% are hard to believe at these shallow depths, even when the lithology is pure shale. On the other hand, TNO's porosities might be a bit optimistic.
The residual error (rightmost column in Figure 3-23) in this interval is quite large, indicating that the mineral model is not able to reproduce the original well logs. Moreover, the multi-mineral model has inserted some gas, probably in attempt to honour the low values for RHOB.

It seems that the choice of mineral end points of the smectite, especially the density value, needs some further adjustment to reduce the effective porosities in these shale zones.

3.3.5 *Formation evaluation using a shaly sand model*

Most wells in the northern Dutch offshore area do not have the full log suite in the Tertiary to run a multi-mineral model. Therefore, a simpler shaly sand model was designed. Using the neutron and density logs, a three-mineral model can be set up which solves for effective porosity (Phie), matrix volume (VSand), and wet clay volume (VWCL). Then, using a suitable shaly-sand saturation model, Sw can be calculated.

The hardest part in these calculations is the choice of the wet clay point. Figure 3-24 lists the most important parameters in the model. The matrix density was set to 2.65 g/cc. Figure 3-25 shows a neutron-density cross plot with the matrix and wet clay points indicated.

The saturation equation used is the Simandoux equation.

Figure 3-26 and Figure 3-27 show the end results.

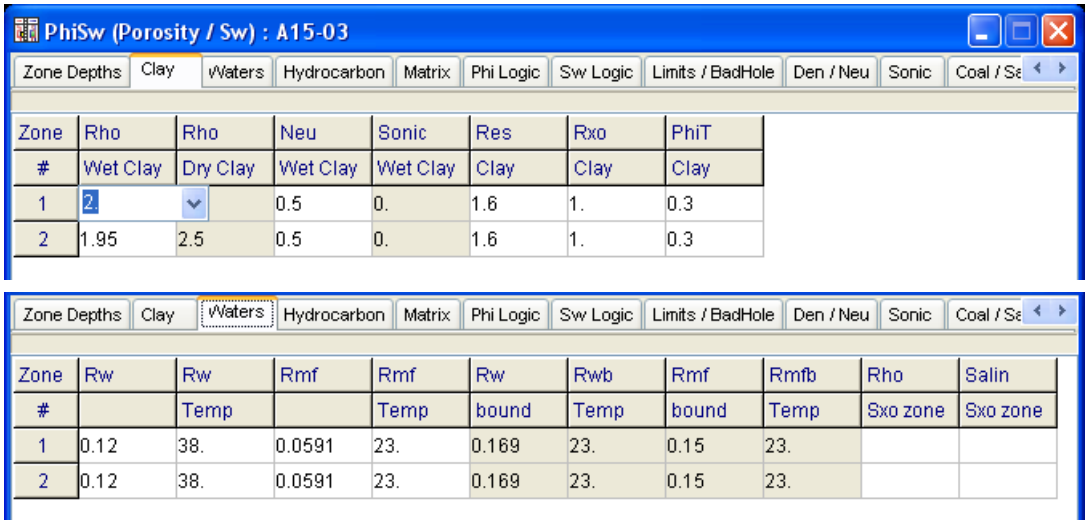

Figure 3-24: Parameters for the shaly sand model used in A15-03.

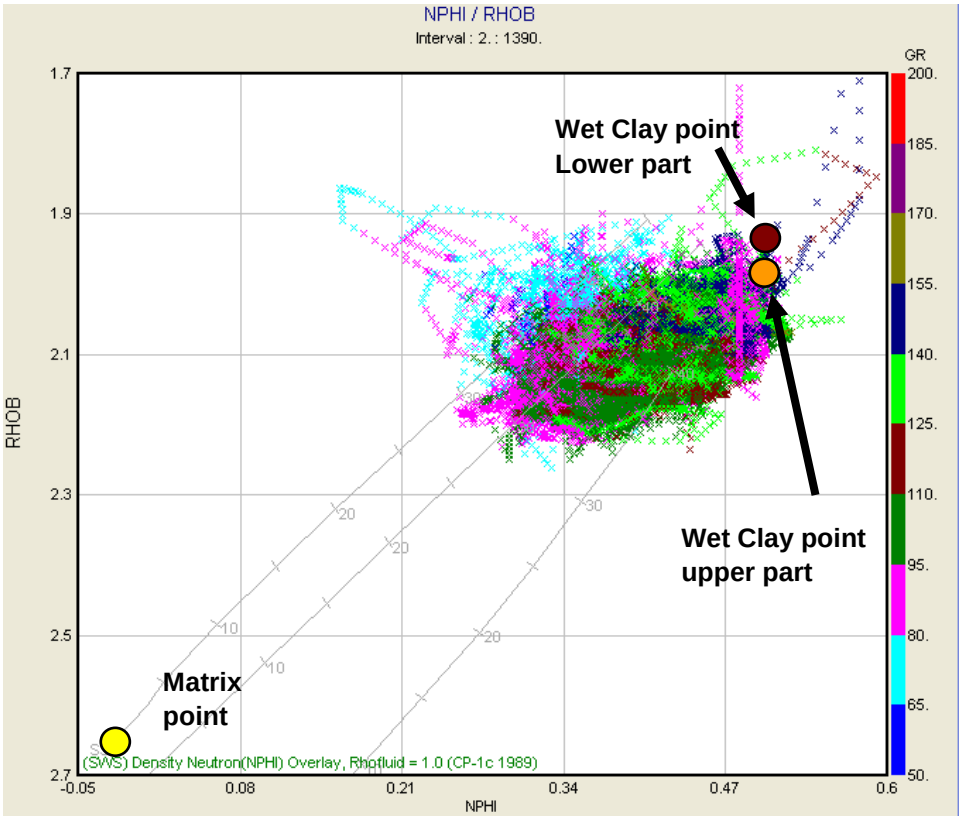

Figure 3-25: Well A15-03 neutron-density cross-plot. GR is on the Z-axis. Indicated are the matrix point and wet clay point.

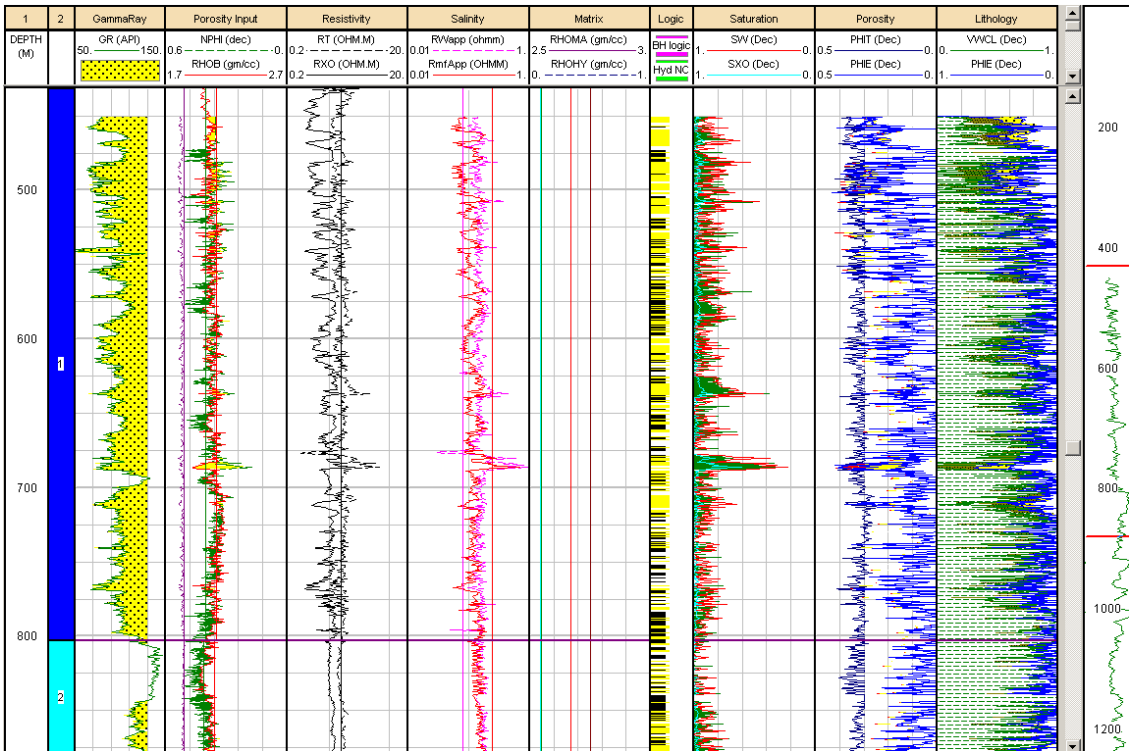

Figure 3-26: Shaly sand analysis in well A15-03 with neutron and density logs and Simandoux equation (Upper part).

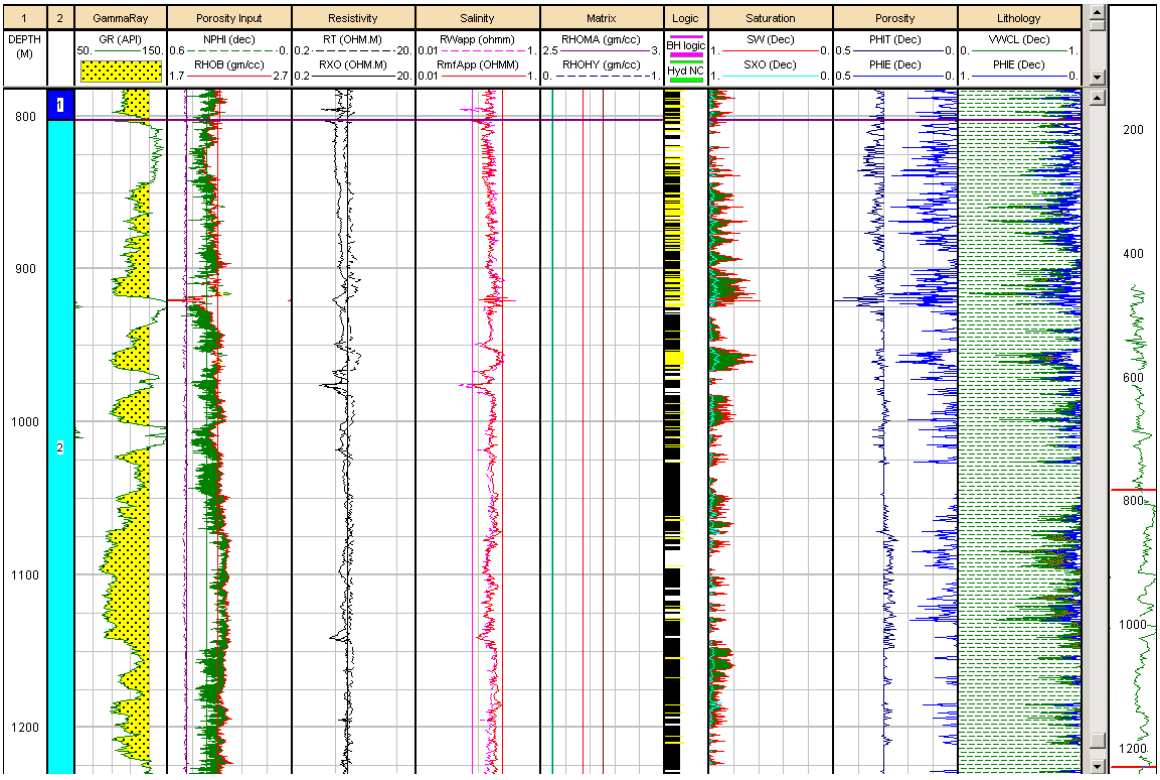

Figure 3-27: Shaly sand analysis in well A15-03 with neutron and density logs and Simandoux equation (Lower part).

3.3.6 *Permeability*

A total number of 38 core plug measurements on permeability were available for well A15-03. As stated above, core plugs were oven-dried, so the porosity measurements actually represent total porosity rather than effective porosity. The measured Helium permeability should thus be cross plotted against effective porosity, which in this case is derived from log measurements. Figure 3-28 shows this cross plot. It is apparent that the scatter is wide, and that the porosity class in which we are most interested (>20%) is strongly underrepresented in the data set.
Therefore, another source of permeability data was involved: the permeability derived from NMR data. Figure 3-29 shows the Timur NMR permeability, cross plotted against effective porosity from the multi-mineral model. Again, the scatter is large, almost two orders of magnitude for a given porosity, but the trend is clear.

In formula:

$$K = 10^{-1.7964 + 14.2768 * \text{Phie}}$$

where K is expressed in milliDarcies, and Phie as a decimal fraction.

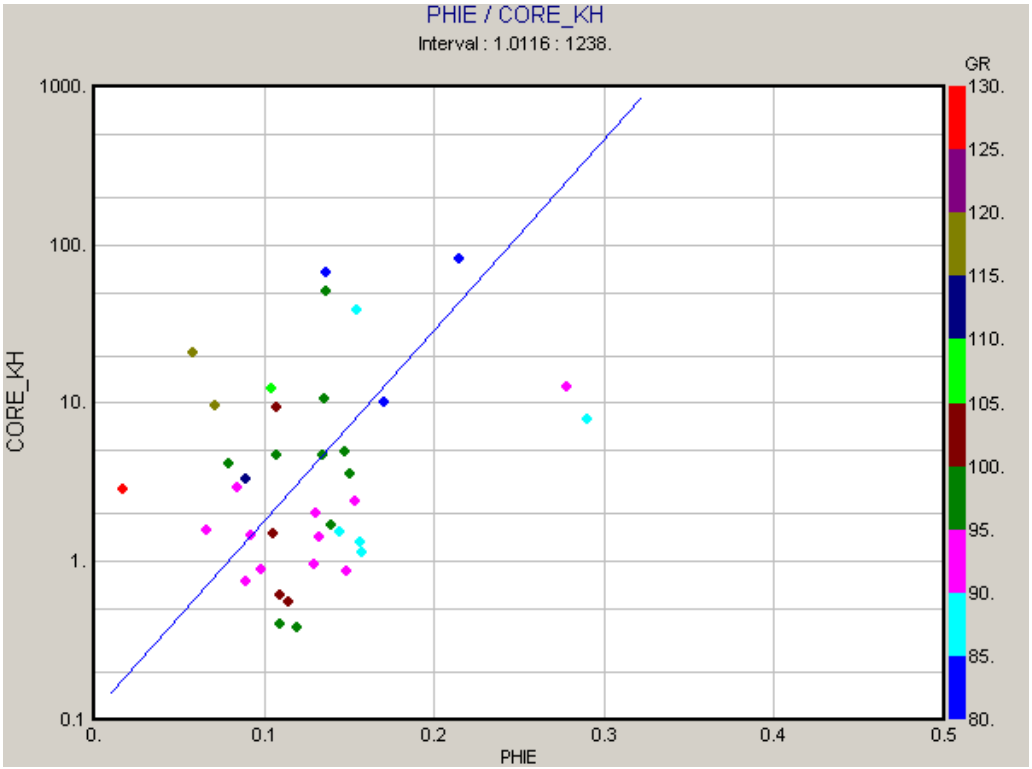

Figure 3-28: A15-03 Core plug helium permeability vs. Phie.

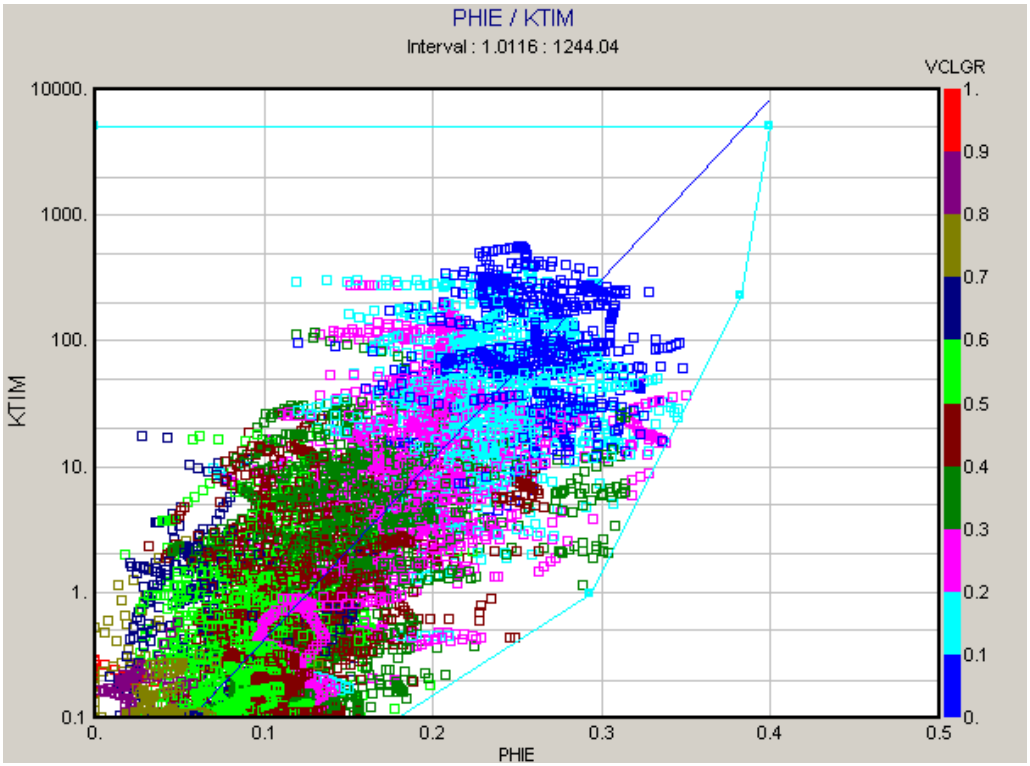

Figure 3-29: A15-03 NMR (Timur) permeability vs. Phie.

3.4 Well A15-02

Well A15-02 had a similar log suite as well A15-03. Shown here (Figure 3-30) are the results for the shaly sand / Simandoux calculations.
The effective porosities are in the same range as those of well A15-03. Also, the gas saturations are comparable, although in general they are even lower than those in A15-03.

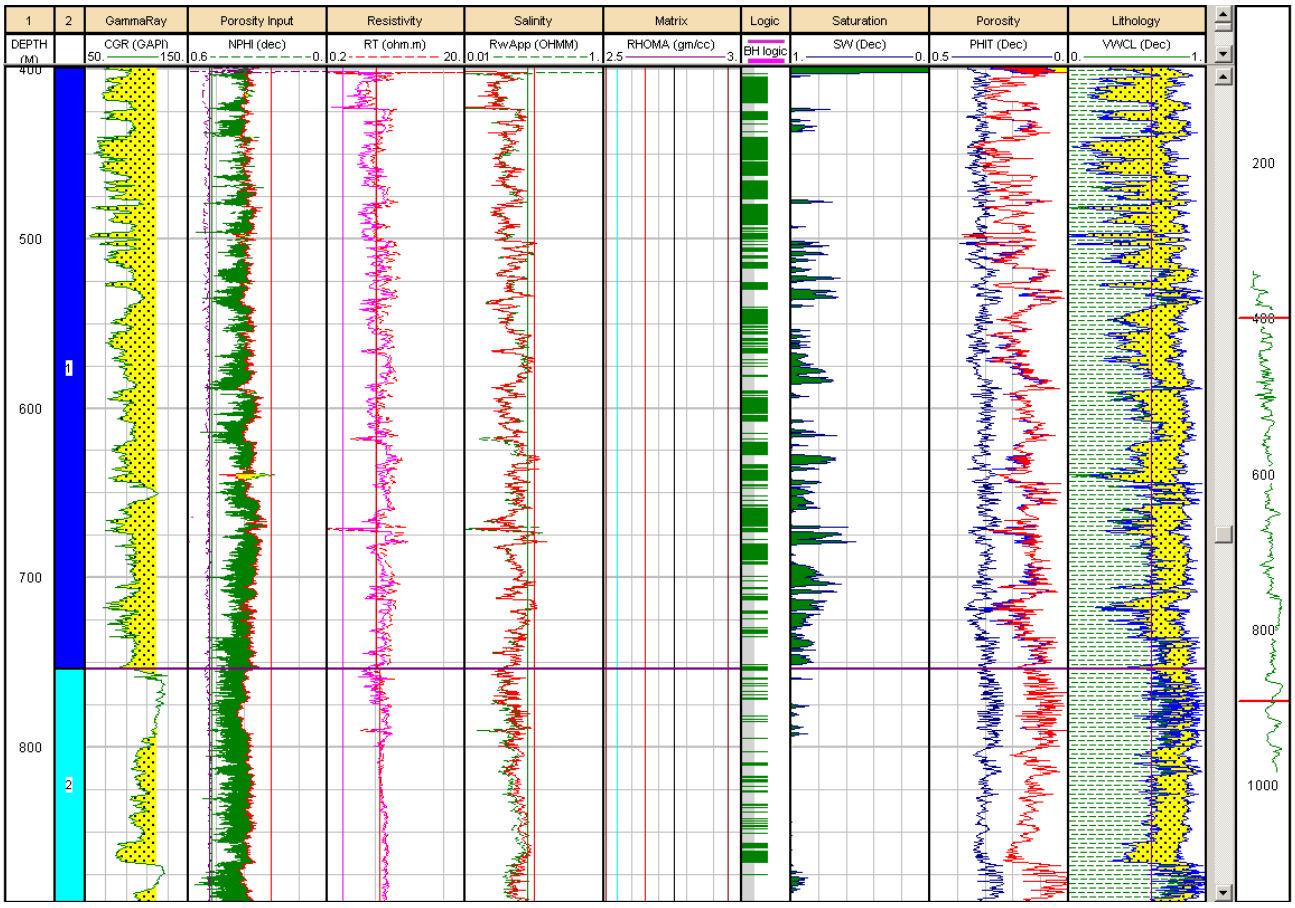

Figure 3-30: Shaly sand analysis in well A15-02 with neutron and density logs and Simandoux equation.

3.5 Well A15-01

Well A15-01 was the first well drilled in the A15 Block, in 1971. Targets were deeper formations such as the Chalk and Scruff. Therefore, in the Tertiary section of the well only a gamma-ray log and a sonic log were recorded. The original sonic had unrealistically low values (around 200 μs/ft instead of the usual 150 μs/ft). Fortunately, A VSP was shot after which a corrected sonic could be constructed. This corrected sonic, together with the gamma-ray log formed the basis for the shaly sand evaluation.
The absence of resistivity logs precludes the calculation of saturation of course.
The GR log was used for VClay determination using a linear transform. Using this clay volume, the sonic was used for effective porosity calculations using the Raymer-Hunt (1980) transform with the following values:
DTma= 90 μs/ft, DTfl=200 μs/ft, and DTclay=168 μs/ft. Figure 3-31 shows the results.

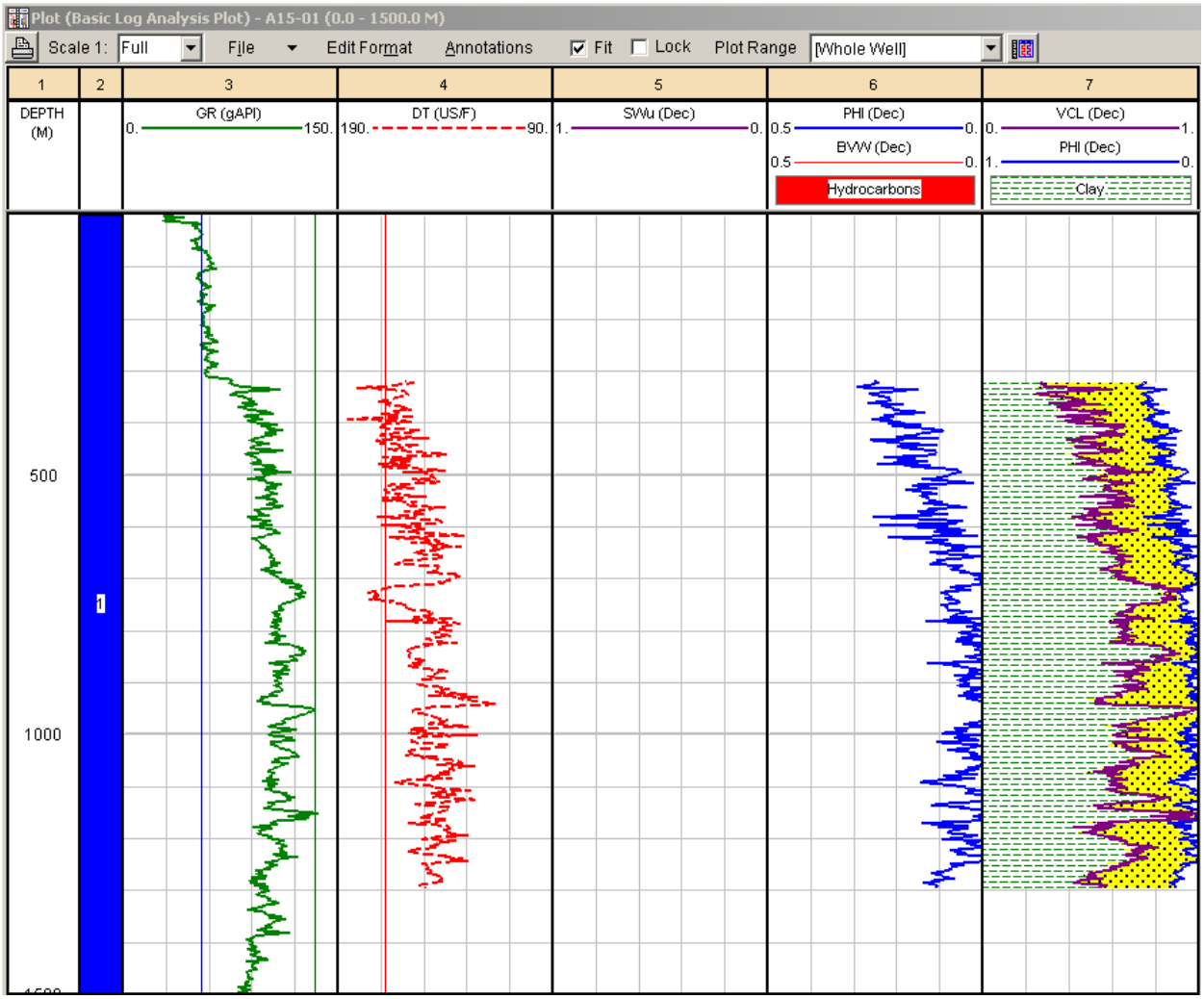

Figure 3-31: Shaly sand analysis in well A15-01 with gamma-ray and sonic logs.

3.6 Well A15-04

For well A15-04, the following logs were available: GR, RHOB, DT, Deep Resistivity. These were spliced logs in LAS format, so log header information was not available.
Apparently, this well suffered from severe bad hole conditions: many suspected washouts caused the density log to produce erroneously high porosity values. Unfortunately there was no caliper log available to unequivocally detect these washouts.
So it was decided to only use the sonic for porosity calculation. As in well A15-01, the GR log provided VClay, and the same DT values for matrix, fluid, and clay were used. Figure 3-32 shows the results. Apart from a dubious streak between 540 and 550 m which shows some gas saturation, the rest of the well is completely dry.

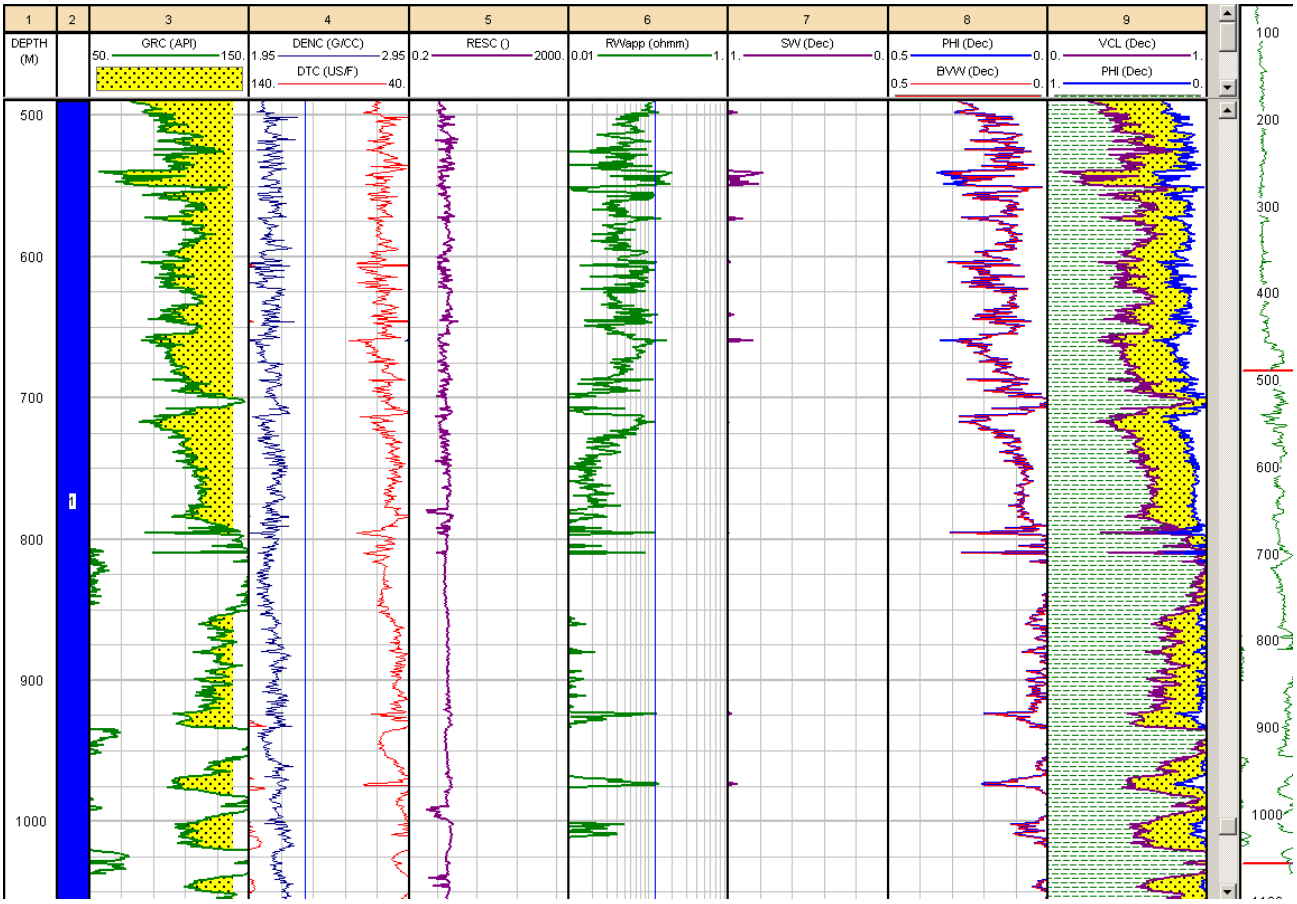

Figure 3-32: Shaly sand analysis in well A15-04 with sonic and density logs and Simandoux equation.

3.7 Comparison of the calculated porosities

In Figure 3-33 the results of the shaly sand porosity calculations are graphically compared. The fact that well A15-03 is overrepresented finds its cause in the sample interval of this well, which is 2 inch, whereas the other wells have a sample interval of 0.5 foot (6 inch).
The porosities in well A15-02 are on the low side in comparison to the other wells. The cause is unknown; for this well exactly the same parameters were used as in well A15-03. Log quality was good in A15-02.
Wells A15-01 and A15-04 have comparable porosity distributions as A15-03.

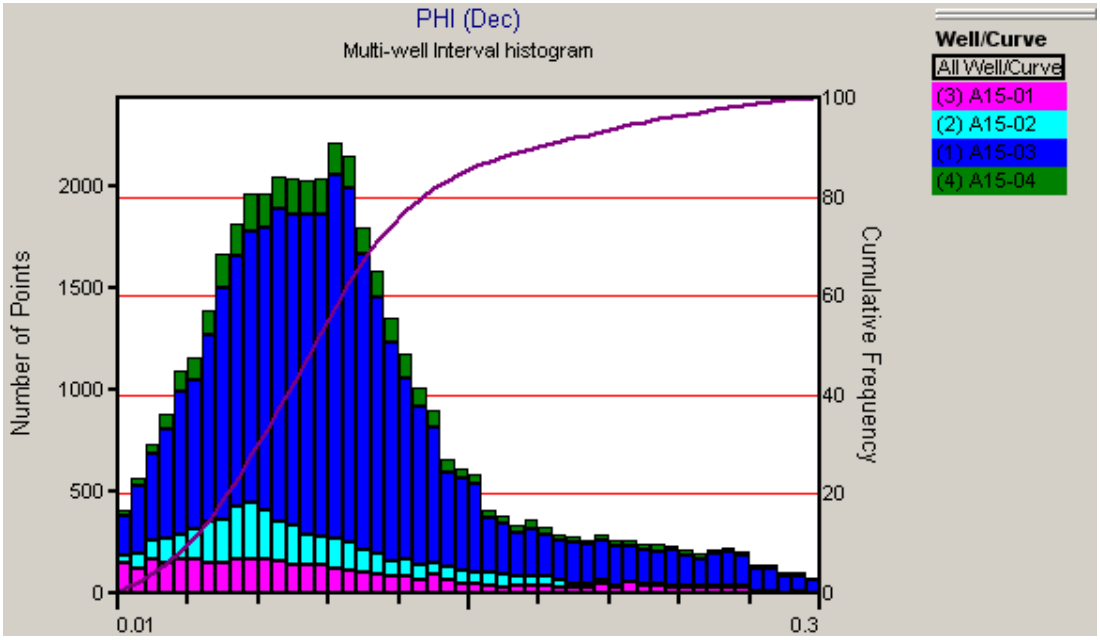

Figure 3-33: Stacked histogram of the effective porosities of the four wells in A15.

3.8 Discussion of the results

3.8.1 *Difficulties in log evaluation*

Based on our experiences with the four wells drilled in the A15 block, evaluation of porosity, shale content, water saturation, and permeability in the Neogene strata is not straightforward. There are several factors that complicate the process of log interpretation.

- Well to well differences. Within the A15 block different logging suites and log sampling rates have been used. This means that each well needs an individual approach.
- Hole conditions. Because the rocks are unconsolidated sands and clays, most wells have many washout sections. This affects all contact-type logging tools, and causes many aberrant readings, especially in the porosity logs.
- KCL / Polymer mud. In order to fight the instability of the unconsolidated sediments that consist for a large part of swelling clays, many operators use KCL/Polymer additives to the drilling mud. This creates a substantial bias in the gamma ray and spectral gamma ray logs.
- Complex lithology. The Neogene sediments of the Eridanos delta contain many minerals that are either heavy, or radioactive, or both. A standard suite of logs (including spectral gamma ray and Pef) cannot resolve all these minerals. In addition, a substantial amount of charcoal particles complicates the interpretation even further.
- Clay-Bound Water. The sediments are in general fine-grained and muddy, and they are unconsolidated. This means that they contain a considerable amount of clay-bound water. This in turn creates challenges for porosity and water saturation evaluation. Core porosities cannot be directly compared to effective porosities, and water saturation calculation based on total porosity concepts need either robust lab measurements for Cation Exchange Capacity, or a volumetric log analysis of the constituting clay minerals, or both.

Despite these complicating factors, a petrophysical evaluation of the Neogene sediments was done on the four A15 wells.
The differences in logging environments and logging suites between the wells are a fact of life. Within the A15 block, it took some time and effort to get used to these different environments. However, it is envisaged that the learning curve will level off as more wells will be processed in follow-up projects.
The deteriorating effects of washed out sections that are present in some wells can be combated, but to the expense of considerable effort and time as was proven by the sonic repair of A15-03 and the density repair of A15-04. Unless it is really necessary, it is advised not to repair the logs that are affected by washouts. Instead leaving the affected logs as they are and setting a Bad Hole Flag for these intervals is probably more appropriate.

With well A15-03 acting as the key well, a multi-mineral model was set up that calculates total and effective porosity, shale volume, and water saturation. Logs involved included gamma ray, Potassium, Thorium, neutron, density, Pef, as well as RT and RXO. Matrix minerals include quartz, K-feldspar, and muscovite, whereas illite and smectite were included as clay minerals. The model produced a low residual error in the sands, but had difficulties in the more shaly intervals, especially in the lower half of the evaluated interval. Residual errors were high which means that the porosities and saturations in these shaly intervals are less reliable. The mineralogy in the ‘cold shales’ could not satisfactorily be resolved which implies that the calculated porosity in these shales is probably not correct.
If we look at the gas saturation calculated by the combined multi-mineral / Dual Water model (Figure 3-20), it is apparent that it calculates a non-neglectable amount of gas in the shalier sections, e.g. in the interval between A60 and A70 (620-625 m). The porosities in these sections are reasonable, so obviously something is not completely right with the parameters in the Dual Water model. This effect is even more apparent in the lower part of the Neogene (Figure 3-21). The much simpler model, the

neutron-density based shaly sand model performs much better in this respect (Figure 3-26, Figure 3-27). This evaluation is also much better in line with the ELAN evaluation done by Schlumberger, which was for a large part based on the NMR measurements. It is therefore recommended to adopt the simple approach consisting of a neutron-density based shaly sand model with a Simandoux saturation model.

3.8.2 *Thin beds*

From Figure 3-23 it can be seen that the reservoir sands are actually thin bedded. For example, the interval 680-690 mAH shows a regular alternation of higher and lower porosity beds, in total 16 beds. This means that the average bed thickness in this interval is about 60 cm, just thick enough to be picked up by the neutron and density logs. The gamma-ray log has a too low resolution to effectively distinguish between beds that are so thin, so any V_{shale} calculation that is based on a GR transform will overestimate V_{shale} in the cleaner beds and underestimate V_{shale} in the muddier beds. This in turn will cause Phie to be underestimated in the cleaner beds, which eventually will result in an underestimation of the gas in place.
It is therefore recommended to derive the V_{shale} from the neutron-density logs, and not from the gamma ray log. If only the GR is available, its resolution might be increased by a method proposed by Geel (2002). The best solution of course would be to utilize borehole image logs, such as FMI. But these are not routinely recorded and are therefore hardly available for the Tertiary.

3.8.3 *Movable water*

The gas-bearing sands A60 and A70 (Q_S9 and N_S8 respectively; Figure 3-20) have a relatively low gas saturation, although this is dependent on which thin bed we are looking at. In A70 for example, the best beds have a saturation of some 80%, while the lower porosity beds have saturations of 50%. It may be questioned whether this gas can be produced water-free.
One way to tackle this problem is to study capillary pressure (Pc) curves. Since well A15-03 is drilled near the crest of the stack of bright spots, these Pc curves can test whether e.g. the A70 sand is at irreducible water saturation. Unfortunately, no Pc curves were available.
Another approach is to study the well tests that have been performed on several reservoir intervals. Although well test interpretation was beyond the scope of the present study, the tabulated raw data of the various DST's carried out in A15-03 gives some information. For example, the sands from the lower part of the Neogene (D10, D20, and D30) did not flow at all, which is a nice confirmation of the high water saturations calculated by the shaly sand model. Another interval (A70) flowed water-free gas at a maximum rate of 300,000 Nm³/d. This is a strong indication that the A70 sand (at least the part that has been perforated) is indeed at irreducible water saturation. Yet two other sands, A60 and A65, produced comingled gas at a maximum rate of 210,000 Nm³/d. During this test water was produced, although it is not clear which of the two sands produced it.
To conclude, sands with a high gas saturation are probably at irreducible conditions and are therefore likely to produce water-free gas. On the other hand, low gas-saturated sands produce also water, and are therefore not at irreducible saturations. This means that their top seals are probably leaking, and the gas in these sands is residual gas.

3.8.4 *Reservoir characteristics*

From our petrophysical analysis it follows that the Neogene sediments are quite distinct from other reservoir rocks in The Netherlands (e.g. Rijswijk Sst, Volpriehausen Sst, Slochteren Sst). The following characteristics apply:

- unconsolidated;
- mostly shaly sands;
- high clay-bound water content;
- complex mineralogy;
- high effective porosities (25-30%);

- generally low gas saturations (<80%);
- thin-bedded.

Summary
A petrophysical evaluation of the Tertiary sediments was done on the four wells drilled to date in the A15 block in the northern Dutch offshore. With well A15-03 acting as the key well, a multi-mineral model was set up that calculates total and effective porosity, shale volume, and water saturation. Logs involved included gamma ray, Potassium, Thorium, neutron, density, Pef, as well as RT and RXO. Matrix minerals include quartz, K-feldspar, and muscovite, whereas illite and smectite were included as clay minerals. The model produced a low residual error in the sands, but had difficulties in the more shaly intervals, especially in the lower half of the evaluated interval. Residual errors were high which means that the porosities and saturations in these intervals are less reliable.
In order to calculate permeability, a relationship was derived from NMR permeability and effective porosity. This relationship agreed very well with core plug measurements.
In wells A15-01 and A15-04 only a minimal log suite was available, so the multi-mineral model could not be used on these wells. A simple shaly sand model was therefore run on A15-03 with fewer logs. Parameters were tweaked so as to reproduce the results of the multi-mineral model.
This shaly sand model was run on wells A15-01, A15-02, and A15-04.

Effective porosities in the sandy intervals range from 15% to 35%, total porosities are in the range 30-45%.

Wells A15-01 and A15-04 were dry, but wells A15-02 and A15-03 were gas-bearing. Gas saturations are in general low. Most of the bright spots identified on seismic contain less than 30% gas. Only a few thin reservoirs contain gas saturations higher than 50%.

4 Biostratigraphy and facies (C2)

4.1 Essence of the geobiological input

The geobiological data provide an age model and a depositional model for the Eridanos succession in the A15 Block and beyond. Due to the core availability in A15, the well data are an important regional standard for future follow ups of this pilot project.

The age model is important to constrain the sequence stratigraphic interpretation, derived from the seismic intepretation, in terms of absolute time. Outside A15, the age model can also be used in future studies to correlate wells and calibrate the seismic interpretations, especially in regions with limited 3D seismic data coverage.

The depositional model is important because it contributes to the understanding of the petroleum system in the A15 Block. The gas occurrences in the A15 Block are constrained to specific stratigraphic intervals with recurring combinations of physical properties. The physical properties of the sediments are determined to a high degree by paleoenvironmental parameters such as climate, productivity and sea level. The depositional model provides the link between the physical properties and the palaeonvironmental parameters.

In a follow up of this project, the depositional model will be put to the test when data from other sites become available. Ultimately, the depositional model will be the essence of a prospectivity workflow that will have predictive value for shallow gas occurrences in the entire northern offshore area.

4.2 Database

At TNO there is a large amount of biostratigraphic data available from the Cenozoic North Sea Group in the A&B Blocks (see Appendix E). The biostratigraphic data from the A15 Block is limited to two wells only: A15-3 and A15-4. The data basically originates from 4 sources, but the data from these sources are complexly intertwined:

1) commercial biostratigraphic work for the Dutch operator Wintershall.
This work incorporates both Micropalaeontology (foraminfera) and Palynology (mainly dinoflagellate cysts, hereafter dinocysts). Most of these have been incorporated in Kuhlmann (2004, PhD thesis). There is one important report concerning well A15-3 by J&G and LPP from 1999:

Biostratigraphy of Wintershall's (now publicly available) A15-3 well. Interval 400m – 1400m. Report JG00094 and LPP report 9918.

2) PhD study by Gesa Kuhlmann
This work mainly compiles and combines both commercial biostratigraphic work (LPP and TNO-NITG) and that from the Geological Survey of the Netherlands. Well A15-3 plays a key-role, while well A15-4 was not yet available at that time. Data from other wells is derived from: A18-2, B16-1, B17-5, B10-3, B13-3, B13-4, B17-6. Marine Palynology (dinocysts), Terrestrial Palynology (pollen and spores) and Micropalaeontology (foraminifera) are incorporated. The title of the thesis:

High resolution stratigraphy and paleoenvironmental changes in the southern North Sea during the Neogene. An integrated study of Late Cenozoic marine deposits from the northern part of the Dutch offshore area. Geologica Ultrajectina, no 245, University of Utrecht,

3) biostratigraphic data from the Geological Survey of the Netherlands
(RGD, TNO-NITG and TNO Geo-Energy & Geo-Information)
A large amount of data from many wells is available and partially incorporated in Kuhlmann (2004). Noteworthy are the high-resolution pollen data from Zagwijn on cored Gelasian intervals from wells A12-3, B10-3, B16-1, A18-2, B13-3 and B17-5. Most data are from 1989-1995. Reports are archived and available on request. One report is very recent and deals with pollen analysis on the cored intervals of well A15-3 and A15-4. These data have been incorporated in the data set and report of UU-student Niels van Helmond.

TNO report-034-UT-2009-01727. Donders, T.H. Koolmees, H.H. Bunnik, F.P.M., 2009. High resolution pollen analysis of cores A15-03 and A15-04 (southern North Sea) across MIS 94-102.

4) MSc Internship by Niels van Helmond (Utrecht University)
A high resolution organic, geochemical and geobiological study on cored sections from the base of the Gelasian of well A15-3 and A15-4. Niels van Helmond carried out palynological analyses and a suite of organic-geochemical analyses, such as the distribution of membrane lipids produced by microorganisms. Most of these analyses are used as paleotemperature proxies. Together with Timme Donders (TNO), existing geobiological data together with new geochemical data were compiled and integrated into one dataset. The cored sections are from the Early Gelasian, the interval with the characteristic bell-shaped cycles and bright spots (interval 890m – 1050m of well A15-3).

TNO report-034-UT-2010-01544/B. Van Helmond, Donders, Verreussel, Bunnik, Munsterman, Weijers, Reichart, Sinninghe Damsté. Palynological and organic geochemical characterization of marine and terrestrial Early Pleistocene climate in northwest Europe. 78 p.

Note: To complete the dataset, TNO carried out additional palynological analyses within this project to raise the dinocyst analyses to the same, high resolution as the pollen and spore data. These data have been integrated in Van Helmonds data set and are presented in this report (Fig. 4-6).

4.3 Methods

4.3.1 *Sampling and splicing of wells*

The borehole samples from A15-3 were used by Kuhlmann et al. (2006) to construct a solid integrated chronostratigraphy for the Upper Neogene deposits. This chronostratigraphy is based on paleomagnetic data and dinoflagellate- and foraminiferal proxies. Hence, A15-03 is used as the reference well for the current shallow gas study and updated here to the latest stratigraphical insights (De Schepper et al., 2009a; 2009b).

All sediment samples used for this study originate from exploration wells A15-3 and A15-4 and are listed in Appendix E. For palynology, remaining material sampled by Kuhlmann was analyzed. For the geochemistry additional samples were taken from the cores. Most of the studied samples are core samples, a minor part are sidewall cores. The two boreholes were spliced on basis of the similar pattern of the gamma-ray log and equivalent biostratigraphic events, using the integrated chronostratigraphy by Kuhlmann (2004), to generate a composite record over depth. Sample depths were corrected according previous studies. Corrected sample depths are listed in Appendix E. A15-3 is used as the reference well, the spliced depths refer to that section. For MIS 94/95, the sample spacing of the composite section is ~1.5 m on average, which equals approximately 2000 yrs with a sedimentation rate of 84 cm/kyr for this interval.

4.3.2 *Palynology*

For palynological analyses, 177 samples were studied (earlier work and this study), of which 120 samples are taken from core A15-3. The samples of A15-3 range between 400 and 1400 metres depth below sea level (mbsl). The majority of the samples, about 70, focus on the Early Pleistocene (~2.5-2.4 Ma) interval between 890.05 and 964.14 mbsl, The 56 studied samples from core A15-4, range between 901.72 and 1057.62 metres spliced depth, (918.4 and 1089.9 mbsl). This interval covers the Pliocene/Pleistocene transition (~2.588 Ma) and the Early Pleistocene. On the interval between 997.26 and 1037.69 metres spliced depth, (1014.3 and 1064 mbsl) no samples were collected/studied, as a result of poor core recovery.

The samples were processed using standard marine palynological procedures (e.g. Wood et al., 1996) involving HCl-HF-HCl digestion, heavy liquid separation, and sieving over 18 µm mesh. For pollen, it is at present generally accepted that morphological characteristics of late Pliocene to early Pleistocene pollen types can directly be related to extant genera and families (see Donders et al., 2009). This correlation potential is a sound basis for floristic analysis of the assemblages and the recognition of similarities with modern vegetation types. Dinocysts and pollen/spores were examined independently by light microscopy, using a binocular microscope, and counted up to ~100 identified cysts and ~300 pollen/spores. Dinocyst taxonomy is according Fensome and Williams (2004).

The occurrence of thermophilous trees and *Picea, Tsuga* and *Osmunda* indicate relatively warmer (wetter) climatic conditions on land. In contrast, occurrences of *Ericales*, *Sphagnum* and herbs in general, suggest relatively cooler and dryer conditions on land. *Pinus* abundance is also strongly related to the relative distance to the coast, and hence may show a correlation with by sea-level changes. The AP/NAP ratio (tree pollen over non-tree pollen), shown in Figure 4-6, represents these changes and is indicative of temperature.

4.3.3 *Organic geochemistry*

For the organic geochemical analyses, 78 unique samples were studied. Most of these samples (41) originate from core A15-4. The studied samples range between 907.8 and 1057.62 metres

spliced depth (925.45 and 1089.9 mbsl). About half of these samples (below 972 metres spliced depth) were obtained from sidewall cores. All 37 samples from A15-3 were obtained from cores. The studied samples range between 890.8 and 964.02 metres of depth below seafloor.

Total organic carbon

Total Organic Carbon (TOC) content of sediment provides information on the amount of organic carbon relative to the mineral fraction. For the determination of the TOC content, about 0.3 g of freeze dried and powdered sediment per sample was weighed and stored in Greiner centrifuge tubes of 15 ml. To remove carbonates, 7,5 ml 1 M HCL was added. After bubbling of gas ceases, the tubes were closed and placed on a shaker for 4 hours. After that, the acid was removed upon centrifugation. This step was repeated for 12 hours on the shaker. Finally, the samples were washed twice with demineralised water and stored in an oven at 40-50°C for 96 hours. To determine the weight loss by the removal of carbonates the dried samples were weighed again. The samples were grinded and ~15 to 20 mg per sample was weighed in tin foil cups. Measurements were performed using a Fisons NA1500 NCS elemental analyzer with a normal Dumas combustion setup. Three external standards, BCR, atropine and acetanilide, were analyzed before and after the series, and after each ten measurements. Measurements were normalized to these standards.

%TOC per gram of sediment was calculated using the following formula:

%TOC = C% * W2/W1

C% = result of NCS analyzer
W1 = weight of sample before decalcification
W2 = weight of sample after decalcification

Biomarkers

Many microorganisms leave behind traces in the sedimentary record in the form of fossilized chemical components. If these components are specific to a certain organism or a group of organisms, these molecules are referred to as biomarkers. In addition to being specific for an organism, these molecular fossils might also provide information on the paleoenvironment and paleoclimate where the organism lived in. Saturated hydrocarbons, termed n-alkanes, are important constituents in different groups of organisms. Marine organisms typically contain short chain (C16-C24) n-alkanes, whereas the leaf waxes of land plants dominantly contain long chain (C25-C35) n-alkanes. Here, specific biomarkers for *Sphagnum* (peat moss) are shown to corroborate the pollen data (Figure 4-6 Detailed palynological and geochemical data summary of the clay-silt couplets in well A15-3 representing the interval with the first glaciations of the Pleistocene. The climatic signature of these cycles provides ground for regional correlation across the basin and explains the origin of the sedimentary cycles and organic matter variations). Detailed results and methods are given in Van Helmond *et al.* (2010).

4.4 Results

4.4.1 *Age Model A15-3*

>> Data source 1 and 2 <<

In well A15-3 a geomagnetic tool has been run along the hole. The resulting magnetic polarity intervals were tied to the global standard and calibrated to Chrons by using a couple of well calibrated biostrat events (Fig. Figure 2-1). Thus, it was possible to pinpoint 1) the Gauss-Matuyama boundary, which is calibrated to the absolute age of 2.56 Ma and to Marine Isotope Stage 103, 2) the X-event, calibrated to 2.44 Ma, 3) the base of the Olduvai, calibrated to 1.94 Ma.
Absolute ages for well A15-3 are listed in Table 4-1.

Table 4-1 Absolute age versus depth and seismic reflector in well A15-3

TNO 2011	MD	Z	Kuhl-mann & Wong, 2008	Log unit Kuhl-mann 2006	unit Age	unit TOP Age (Ma)	unit Base Age (Ma)	PWD
X_S13	431.42	390.84	**S13**	18	Gela-	1.8		
W_S12	470.91	429.46	**S12**	17	sian		1.9	050
V	482.00	440.31						
U_S11	532.60	489.86	**S11**	16				
T	539.00	496.13						
S_S10	583.26	539.50	**S10**	15				
R	597.00	552.96						
Q_S9	633.88	589.10						
P	643.00	598.03	**S9**	14				
O	660.00	614.69						
N_S8	689.84	643.90	**S8**	13				50100
M_S7	712.00	665.59	**S7**	12				
L	769.00	721.35		11				
K_S6	802.00	753.63	**S6**					
J	845.00	795.69		10		2.16	2.44	150
I_S5	918.00	867.04		9		2.44		
H	967.00	914.90		8				
G	1003.00	950.08	**S5**	7				
F	1028.00	974.51		6				
E	1070.00	1015.55					2.58	200
D_S4	1100.00	1044.89	**S4**	4 + 5	Piacen-	2.58		
C_S3	1142.00	1085.97	**S3**	3	zian		3.6	200
B_S2	1182.00	1125.11	**S2**	2	Zan-			
A_S1	1205.00	1147.64	**S1**	1	clean		5.2	200
MMU	1247.00	1188.72						

Figure 4-1 Stratigraphic framework and biostratigraphic events for the Gelasian in well A15-3

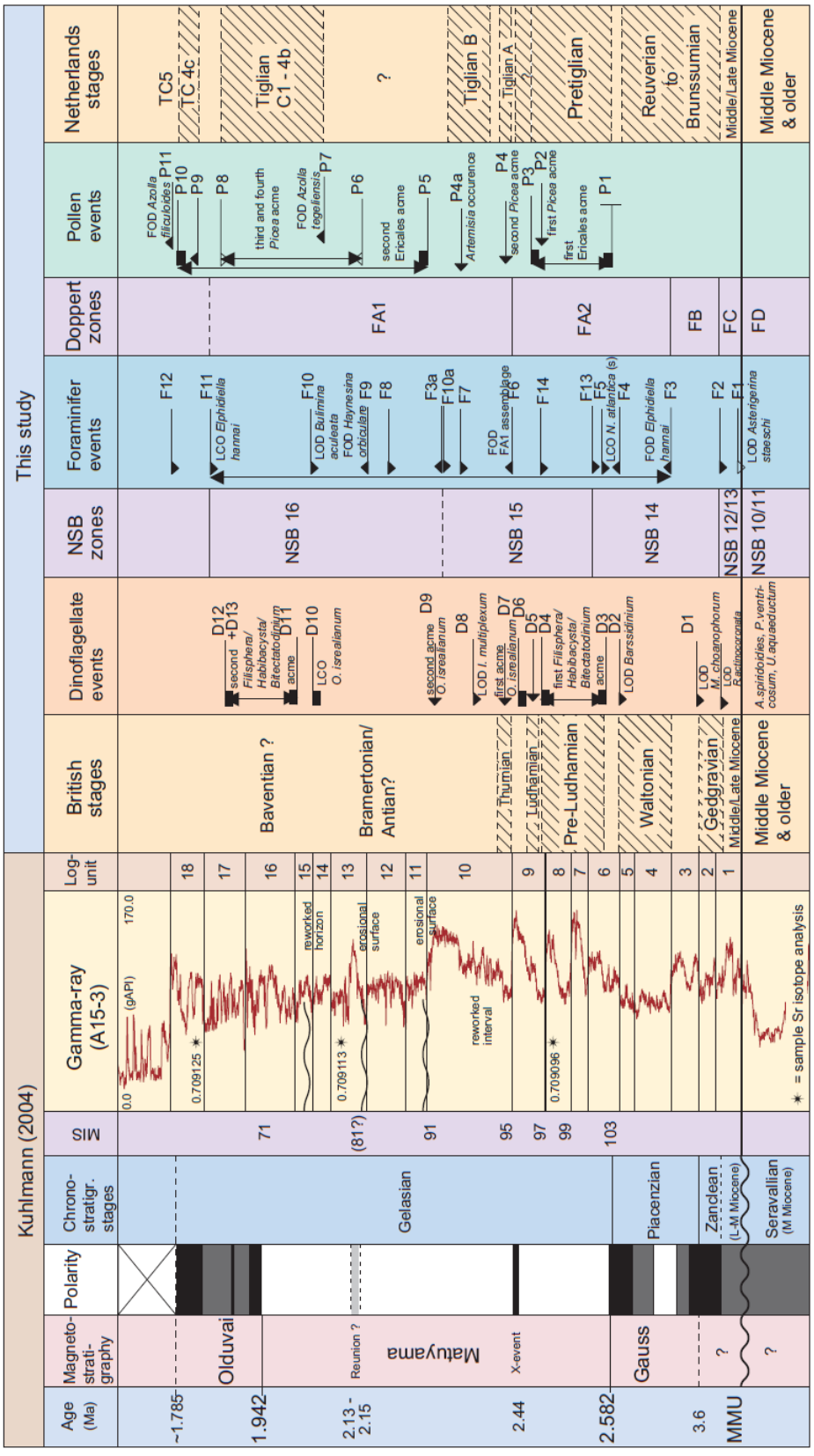

4.4.2 *Depositional model*

>> Data source 1, 2, 3 and 4 <<

Perhaps the most important aspect of the Neogene Eridanos succession in the A15 Block, is the strong coupling of sediment deposition and climate. The Eridanos delta sediments were laid down at the time the first ice caps appeared on the Scandinavian shield. This so-called *onset of northern Hemisphere glaciations* resulted in a series of glacial-interglacial cycles that had a profound impact on the Eridanos behaviour and on the resulting basin-fill. These first glacial-interglacial cycles, unlike the present ones, were paced by the 40 kyr obliquity cycles. Figure 4-2 clearly shows the strong coupling or even forcing of sediment deposition and climate. The marine dinocyst record displays a warm-cool-cold cyclicity that is corroborated by the terrestrial pollen record (shown in Figure 4-6). The warmest intervals or interglacials are coupled to the most coarse-grained sediments, and the coldest intervals or glacials are linked to the most fine-grained sediments. The sea level trend is in line with the expected trend associated with ice sheet build-up: high sea levels during the interglacials and low sea levels during the glacials. The relevance of these climatic cycles is the fact they occur basin-wide and control the deposition of clay - silt couplets with good sealing capacity (clays) and reservoir bodies with a likely biogenic source (enhanced TOC in the silts, see Figure 4-6).

4.4.3 *Long-term sea-level trend*

The long-term sea level trend is shallowing (Figure 4-3). The on-going shallowing trend is controlled by infill of accomodation space through the advancing delta. In the lower part, the Eridanos succession in well A15-3 contains open marine dinoflagellate cyst and benthic foraminifera assemblages. These roughly correlate with the toe sets of the delta. The part with the characteristic bell-shaped GR-cycles, is transitional, with strongly fluctuating sea levels. In the middle part, the Eridanos succession is restricted marine, with high-dominance and low-diversity dinoflagellate cyst assemblages. A short-lived return to an open marine setting is achieved in the upper part, with abundant dinoflagellate cysts. The uppermost part of the Eridanos succession is basically non-marine. The general sea level trend inferred from geobiological data is listed against the log units in Table 5-2.

Table 4-2 Paleoenvironment with respect to sea level. Interpretation is based on geobiological data.

Log unit TNO 2011	**Top A15-3**	**Base A15-3**	**Paleoenvironment**
W-X	400	500	Non-marine, deltaic or paralic
T-V	500	600	Open marine
L-S	600	800	Restricted marine
E-K	800	1230	Transitional: open – restricted marine
A-D	1230	1050	Open marine

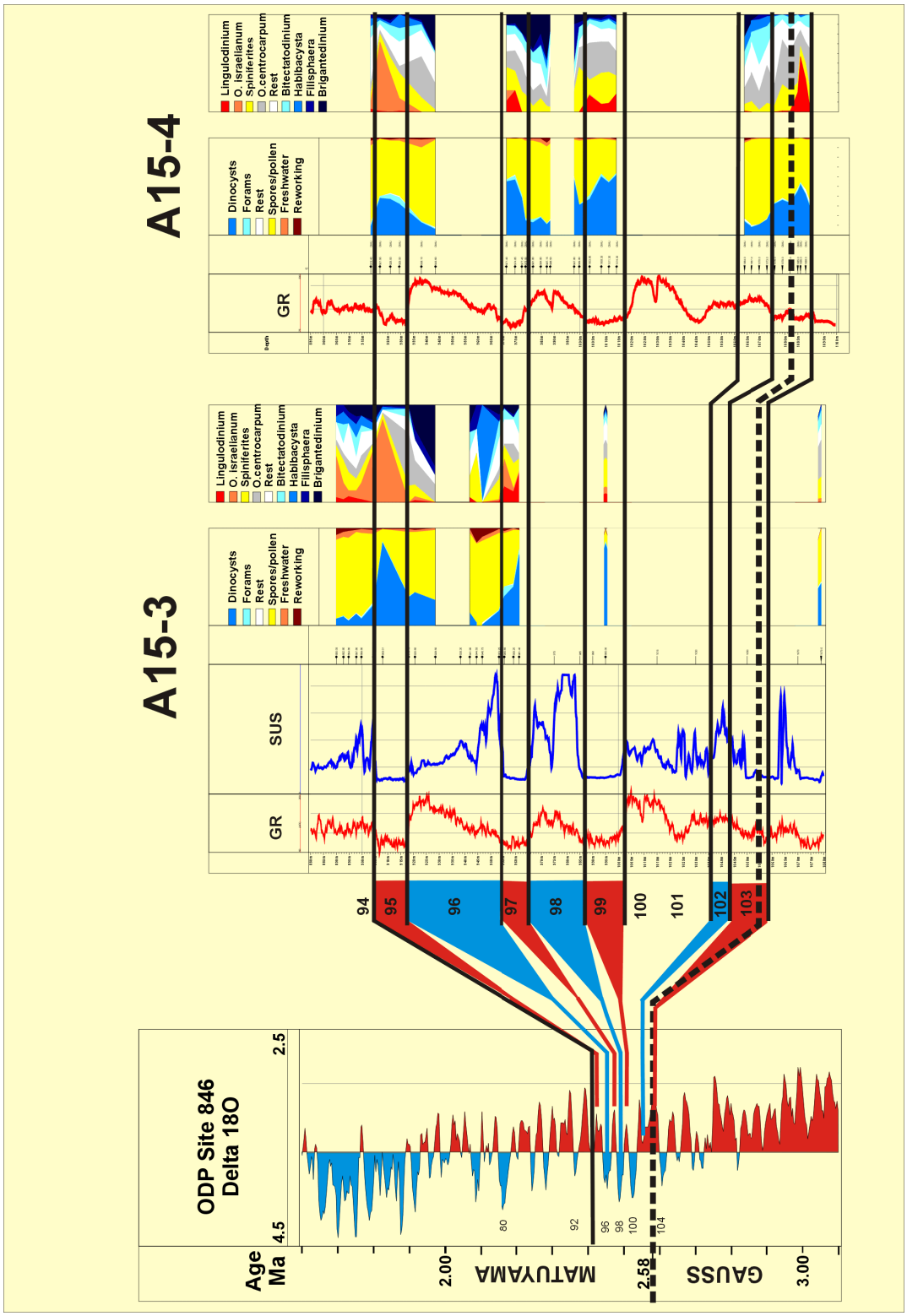

Figure 4-2 Glacial-interglacial cycles derived from the dinocyst record and calibrated to Marine Isotope Stages

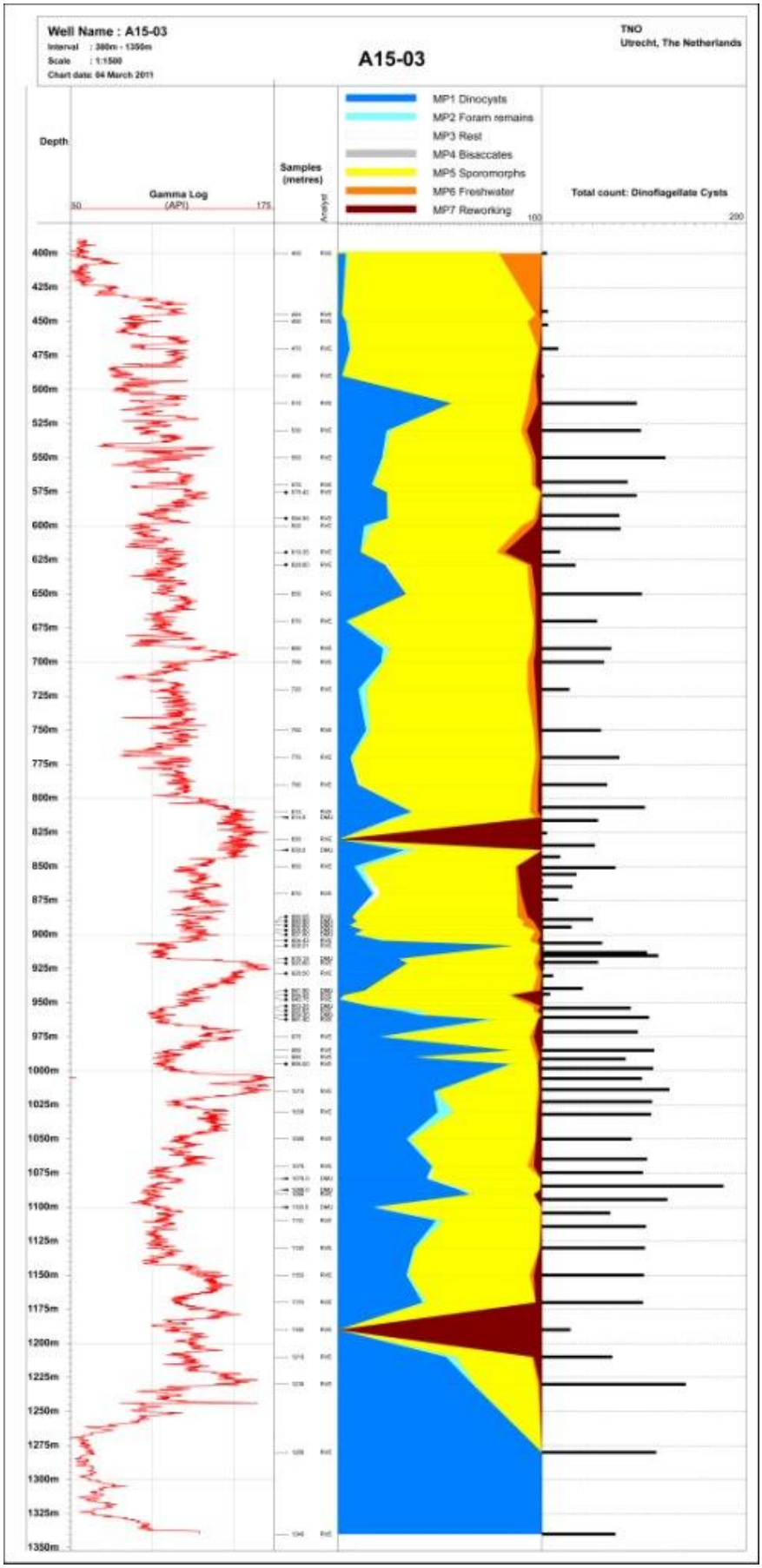

Figure 4-3 Marine (blue) versus Terrestrial (yellow and brown) palynomorphs, showing an overall shallowing trend

4.4.4 *Sea level, Sea Surface Temperature and climate*

Sea level is strongly controlled by the climate: the glacial force low sea levels, the interglacials force sea level to return to “normal” levels. One intriguing interval remains unexplained: the upper part of the Gelasian in well A15-3, Log unit T-V. The palynological assemblages indicate **open marine conditions in combination with cold Sea Surface Temperatures** (Fig. 4-4)**.** A possible explanation may be a significant “melting event” that has been recorded in the literature. This melting event appeared to be related to a temporary change in oceanic circulation: for a short duration of time warm Atlantic waters flowed west of Iceland into the arctic (Baumann and Huber, 1999). This warm water current caused melting of the existing sea ice cap and possibly pushed the cold arctic surface waters into the proto-North Sea.

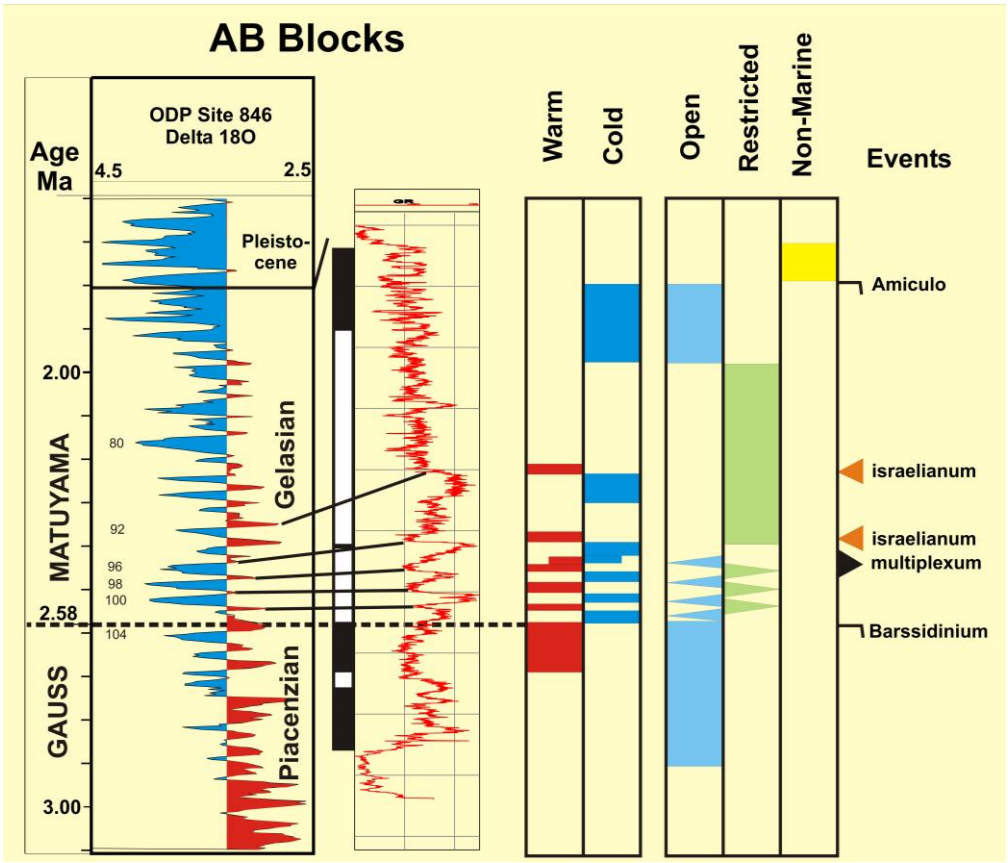

Figure 4-4 Summary of paleoenvironmental trends in well A15-3, showing the relationship between sea level, climate and Sea Surface Temperature

4.4.5 *Long term climate trend*

>> Data source 1 <<

A long term cooling trend is observed from MMU to the top of the Eridanos succession. The cooling trend can be derived from the increase in the abundance of “cool preference” dinoflagellate cysts, concomitant with a decrease in abundance of “warm preference” dinoflagellate cysts (Fig. 4-5). This trend is punctuated by a couple of distinct cold and warm peaks. These peaks are important from a

hydrocarbon perspective, because the rapid glacial-interglacial alternations lead to the strong porosity contrasts in the silt-clay couplets. In addition, the glacial-interglacial cycles may be related to biogenic gas generation and are possible closed petroleum systems (source-reservoir-seal). In the Eridanos successions the most distinct glacial-interglacial couplets are the G, H and I log units, which are correlated to the Early Gelasian Marine Isotope Stages 100 to 98 (Table 5-3, Fig. 4.2). Data density is extremely high in these glacial-interglacial couplets. In the rest of the Eridanos succession, the data density is much lower and the evidence for glacial-interglacial cycles is less obvious. Probably, log unit C and D also represent a glacial-interglacial cycle.

Table 4-3 Glacial-interglacial cycles and their relationship to SST and marine isotope stages (MIS)

Log unit TNO 2011	**SST**	**MIS**
T-V	Cold	?73-71
L	Warm	91
K	Cold	92
J lower	Warm	95
I upper	Cold	96
I lower	Warm	97
H upper	Cold	98
H lower	Warm	99
G upper	Cold	100
G lower	Warm	101
D lower	Warm	?
C	Cold	?M2

4.4.6 *High resolution trends in the clay-silt couplets from Log Units E-J*

>> Data source 4 <<

The data in Fig. 4-6 show **high TOC contents in the silts** (low gamma ray), coupled to **high SST** (based on dinoflagellate cysts), and **relatively warm climate** (increased forest cover based on pollen analyses). Shaded bars show colder intervals where open landscapes increase regionally, SST decreases and the relative distance to the coast decreases (high sporomorph/dinocyst; SD ratio). These climatically controlled clayey intervals represent cold conditions and occur basin wide and act as regional seals.

Note that pollen preservation is reasonably good, but shows the effects of relatively long-distance transport since the assemblages are dominated by comparatively and few exclusively wind-pollinated taxa that disperse well. Hence, the results are not directly representative for the vegetation cover on-land, but changes should be interpreted as the relative dominance of certain environments and vegetation types. Typical Pliocene elements in the succession are *Taxodium, Sciadopitys, Carya, Pterocarya* and *Osmunda.*

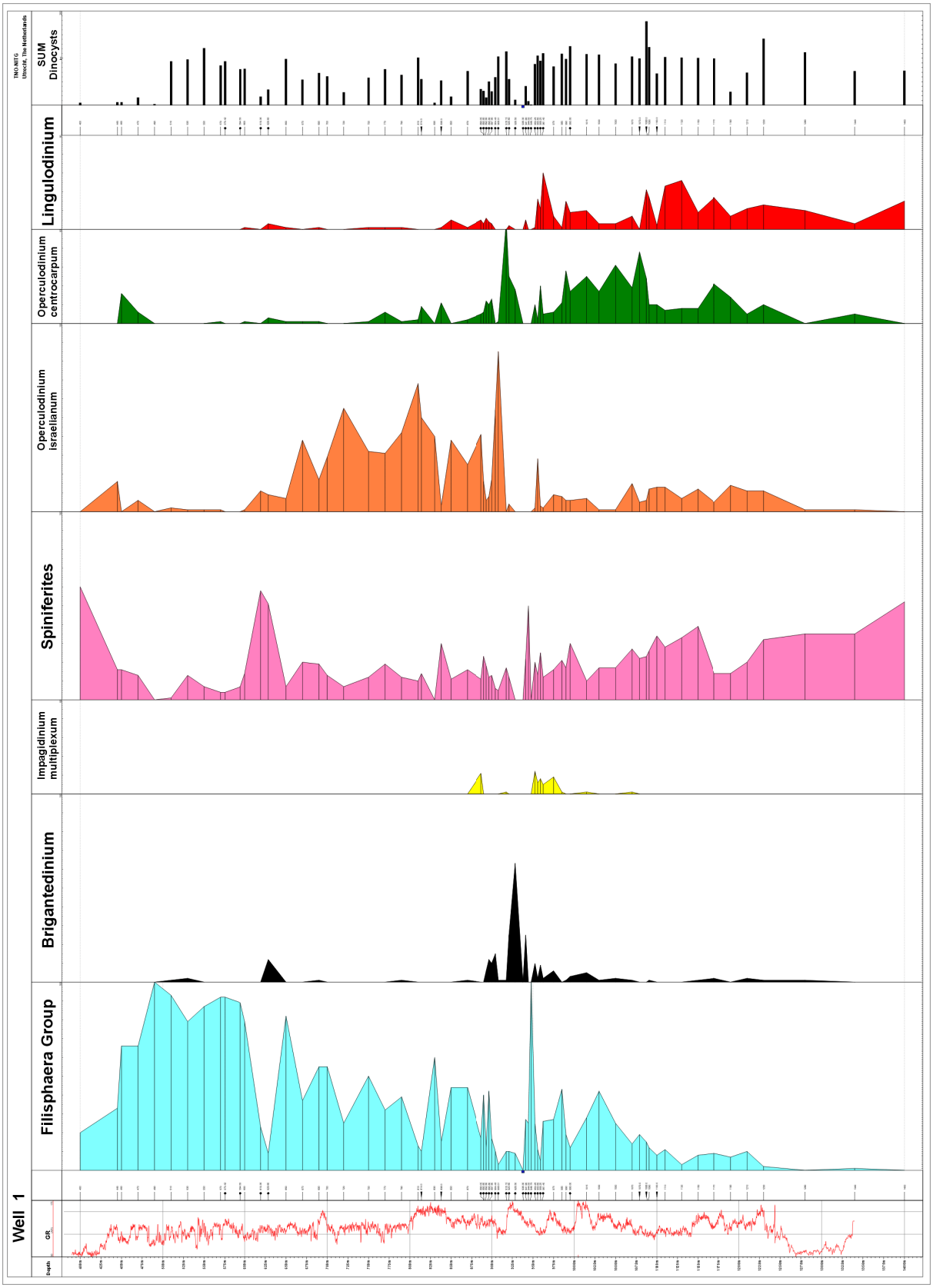

Figure 4-5 Main trends in dinocysts taxa along well A15-03 showing the overall cooling trend (blue curve; *Filisphaera* Group). Restricted marine conditions are indicated by the dominance of *Operculodinium israelianum*. A short-lived return to open marine conditions os observed in interval 500m – 600m (high SUM in dinocysts)

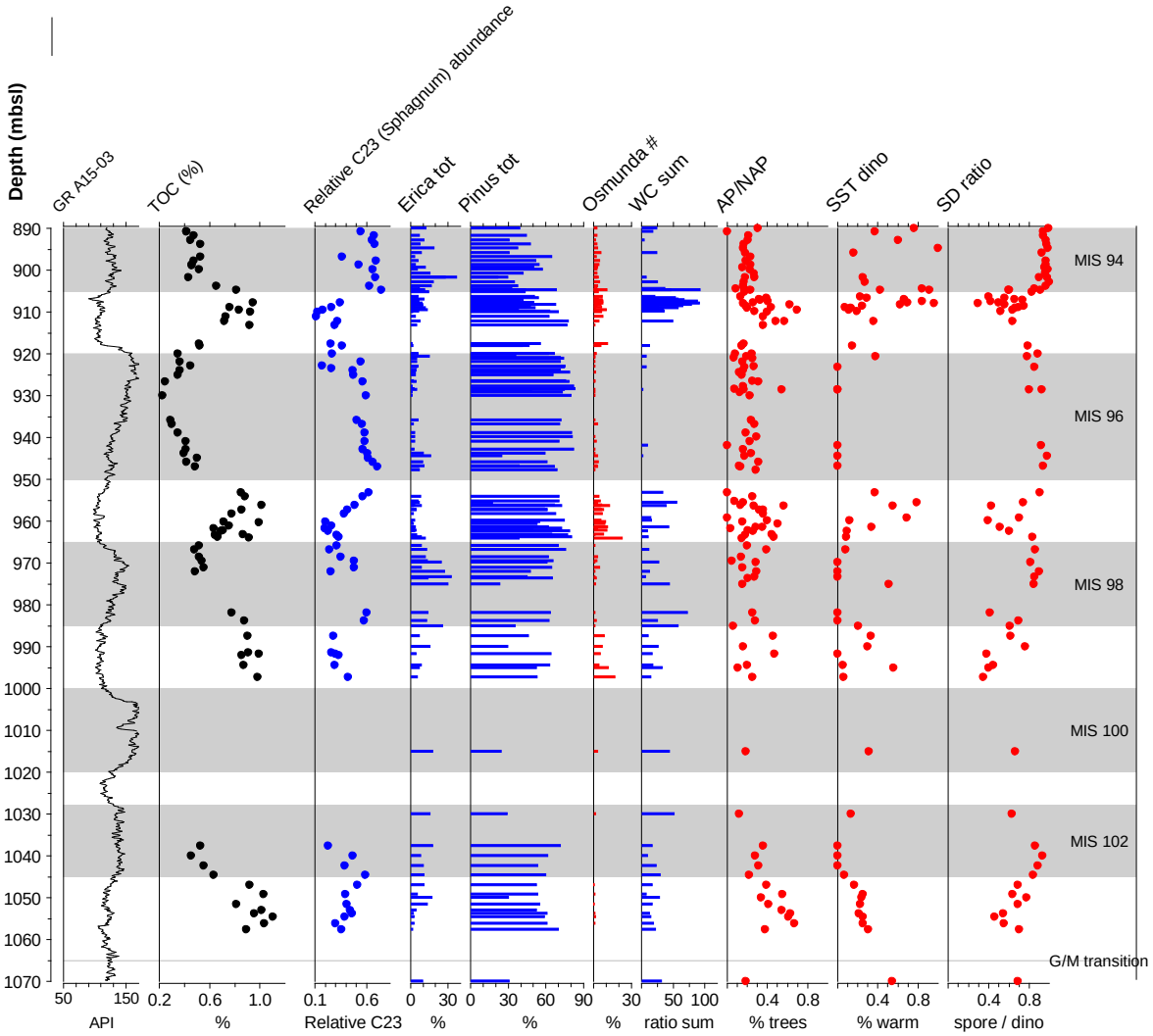

Figure 4-6 Detailed palynological and geochemical data summary of the clay-silt couplets in well A15-3 representing the interval with the first glaciations of the Pleistocene. The climatic signature of these cycles provides ground for regional correlation across the basin and explains the origin of the sedimentary cycles and organic matter variations

TOC = total organic carbon
C23 = sphagnum (peat moss)-derived alkane concentration indicative of cool periods
***Erica* tot** = total ericaceae (heath vegetation) pollen, indicative of cool phases
***Pinus* tot** = total *Pinus* (pine pollen) indicative of distance to shore
***Osmunda* #** = *Osmunda* (fern) spores indicative of warm periods
WC sum = sum (total counts) on which the warm / cold SST_{dino} ratio is based, very low values preclude confident interpretation
AP/NAP = ratio of arboreal (tree) to non-arboreal pollen indicative of temperature changes on land (excl *Pinus*, aquatic / *Osmunda* / Ericaceae pollen).
SST_{dino} = relative sea surface temperature changes based on indicative dinoflagellate cysts (see Fig. 4-5)
SD ratio = sporomorph to dinocyst ratio showing relative contribution of terrestrial vs. marine organic matter input and distance to the coast.
Grey shaded areas indicate position of marine isotope stages (MIS) glacial intervals based on stratigraphic correlation.

5 Conceptual model (C1d)

5.1 Synthesis from C2

Based on the Biostratigraphic- and paleoenvironmental analyses (C2), the following conclusions are drawn:

- In the A15 Block an excellent chronostratigraphic framework is available for the Eridanos succession. The precise coupling to absolute age is derived from geomagnetic polarity data of well A15-3. The polarity intervals are coupled to the global standard by a number of well calibrated biostratigraphic events.
- A strong coupling exists between climate and sediment properties.
- Glacial-interglacial cycles show a marked contrast in grainsize, sea surface temperature and climate.
- Interglacials are characterized by:
    - Relatively warm climate and relatively high Sea Surface Temperatures
    - High freshwater input at the base of the interglacials
    - Relatively open marine conditions
    - Relatively coarse grainsize (moderate to good reservoir properties)
    - Relatively high sea level
    - Relatively high TOC content (possible source for biogenic gas)
- Glacials are characterized by:
    - Relatively cold climate and relatively low Sea Surface Temperatures
    - Almost no freshwater input
    - Relatively restricted marine conditions (water stratification)
    - Very fine grainsizes (excellent seal properties)
    - Relatively low sea levels
    - Relatively low TOC content

5.2 Sequence stratigraphic concept applied

Based on the chronostratigraphic framework, the paleoclimate model and the sedimentary facies analysis, together with the architectural elements of the delta obtained from seismic interpretation (see section 2), a sequence-stratigraphic subdivision was made. This interpretation was performed jointly with dGB and served as the main input for the construction of the (multi) Horizon Cube (see section 7).

The use of well log data as aid in sequence-stratigraphic interpretation needs one important consideration. Classically, GR peaks are seen as potential Maximum Flooding Surfaces (MFS), since it is generally assumed that the highest clay content is deposited during flooding of a basin (Figure 5-1). This, potentially, results in condensed clayey sections. This assumption is importantly biased by the idea that during sea-level highstand (warm climatic conditions), the largest part of the shelf is submerged and no source for clastic sediment supply exists. However, as was demonstrated in this study, the warmest intervals, or interglacials, are coupled to the coarser-grained sediments, and the coldest intervals or glacials are linked to the finer-grained sediments. During glacial conditions, supply of coars(er) grained sediment is reduced, since permafrost conditions and the glacial cover impede the transport of sediments to the basin. This concept has been used to subdivide the studied interval into depostional sequences that reflect the ratio between

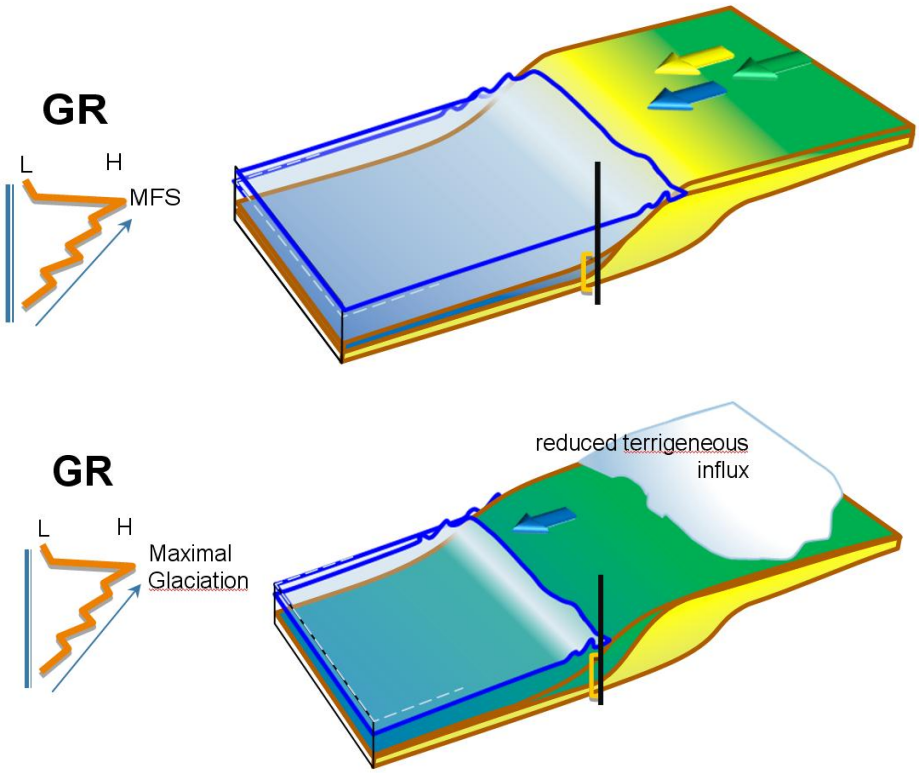

Figure 5-1 Similar GR responses in a) sea-level highstand situation according the classical “Exxon” concept (upper image) and b) sea-level lowstand situation according glacial model presented here (lower image).

accommodation (gain or loss) and sediment supply during a certain segment of the glacioeustatic sealevel curve (Fig. 5-2). The depositional sequences are bounded by key surfaces that represent transitions between curve segments that are marked by different accommodation/supply ratios and, as a consequence, have different internal geometry (see Figs. 5-2A). The bounding surfaces are either unconformities (sequence boundaries) or maximum flooding surfaces (MFS). It is here advocated to use the sequences and their bounding surfaces to constrain property distribution throughout the A15 cube, since it prevents the properties to “cross” the genetic units. Due to the clinoform geometry that is produced during progradational phases (or growth) of the delta development, identical lithologies may be hosted by diachronously deposited units. The clinoforms are usually bounded by finer grained layers representing times of limited clastic deposition and which may act as (partial) baffles for fluid flow. These bounding surfaces are the better correlation surfaces, since they represent more-or-less time equivalent surfaces that can be linked to climatic control. The internal layering (stratification) of the clinoform is produced by lower order progradation of individual sediment packages and represent the highest level of correlation possible (see Fig. 5-3). Results of the sequence-stratigraphic interpretation are shown in Figure 5-4 and Appendix F.

5.3 Horizon Cube and Wheeler transformed seismic data

The basic seismic horizon interpretation (see chapter 2) is well able to trace the major bounding surfaces that delineate the geometry of the individual sequences identified. Tracing all internal stratification in the same manner is time consuming and it was therefore decided to produce a “Horizon Cube” (functionality of OpendTect and performed by dGB, see accompanying report).

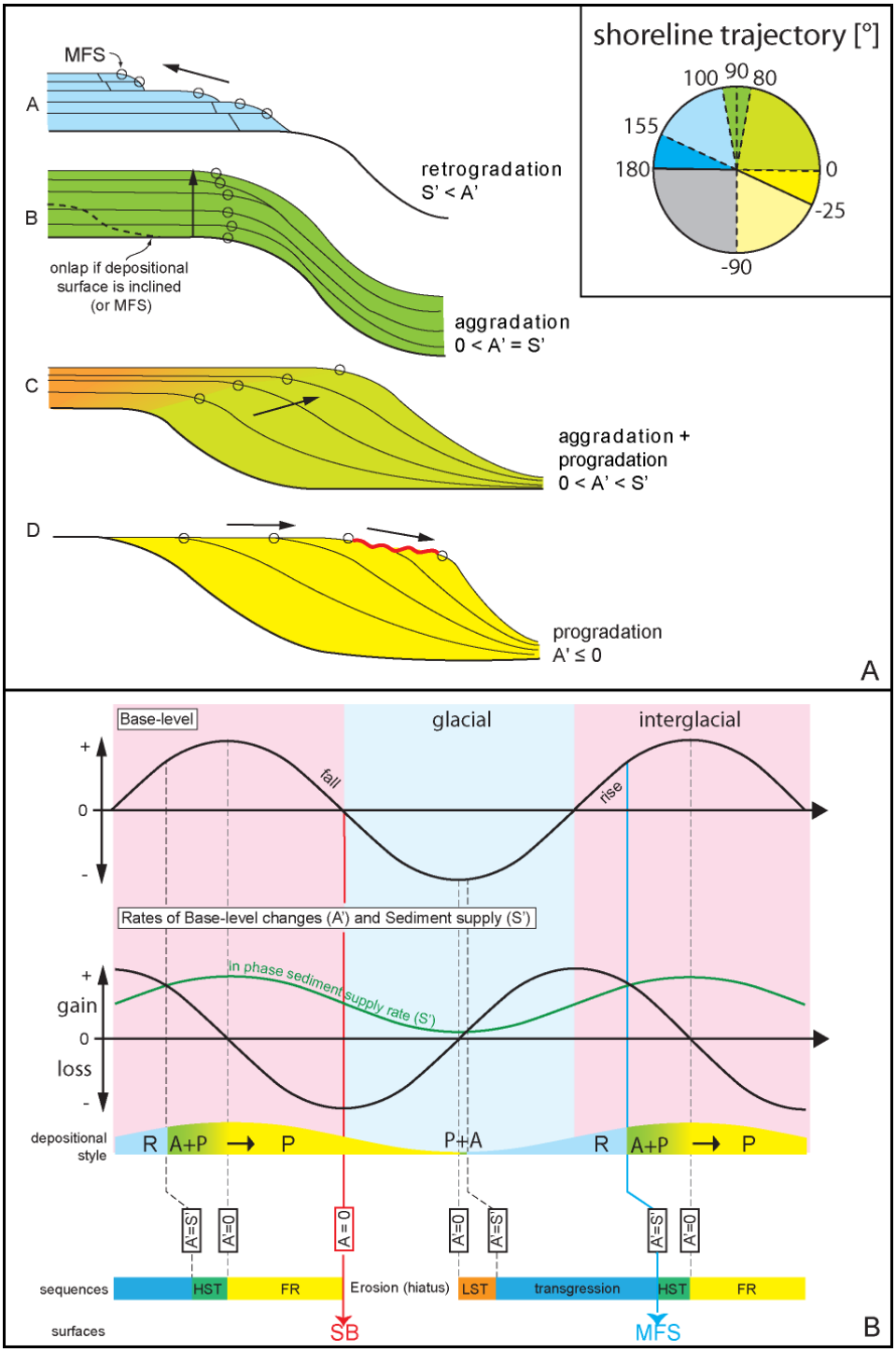

Figure 5-2 A) Depositional sequence types vs. the ration between accommodation change and sediment supply. Inset shows how the position of the shoreline throughout the sequence (the shoreline trajectory cf. Helland-Hansen and Martinsen,, 1996) is indicative for the depositional behaviour. B) Conceptual model explaining relationship between climatically controlled variations in sediment supply and accommodation (glacioeustasy).The periglacial setting of the Pleistocene Eridanos delta is best explained by an in-phase relationship, where low supply occurs at sea-level lowstand (glacials). The diagram explains that lowstand deposits (fans) are unlikely to form due to 1) limited sediment supply to the basin and 2) a short time window. Instead, highstand deposits are thick and prograding due to both sufficient accommodation and supply. Sequences as in Figure 5-4. Based on Catuneanu (2006) and ten Veen (2008).

This cube is guided by the basis seismic interpretations, the seismic amplitude cube and a steering cube (see dGB report) and as such, traces internal reflectors within the identified sequences. The resulting Horizon Cube consists of 757 horizons. Main drawback of the Horizon Cube is that the vertical resolution is limited by the seismic resolution. In order to obtain a vertical resolution comparable to that of the well logs a further subdivision of the Horizon Cube should be made, for instance by using the layering process in Petrels©. This last step was not part of this study.
By flattening the 757 horizon in the Horizon Cube, all horizons are stacked in a chronological order that by approximation represents the chronostratigraphy of the stacked delta sequence. This representation is referred to as Wheeler transformed domain and is useful for studying the evolution of deposition. Gaps in the Wheeler domain represent hiatuses caused by erosion or non-deposition. The extent of each layer is immediately apparent and shifts in the centre of deposition over geologic time can be easily deduced and related to relative base level changes. Another important application of the Wheeler cube is that seismic attributes (here OpendTect's discontinuity attribute)

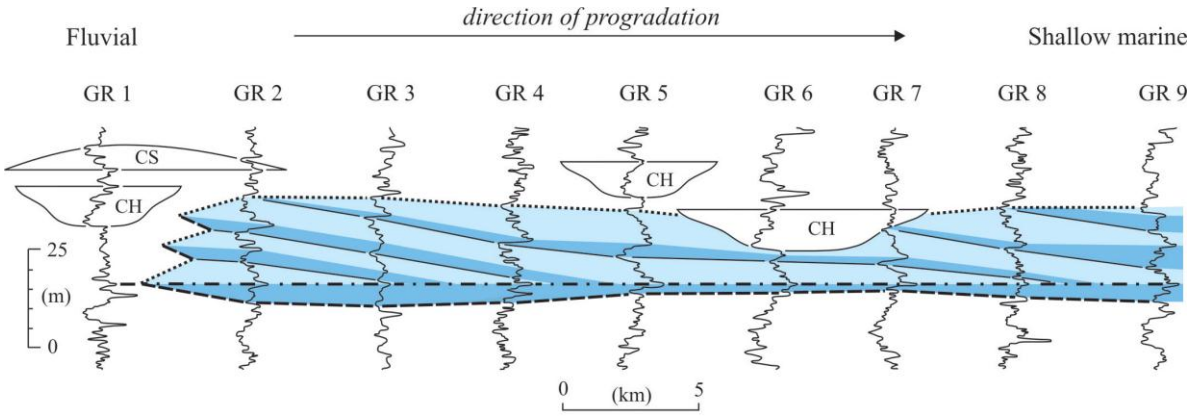

Figure 5-3 Example of sequence stratigraphic interpretation (based on gamma ray log GR) to illustrate reservoir compartimentalization of a deltaic depositional sequence due to internal stratification. Bounding surfaces of individual sequences represent the higher order correlation surfaces, whereas the internal stratification enables higher resolution correlation. Based on Catuneanu (2006).

can be appended to each flattened horizon. As such, a seismic volume is produced that only contains seismic information at the identified horizons. This volume is referred to as Wheeler transformed seismic cube. By time-slicing through this data, stratigraphic trends or morphological features may be observed that are otherwise obscured by structural deformations. For instance, paleocoastlines, channels, iceberg scratch marks, and other morphological features can be of great help to support the sequence stratigraphic interpretation (Fig. 5-5).
Ideally, the sequency-stratigraphic interpretation is an iterative process and may require several loops of 1) basic seismic interpretation, 2) Horizon Cube building, 3) Wheeler transform, 4) QC and, if necessary, 5) re-interpretation of the key bounding surfaces.

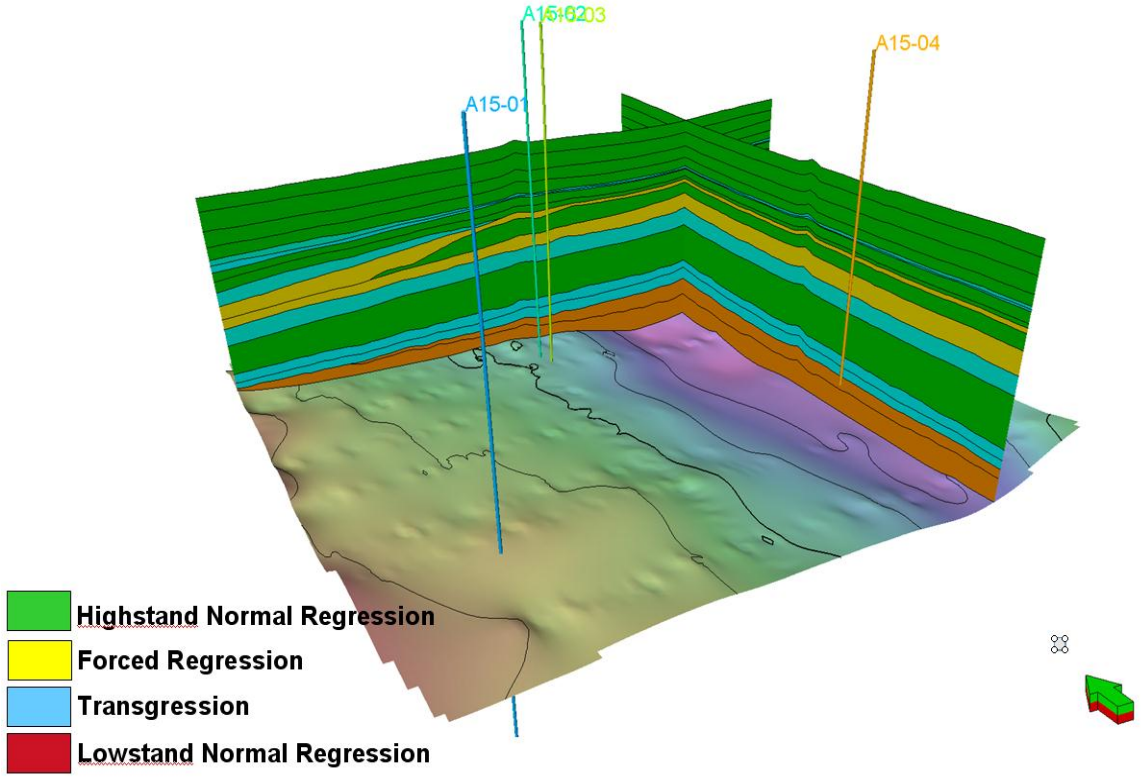

Figure 5-4 Sequence-stratigraphic interpretation of block A15. Boundaries between the depositional elements correspond to the 13 interpreted horizons (S1-S13) supplemented with two additional horizon interpretations provided by dGB (see section 7). Sequences types are explained in Figure 5-2.

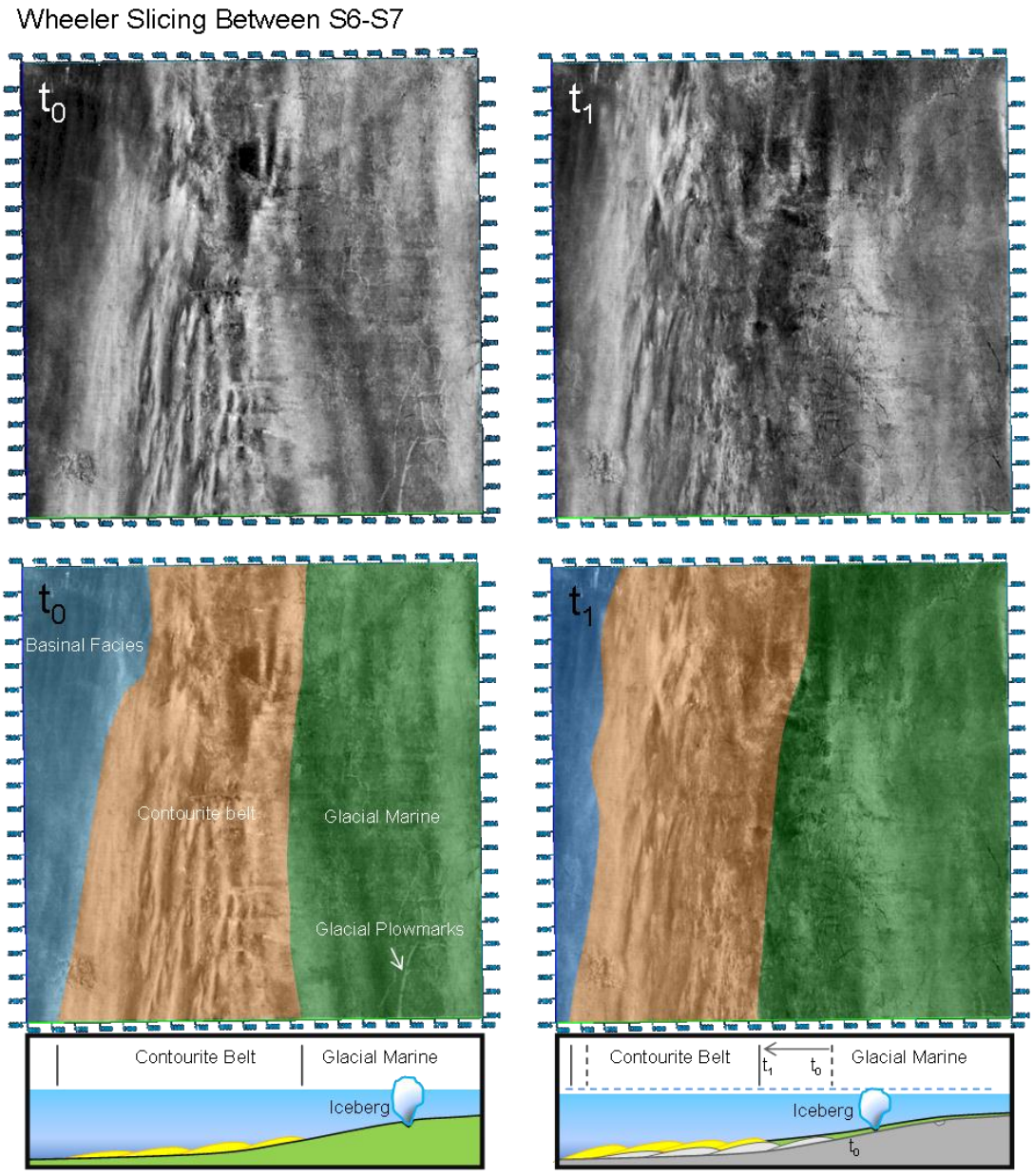

Figure 5-5 Representation of the discontinuity attribute in the Wheeler domain within the sequence defined between horizon S6 and S7. In this example, comparison of two chronostratigraphic slices (t_0 and t) enable to see the seaward shift of facies belts, which is interpreted as progradation (shown in cross-sectional views at bottom)

6 Seismic inversion and property modelling (by dGB)

In order to map porosity and gas saturation for the A15 block it was decided to invert the available seismic amplitude cube to acoustic impedance. Subsequently, the impedance cube was used for property distribution using Neural Network training. The A15 well data presented in the previous chapters forms the essential input to calibrate and test the reservoir mapping. These exercises were performed by de Groot Bril (dGB). For description of the workflow and results the reader is referred to the dGB report accompanying this document.

The following general conclusions are drawn from this study:

- An accurate initial model was created using a HorizonCube of very good quality, following the seismic reflectivity over the entire interval of interest.

- The deterministic inversion to acoustic impedance is considered successful. This is demonstrated by the low overall synthetic seismic error derived from the impedance volume, and the good synthetic-to-seismic match of the inverted impedance. Like any deterministic inversion the output resolution is bound to the bandwidth of the seismic and sampling rate, thus lower than the log resolution (up to 500Hz). The modelled volumes have thus a maximum resolution of 2 meters, which is more than enough to map the interesting areas from the output volumes

- The prediction of porosity from lithological/depositional information was not feasible. There is too little log information to establish proper relations, regardless of the log quality and hydrocarbon content

- The prediction of porosity and the localization of gas-saturated areas using impedance is of low quality. The match of the porosity volume with the logs is of medium quality. However, doubts remain on the distinction between gas-related and porosity-related anomalies in the low impedance areas.

- No reliable relation between seismic, impedance, volume of clay and water saturation was found when training the neural networks.

Recommendations concerning the procedures and discussion of results of the dGB study are presented in Chapter 7.

7 Recommendations

7.1 Seismic inversion

Recommendation: The use of acoustic inversion to produce (for instance) impedance cubes that are subsequently used to steer NN property distribution is not recommended. The NN modeling, alone, however, is a technique that has great potential (see next recommendation), provided that it is applied to and steered by a high-resolution geobody model that accurately, i.e. at the log resolution describes the internal geometry of the studied succession.
Motivation: One of the conclusions of dGB's analysis is that 2m resolution of the modelled volumes is more than enough to map the interesting areas from the output volumes. However, TNO believes that there are the two main reasons for the mediocre correlation between the porosity cube and the porosity logs:
1) The depth interval of interest has a predominant frequency of 70 Hz. With an average seismic velocity of 2000 m/s the seismic wavelength is about 30 m. This results in a limit of separation (1/4 λ) of 7.5 m. Most of the target sands have thicknesses of ~5 m or less which means that the seismic amplitude of the sands will be influenced by the over-and underlying lithologies. Any property prediction based on inversion of the seismic amplitude is thus bound to fail in these thin sands. Even with a higher predominant frequency (say 150 Hz) the standard seismic sampling rate of 4 ms is not sufficient. At this sampling rate, a sand sequence of 5 m thick is represented by one, or at most, two seismic samples. The seismic inversion results have the same sample rate. Using the impedance cube to train the neural network distribution of properties thus results in averaging of well log properties that have much higher resolutions (typically 0.5 - 1 ft).
2) Doubts remain on the distinction between gas-related and porosity-related anomalies in the low impedance areas. In other words, bright spots are reproduced in the inversion cube and thus in the property modelling results as well.

7.2 Neural Network (NN) property modeling

Recommendation: A NN modeling modeling approach is advocated that need to be steered by the internal geometry of the delta succession and interpolated well logs.
Motivation: All depositional sequences represent a certain facies type (systems tract) and internal layering of these sequences is accurately represented by the Horizon Cube. The 756 horizon in the Horizon Cube should provide sufficient means to construct a detailed geomodel that can be populated with properties using standard functionality (e.g. using Petrel). Key is that the modeling performed must be able to reproduce the sediment properties at the well location at a desired resolution. This resolution should be determined on fore hand.

7.3 Seismic vs. log resolution

Recommendation: It is recommended to use higher seismic sampling rates for shallow/Tertiary targets, preferably 2 ms or less. It is also recommended to use different seismic acquisition parameters in order to obtain higher predominant frequencies. Possible examples include a closer hydrophone spacing, high-frequency hydrophones and boomer, smaller airguns, reduced streamer depth. Regarding the fact that most of the available seismic data was processed with 2-3 s targets in mind, existing (pre-stack) seismic data might be re-processed with the objective to improve the <1500 ms interval.

Motivation: Basically, this pertains to the motivation of 7.1., with the additional remark that the seismic data, when it is used to steer property prediction, should be of such resolution that it is able to reproduce thin interbedded sequences at resolution comparable to that of the well logs.

7.4 Horizon Cube

Recommendation: The use of the HorizonCube functionality of dGB's OpendTect is recommended
Motivation: Following the earlier recommendation that a detailed geometrical model (geobody model), with a resolution equal to the well-log data, should form the basis for property distribution, we recommend the use of a multi-layer horizon interpretation. There are several ways to produce such a multi-layer horizon interpretation: 1) seismic interpretation of more horizons to include also the internal geometry of depositional sequences. Subsequently, the horizon interpretation can be refined using model layering, applying the proper stratigraphic rules and a resolution (layer thickness) that equals that of the well-log. This method is time consuming and therefore it is suggested to 2) make use of the HorizonCube functionality of dGB's OpendTect. At this point it is not known whether the latter option is more cost effective.

7.5 Wheeler Cube

Recommendation: The Wheeler Cube is not essential for property distribution studies.
Motivation Ideally, the sequence-stratigraphic interpretation is an iterative process and may require several loops of 1) basic seismic interpretation, 2) Horizon Cube building, 3) Wheeler transform, 4) QC and, if necessary, 5) re-interpretation of the key bounding surfaces. Although the Wheeler Cube may be of great help to support the sequence-stratigrahic interpretation, it is not essential for generation of the high-resolution geobody construction mentioned before.

7.6 Pre- vs. post stack data

Recommendation: If possible AVO analysis should be performed on pre-stack data, since AVO is the inversion technique that has the best potential for discriminating porosity from saturation effects. Before acquiring pre-stack data, a feasibility study of possible AVO effects vs. gas saturation can be performed. Such approach builds on Gassmann's (1951) model for fluid substitution.
Motivation: For this project post-stack seismic data was used and pre-stack data was not available. However high-porosity gas saturated areas are the kind of geology for which AVO analysis is required, since substitution of hydrocarbon for water will result in a lowering of bulk density and an increase in Vs.

7.7 Synthetic seismic

Recommendation: It is not recommended to put too much effort in matching synthetic seismic in gas-bearing wells. Instead, the dry wells should be used to tie the well logs to the seismic.
Motivation: TNO had severe difficulties in tying the well logs to the seismic. The well with theoretically speaking the best log suite, A15-03, had the poorest tie to the seismic. We don't know the exact cause. The quality of the logs (most notably the sonic log) certainly plays a role, but other effects cannot be ruled out. Invasion effects for example might introduce a mismatch between the calculated acoustic impedances from well logs and derived from seismic. This is especially true for wells with gas-bearing sands. Attempts could of course be made to generate sonic and density logs

that do not suffer from invasion effects and could produce synthetic seismic in a virgin formation. But other problems remain, such as the dimming effect which is very prominent in the A15 survey. This can not be resolved by a standard synthetic seismic calculation, but should be tackled by e.g. ray tracing techniques. Such an approach is beyond the scope of the current study.

7.8 Petrophysics

Recommendation 1: Perform gamma-ray normalization for all wells in the project. This can be done in Petrel, for example.
Motivation 1: Wells were drilled with different amounts of KCl/polymer additives, resulting in gamma-ray logs with varying readings in the different wells. Although it is not a real problem for correlation purposes, it creates additional work during the log evaluation process.

Recommendation 2: For future log evaluations, it is recommended to use a simple neutron-density based shaly sand model instead of a sophisticated multi-mineral model.
Motivation 2: It is much faster, and also much better in predicting effective porosities and gas saturations in the shaly zones.

Recommendation 3: Unless it is really necessary, it is advised not to repair the logs that are affected by washouts. Instead leaving the affected logs as they are and setting a Bad Hole Flag for these intervals is probably more appropriate.
Motivation 3: The deteriorating effects of washed out sections that are present in some wells can be combated, but to the expense of considerable effort and time as was proven by the sonic repair of A15-03 and the density repair of A15-04.

Recommendation 4: It is recommended to derive V_{shale} from the neutron-density logs, not from the gamma ray log.
Motivation 4: The gamma-ray log has a too low resolution to effectively distinguish between beds that are thinner than 60 cm, so any V_{shale} calculation that is based on a GR transform will overestimate V_{shale} in the cleaner beds and underestimate V_{shale} in the muddier beds. This will result in an underestimation of the gas in place. The neutron and density logs have a higher resolution than the GR log and are able to distinguish between these thin beds.

7.9 Biostratigraphy and facies

Recommendation 1: Detailed correlation between wells is possible and should be performed using the established scheme. Especially dinoflagellate cysts data are critical for age calibration and are the principle proxy in this setting.
Motivation 1: The high-resolution multi proxy analyses from A15-3 and A15-4 show that, based on the age calibration points (biostratigraphic markers) and available logs, a well-to-well correlation can be made whereby the paleoenvironmental trends derived from the data overlap very well. These include trends in TOC, marine/terrestrial ratios, and paleotemperatures. The dinocyst data have proven most useful as they provide correlation horizons and paleoenvironmental interpretations. Detailed pollen counts are not critical but identification of major groups provide a marine/terrestrial signal which is critical for interpretation. Foraminiferal data have been supporting in the development of the age model but are not critical in further application. If needed in the development of a regional stratigraphic model they can provide further paleodepth interpretations.

Recommendation 2: Cuttings material can be suitable for correlation if the resolution is high enough.
Motivation 2: In A15-3 a combination of core samples, sidewall cores and cuttings are available. Inclusion of the latter does not disturb the data interpretation since mainly quantitative trends are important in the age dating and facies analysis.
Recommendation 3: Stratigraphic model and related facies information (paleoenvironment) is useful in relating the well data to the different plays in the shallow gas system. Spatial distribution of the facies/depositional elements based on the biostratigraphical analyses is therefore needed.
Motivation 3: The quantitative paleoenvironmental data derived from biostratigraphical analyses (species counts) provide a qualitative interpretation of the interpreted seismic surfaces, e.g. sea level trends derived from marine/terrestrial ratios compared with a sequence stratigraphic interpretation. The species composition, furthermore, is a direct representation of the depositional environment. E.g. marine organisms indicative of open water conditions show a pro-delta setting, whereas brackish assemblages and/or organisms indicative of high-energy conditions point to upslope shallow environments above wave base, which results in a much more heterogeneous sedimentation. Especially the derived paleoclimatic trends relate the sedimentary properties (e.g. high TOC) to certain sequences and help predict the regional occurrence of these intervals. These interpretations feed into petroleum systems analysis and are independent of the seismic interpretations and therefore a significant verification.

8 Conclusions

This report describes a best-practise workflow for assessment of the distribution and properties of both bright-spot occurrences and their hosting sediments in Tertiary Eridanos delta sediments of the A15 block.

The project includes 3 main work packages that involve refinement of the 3D geological model of the delta reservoir. This model was built on sequence-stratigraphic principles, using 1) high resolution seismic interpretation and automated horizon tracking techniques, combined with 2) established temporal and/or spatial relationships between the occurrence of shallow gas and depositional elements (paleoenvironments). In addition, 3) petrophysical properties (Phi, S_w, V_{shale}) of the delta sediment were evaluated, and formed the input for 4) Neural Network modelling trained by seismic inversion cubes to distribute the most relevant model properties through the obtained geological model.

The combined workflow of TNO and dGB produced the following results:

Geological model (1 and 2):

- In the A15 Block a good chronostratigraphic framework is available for the Eridanos succession. The precise coupling to absolute age is derived from geomagnetic polarity data of well A15-3. The polarity intervals are coupled to the global standard by a number of well calibrated biostratigraphic events.
- A strong coupling exists between climate and sediment properties.
- Specific intervals are of interest, the intervals that are interpreted as glacial-interglacial cycles. The glacial-interglacial cycles show a marked contrast in grainsize, sea surface temperature and climate.
- Interglacials are characterized by:
  - Relatively warm climate and relatively high Sea Surface Temperatures
  - High freshwater input at the base of the interglacials
  - Relatively open marine conditions
  - Relatively coarse grainsize (moderate to good reservoir properties)
  - Relatively high sea level
  - Relatively high TOC content (possible source for biogenic gas)
- Glacials are characterized by:
  - Relatively cold climate and relatively low Sea Surface Temperatures
  - Almost no freshwater input
  - Relatively restricted marine conditions (water stratification)
  - Very fine grainsizes (excellent seal properties)
  - Relatively low sea levels
  - Relatively low TOC content

Petrophysics (3):

- A multi-mineral model was developed and applied on well A15-03 that calculates total and effective porosity, shale volume, and water saturation. The model produced a low residual error in the sands, but had difficulties in the more shaly intervals.
- Alternatively, a shaly sand model was run on A15-03, and later on wells A15-01, A15-02, and A15-04.
- Effective porosities in the sandy intervals range from 15% to 35%, total porosities are in the range 30-45%.

- In order to calculate permeability, a relationship was derived from NMR permeability and effective porosity. This relationship agreed very well with core plug measurements.

- Wells A15-01 and A15-04 were dry, but wells A15-02 and A15-03 were gas-bearing. Gas saturations are in general low. Most of the bright spots identified on seismic contain less than 30% gas. Only a few thin reservoirs contain gas saturations higher than 50%.
- To conclude, sands with high gas saturation are probably at irreducible conditions and are therefore likely to produce water-free gas. On the other hand, low gas-saturated sands produce also water, and are therefore not at irreducible saturations. This means that their top seals are probably leaking, and the gas in these sands is residual gas.

Seismic inversion (4):

- An accurate initial model was created using a HorizonCube of very good quality, following the seismic reflectivity over the entire interval of interest.
- The inversion to impedance is considered successful. This is demonstrated by the low overall synthetic seismic error derived from the impedance volume, and the good synthetic-to-seismic match of the inverted impedance.
- No reliable fit between seismic, impedance, volume of clay and water saturation could be established using trained neural network modelling. This is most importantly caused by the resolution difference between seismic (amplitude and inverted) data and well-log data.

9 References

Baumann, K.-H. and Huber, R., 1999.
Sea-surface gradients between the North Atlantic and the Norwegian Sea during the last 3.1 M.y.: comparison of sites 982 and 985. In: M.E. Raymo, E. Jansen, P. Blum and T.D. Herbert (Eds). Proceedings of the Ocean Drilling Program, Scientific Results: 179-190.

Bouma, A. 1973.

Catuneanu, O., 2006.
Principles of Sequence Stratigraphy. Elsevier, Amsterdam. 375 pp.

Ellis, D.V. & J.M. Singer, 2008.
Well logging for Earth Sciences, 2nd edition. Springer, 692 p.

Gassmann, F., 1951.
Elastic waves through a packing of spheres. Geophysics, 16, 673-685.

Geel, C.R., 2002.
Enhancing the gamma-ray log through geological input: Evaluating thin-bedded turbidite sequences, in M. Lovell and N. Parkinson, eds., Geological applications of well logs: AAPG Methods in Exploration No. 13, p. 15–26.

De Haan, H., 2010.
Unconventional gas in the Netherlands. PGK lecture

Helland-Hansen, W., Martinsen, O.J., 1996.
Shoreline trajectories and sequences: description of variable depositional-dip scenarios. Journal of Sedimentary Research 66 (4), 670–688.

Van Helmond, Donders, Verreussel, Bunnik, Munsterman, Weijers, Reichart, Sinninghe Damsté, 2010.
Palynological and organic geochemical characterization of marine and terrestrial Early Pleistocene climate in northwest Europe. TNO report-034-UT-2010-01544/B, 78 p.

Kuhlmann, G., 2004.
High resolution stratigraphy and paleoenvironmental changes in the southern North Sea during the Neogene — an integrated study of Late Cenozoic marine deposits from the northern part of the Dutch offshore area. Ph.D. thesis, Utrecht University, Geologica Ultraiectina, Mededelingen van de Faculteit Aardwetenschappen, No. 245, 205 pp.

Kuhlmann, G., Langereis, C., Munsterman, D., van Leeuwen, R.J., Verreussel, R., Meulenkamp, J., Wong, T., 2006.
Chronostratigraphy of Late Neogene sediments in the southern North Sea Basin and paleoenvironmental interpretations. Palaeogeography, Palaeoclimatology, Palaeoecology 239, 426–455.

Kuhlmann, G., Langereis, C.G., Munsterman, D., van Leeuwen, R.-J., Verreussel, R., Meulenkamp, J.E., Wong, Th.E., 2006b.

Integrated chronostratigraphy of the Pliocene–Pleistocene interval and its relation to the regional stratigraphical stages in the southern North Sea region. Netherlands Journal of Geosciences-Geologie enMijnbouw 85 (1), 19–35.

Overeem, I., Weltje, G. J., Bishop-Kay, C. and Kroonenberg, S. B., 2001.
The Late Cenozoic Eridanos delta system in the Southern North Sea Basin: a climate signal in sediment supply? Basin Research 13(3), 1365-2117.

Panterra, 1999.
Sedimentology And Petrography Of Upper North Sea Group, Well A15-3. Final Report, 176 p.

Raymer, L.L., Hunt, E.R., and Gardner, J.S. (1980).
An improved Sonic Transit time – to – Porosity Transform. Trans., SPWLA.

Reid, P.I. & R.C. Minton, 1992.
New Water-Based Muds for Tertiary Shale Control. SPE Drilling Engineering 7, p237-241. SPE Paper 23077-PA.

De Schepper, S., M. J. Head, and J. Groeneveld, 2009.
North Atlantic Current variability through marine isotope stage M2 (circa 3.3 Ma) during the mid-Pliocene, Paleoceanography, 24, PA4206, doi:10.1029/2008PA001725.

De Schepper, S., Head, M.J., 2009.
PLIOCENE AND PLEISTOCENE DINOFLAGELLATE CYST AND ACRITARCH ZONATION OF DSDP HOLE 610A, EASTERN NORTH ATLANTIC. Palynology Volume: 33 Pages: 179-218

Weatherford, 2007.
Log Interpretation Charts Compact™ Tool Series. Weatherford, Houston, Texas, 66 p.

Ten Veen, J.H., Mikes, D., Postma, G. and Steel, R.J., 2008.
Shelf-edge delta architecture resulting from in- and out phase changes in supply and sea-level in ice-house periods. 26th Regional Meeting of International Association of Sedimentologists (IAS).

10 Signature

Utrecht,July 2011

	Johan ten Veen
Head of department	Author

Appendices

Appendix A - Well correlation for A15 wells – flattened on X_S13 marker

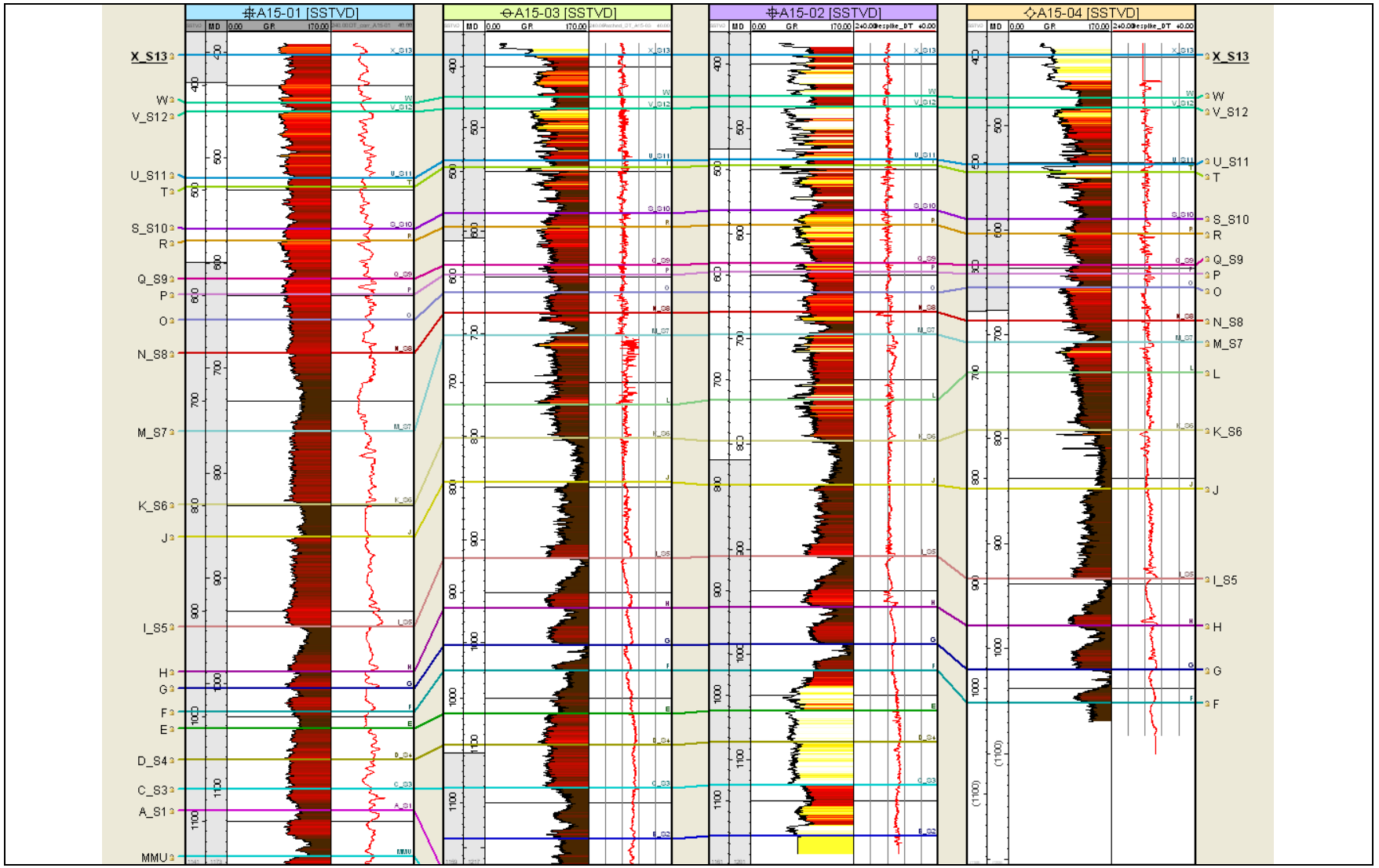

Appendix B - TNO nomenclature - log units defined per well.

Well	A15-01		A15-02		A15-03		A15-04	
Log unit	TVDSS, m	MD, m	TVDSS, m	MD, m	TVDSS, m	MD, m	TVDSS, m	MD, m
X_S13	-371.81	402.98	-391.75	430.78	-389.53	430.08	-398.32	433.32
W	-416.82	448	-430.6	469.64	-429.46	470.91	-438.92	473.92
V_S12	-425.45	456.62	-440.81	479.85	-440.31	482	-448.34	483.35
U_S11	-488.87	520.05	-491.13	530.17	-489.86	532.6	-501.78	536.94
T	-496.71	527.9	-496.23	535.28	-496.13	539	-509.5	544.7
S_S10	-536.79	567.98	-539.41	578.46	-539.5	583.26	-553.85	589.39
R	-547.62	578.81	-552.92	591.97	-552.96	597	-567.48	603.15
Q_S9	-583.97	615.16	-589.47	628.53	-589.1	633.88	-597.69	633.69
P	-598.6	629.8	-597.99	637.05	-598.03	643	-606.2	642.29
O	-623.43	654.63	-616.67	655.73	-614.69	660	-618.53	654.76
N_S8	-655.18	686.38	-635.42	674.48	-634.31	680.04	-650.79	687.35
M_S7	-729.24	760.45	-656.82	695.88	-655.91	702.11	-671.42	708.19
L	na	na	-718.92	757.99	-721.35	769	-699.78	736.83
K_S6	-798.6	829.81	-758.02	797.1	-753.63	802	-754.43	792
J	-829.19	860.4	-799.96	839.04	-795.41	844.71	-810.23	848.07
I_S5	-914.36	945.58	-868.08	907.17	-867.04	918	-896.02	933.91
H	-957.22	988.44	-916.57	955.66	-914.9	967	-940.65	978.55
G	-972.94	1004.16	-951.22	990.32	-950.08	1003	-982.56	1020.46
F	-995.45	1026.67	-976.28	1015.38	-974.51	1028	-1013.6	1051.51
E	-1011.24	1042.46	-1014.82	1053.92	-1015.55	1070	NA	NA
D_S4	-1041.44	1072.66	-1044.79	1083.89	-1044.89	1100	NA	NA
C_S3	-1068.9	1100.12	-1084.81	1123.91	-1085.97	1142	NA	NA
B_S2	NA	NA	-1133.49	1172.6	-1134.26	1191.35	NA	NA
A_S1	-1089.77	1120.99	NA	NA	-1166.51	1224.29	NA	NA
MMU	-1133.49	1164.71	NA	NA	-1192.81	1251.19	NA	NA

Appendix C - Difference in seismic-log unit correspondence after TZ calibration applied. TNO markers (left) vs Gesa Kuhlmann's markers (right)

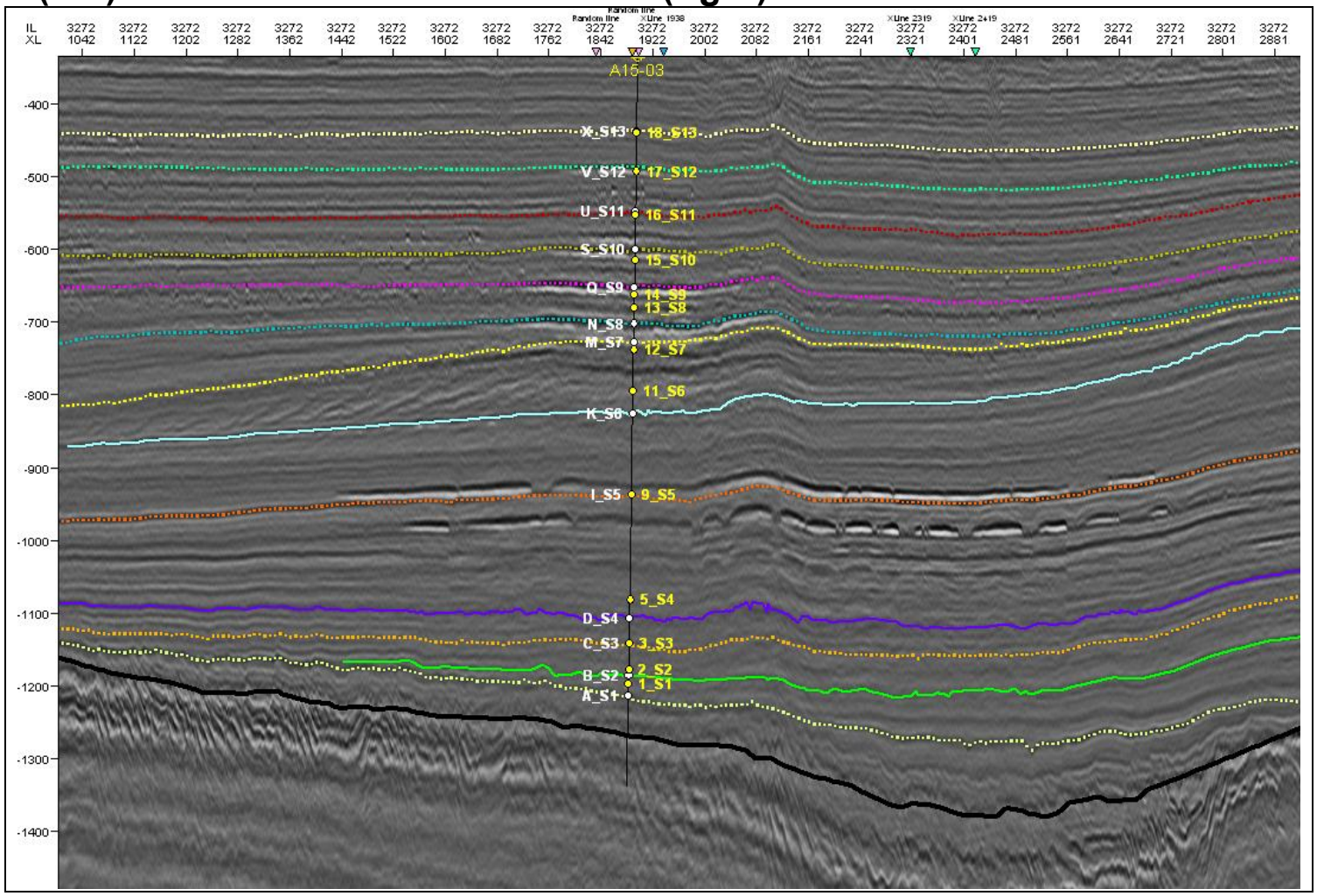

Appendix D – Inline 3272. All seismic units and GR log displayed along the well A15-03.

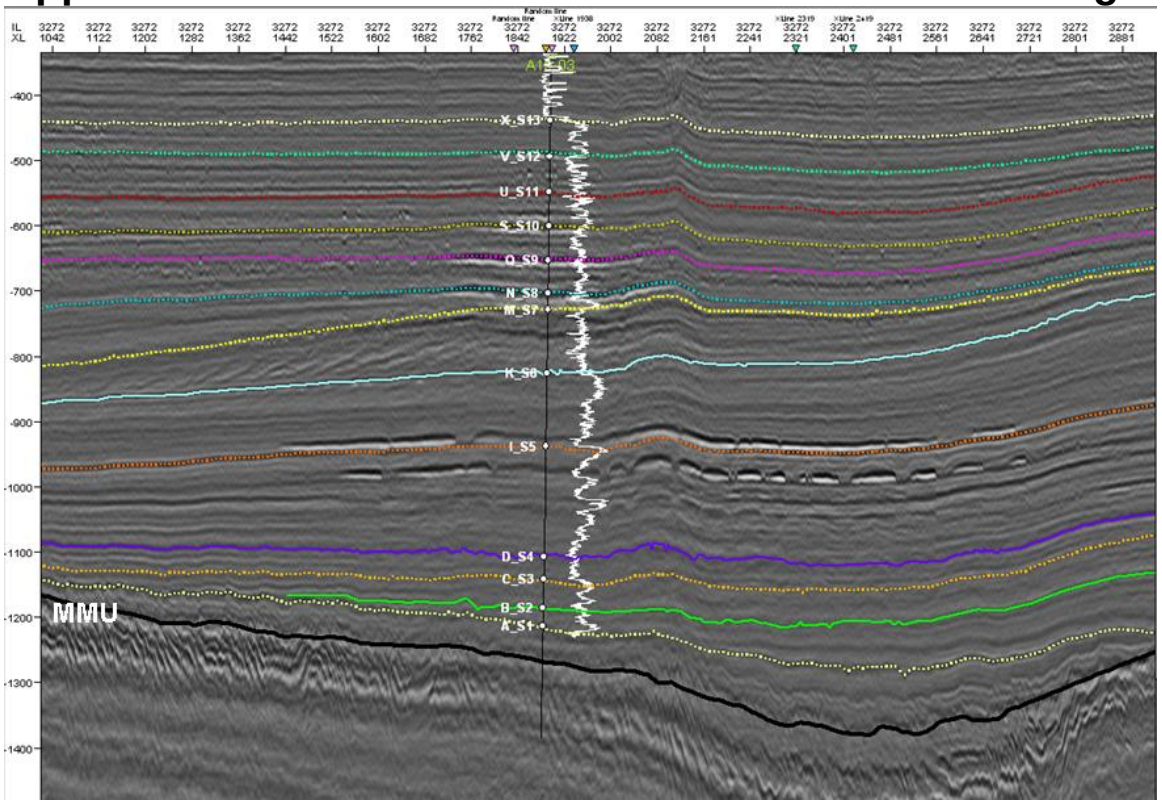

Appendix E – A15-3 and A15-4 sample list

Nr.	TNO label	Core	Depth (mbsl)	Splice depth (mbsl) to core A15-3	Box
1	1 CO	A15-3	890.8	890.8	
2	2 CO	A15-3	891.75	891.75	
3	6 CO	A15-3	892.8	892.8	
4	8 CO	A15-3	893.8	893.8	
5	12 CO	A15-3	896.8	896.8	
6	13 CO	A15-3	897.8	897.8	
7	15 CO	A15-3	898.8	898.8	
8	17 CO	A15-3	899.8	899.8	6-1
9	20 CO	A15-3	901.8	901.8	6-4
10	23 CO	A15-3	903.85	903.85	6-6
11	24 CO	A15-3	904.8	904.8	6-7
12	32 CO	A15-4	925.45	907.8	
13	36 CO	A15-4	926.8	908.97	
14	38 CO	A15-4	927.45	909.53	
15	40 CO	A15-4	928	910.01	
16	42 CO	A15-4	928.75	911.06	
17	44 CO	A15-4	929.55	912.19	
18	45 CO	A15-4	930.25	913.21	
19	48 CO	A15-3	917.55	917.55	8-1
20	49 CO	A15-3	918.15	918.15	8-2
21	51 CO	A15-3	920	920	8-4
22	55 CO	A15-3	921.95	921.95	8-6
23	57 CO	A15-3	924	924	8-8
24	60 CO	A15-3	925	925	8-10
25	62 CO	A15-3	926.7	926.7	9-1
26	67 CO	A15-3	929.95	929.95	9-5
27	68 CO	A15-3	935.9	935.9	10-2
28	69 CO	A15-3	936.9	936.9	10-3
29	72 CO	A15-3	938.9	938.9	10-5
30	75 CO	A15-3	940.9	940.9	10-7
31	77 CO	A15-3	942.9	942.9	10-9
32	79 CO	A15-3	943.85	943.85	10-10
33	80 CO	A15-3	944.9	944.9	11-1
34	81 CO	A15-3	945.9	945.9	11-2
35	85 CO	A15-3	946.91	946.91	11-3
36	86 CO	A15-3	953.25	953.25	12-1
37	87 CO	A15-3	954.15	954.15	12-2
38	89 CO	A15-3	956.18	956.18	12-4
39	92 CO	A15-3	957.3	957.3	12-5
40	94 CO	A15-3	958.25	958.25	12-6
41	97 CO	A15-3	960.33	960.33	12-9
42	101 CO	A15-3	962.2	962.2	13-1
43	103 CO	A15-3	963.17	963.17	13-2
44	104 CO	A15-3	964.02	964.02	13-3
45	126 CO	A15-4	975.1	960.1	
46	129 CO	A15-4	976.1	961.1	
47	131 CO	A15-4	976.8	961.8	

48	133 CO	A15-4	977.45	962.45	
49	136 CO	A15-4	978.3	963.3	
50	137 CO	A15-4	978.85	963.85	
51	143 CO	A15-4	980.8	965.8	
52	146 CO	A15-4	981.8	966.8	
53	151 CO	A15-4	983.5	968.5	
54	154 CO	A15-4	984.5	969.5	
55	158 CO	A15-4	986.15	971.06	
56	161 CO	A15-4	987.15	972	
57	CO	A15-4	997.8	981.91	
58	CO	A15-4	999.8	983.77	
59	CO	A15-4	1003.8	987.49	
60	CO	A15-4	1008.35	991.72	
61	CO	A15-4	1011.3	994.47	
62	CO	A15-4	1014.3	997.26	
63	SC	A15-4	937.8	922.8	
64	SC	A15-4	938.45	923.45	
65	SC	A15-4	1008.05	991.44	
66	SC	A15-4	1008.75	992.09	
67	SC	A15-4	1064	1037.69	
68	SC	A15-4	1067	1040	
69	SC	A15-4	1070	1042.31	
70	SC	A15-4	1073	1044.62	
71	SC	A15-4	1076	1046.92	
72	SC	A15-4	1079	1049.23	
73	SC	A15-4	1082	1051.54	
74	SC	A15-4	1084	1053.08	
75	SC	A15-4	1085	1053.85	
76	SC	A15-4	1086	1054.62	
77	SC	A15-4	1088	1056.15	
78	SC	A15-4	1089.9	1057.62	

Appendix F – Correlation bio- and chronostraitraphy with seismic- and log units. Sequence stratigraphic interpretation is compared with previous interpretations and sustained by paleoenvironmental interpretations

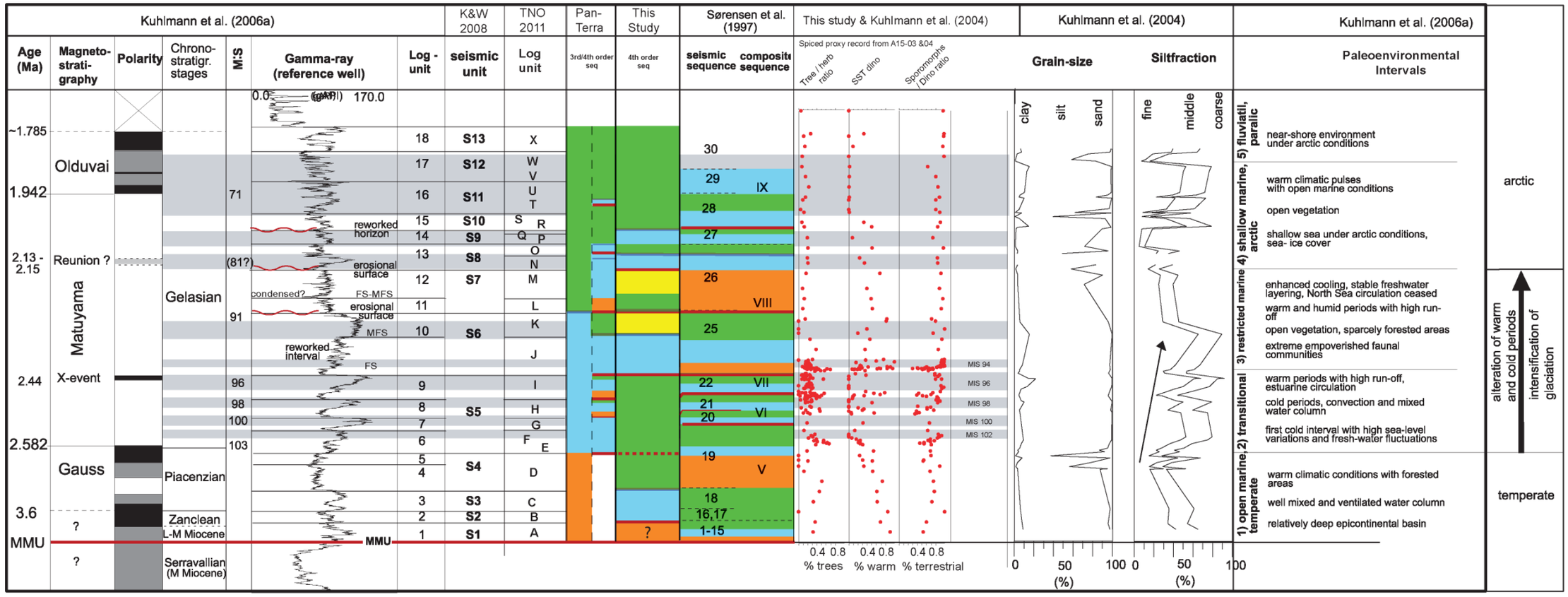

Appendix G – Mineralogical analysis of A15-03 cores

Table G1 - Semi-quantitative results of the whole rock and clay fraction (<2μm) XRD analysis on sandstone, siltstone and claystone samples from the Upper North Sea Group, Well A15-3. From Panterra (1999).

Well	Log Depth (m)	Sample Nº	Litho-stratigraphic Unit	Reservoir Unit	Litho-facies	Lithofacies Association	Rock Classification (Pettijohn, 1975)	Whole Rock Composition (%BW)													Clay Fraction (%BW)				Remarks	Grain Density (g/ml)
								Quartz	Orthoclase	Albite	Wavellite	Calcite	Dolomite	Ankerite	Siderite	Anhydrite	Pyrite	Illite/Mica	Kaolinite	Chlorite	Illite/Smectite	Chlorite/Kaolinite	Illite	Kaolinite	Chlorite	Illite/Smectite	% Smectite in Illite/Smectite	Calculated
A15-3	485.00	SWS 29	Upper North Sea Group	A10		?Lower shoreface	Subarkose	76	7	2	-	-	-	-	-	-	-	8	-	-	6	1	43	7	11	39	75% smectite	2.65
	498.00	SWS 28				?Lower shoreface																	62	14	24	tr		
	572.18	-		A40	JI,M,lp	Offshore	Claystone/Siltstone																					
	572.92	5			M,J,lp	Offshore	Claystone	8	2	1	-	1	-	-	-	-	-	54	3	3	28	-	49	10	9	32	unresolved	2.70
	591.35	11		A50	Ju,ro	Lower shoreface	Mudstone/Siltstone																					
	592.95	S 17			Ju/M,ro	Lower shoreface	Siltstone																					
	594.32	23			M,J,lp	Offshore	Claystone/Feldsp. Greywacke	44	5	2	-	5	2	-	3	-	-	23	2	2	12	-	49	17	9	25	unresolved	2.70
	616.28	26			JI,lp	Lower shoreface	Siltstone																					
	628.46	75			M,J,mb	Offshore	Claystone	22	3	2	-	4	2	-	-	-	-	45	4	4	14	-	47	15	8	30	75% smectite	2.70
	663.90	RSWS 2		A70																								
	667.00	SWS 21				?Lower shoreface	Subarkose	61	7	4	4	1	-	-	-	2	-	13	-	2	6	-	57	-	13	30	unresolved	2.68
	826.00	SWS 16		A80		?Basin	Claystone	8	5	2	-	-	-	-	-	-	-	65	3	4	13	-	56	7	8	29	75% smectite	2.72
	895.67	S 107			S1,dl	Sheet turbidites	Subarkose																					
	897.03	113			M,J,lp	Sheet turbidites	Claystone	12	3	1	-	1	-	1	1	-	-	60	5	3	13	-	53	18	7	22	75% smectite	2.72
	907.15	153		D10	M,J,mb	Basin	Claystone	9	2	1	-	3	-	1	1	-	-	61	5	5	12	-	43	14	4	39	75% smectite	2.73
	911.00	RSWS 11				?Turbidites																	39	13	10	38		
	922.95	181			M,J,mb	Basin	Claystone	5	2	1	-	tr	1	-	1	-	-	78	3	4	5	-	64	11	10	14	unresolved	2.75
	940.22	236			M,J,mb	Basin	Claystone	20	5	2	-	7	1	-	2	-	-	46	8	tr	9	-	54	15	3	28	75% smectite	2.71
	951.87	278		D20	M,J,mb	Basin	Silty Claystone	7	2	1	-	1	-	tr	-	-	tr	69	2	3	15	-	38	11	4	47	75% smectite	2.72
	953.46	285			M,J,mb	Destratified turbidites	Silty Claystone/Arg. Siltstone																					
	956.16	296		D20	M,J,mb	Basin	Mudstone																					
	998.50	RSWS 4		D30		?Turbidites																	36	10	12	40		
	1087.00	SWS 6		D40		?Turbidites	Feldspathic Greywacke	28	3	1	-	9	-	-	-	-	1	42	3	2	11	-	49	15	8	28	75% smectite	2.71
	484-502	DST #5 No 19	Upper North Sea Group	A10				61	6	3	3	1	-	1	-	2	tr	4	-	-	-	-	48	8	17	27	75% smectite	
	484-502	DST #5 No 20						61	6	3	3	1	1	-	-	-	tr	5	-	-	-	1	34	6	12	48	75% smectite	
	484-502	DST #5 No 27						71	6	3	2	1	1	-	-	-	tr	10	-	-	5	1	45	8	16	31	75% smectite	
	484-502	DST #5 No 28						83	6	2	2	1	1	-	-	-	tr	5	-	-	-	1	43	8	15	34	75% smectite	
	679.5-686.5	DST Sample 2		A70				71	5	4	4	1	-	1	-	2	1	-	-	3	9	-						
	679.5-686.5	DST Sample 6						63	6	3	8	tr	-	1	-	2	tr	-	-	3	15	-						
	679.5-686.5	DST/SC 1 bottom						55	8	5	6	1	-	1	-	-	1	21	-	2	-	-						
	679.5-686.5	DST/SC middle						60	7	4	13	-	-	1	-	-	-	14	-	1	-	-						
	679.5-686.5	DST/SC 2 bottom						62	6	4	6	-	-	1	1	-	1	18	-	1	-	-						

tr = trace

Mineral Density (g/ml)

Quartz	2.65	Calcite	2.72	Anhydrite	2.95
Orthoclase	2.57	Dolomite	2.86	Pyrite	4.99
Albite	2.62	Ankerite	3.02	Illite/Mica	2.75
Wavellite	3.23	Siderite	3.96	Kaolinite	2.60

Chlorite	2.95
Illite/Smecti	2.63
Chlorite/Ka	2.78

Table G2 - Detrital composition of sandstone, siltstone and claystone samples from the Upper North Sea Group, Well A15-3. From Panterra (1999).

Log Depth (m)	Plug Nº	Litho-stratigraphic Unit	Reservoir Unit	Litho-facies	Lithofacies Association	Rock Classification (Pettijohn, 1975)	Detrital Components (%)																		
							Monocrystalline Quartz	Polycrystalline Quartz	K-Feldspar	Plagioclase	Claystone Fragments	Carbonate Fragments	Metamorphic Fragments	Mica	Heavy Minerals	Glauconite	Carbonaceous Material	Fossils/Bioclasts	Clay Pellets	Altered Grains	Clay Pellicles	Detrital Clay Matrix	Clay Burrows	Pseudomatrix
485.00	SWS 29	Upper North Sea Gr.	A10		?Lower shoreface	Subarkose	49.7	3.7	6.0	-	-	-	0.7	tr	1.3	-	-	tr	2.7	-	6.7	-	-	0.3
498.00	SWS 28				?Lower shoreface																				
572.18	-		A40	Jl,M,lp	Offshore	Claystone/Siltstone	32.3	-	6.7	-	-	1.0	-	6.3	0.3	tr	4.7	-	-	0.3	-	43.7	-	-
572.92	5			M,J,lp	Offshore	Claystone	4.0	-	0.3	-	-	-	-	1.3	tr	-	2.7	tr	-	-	-	88.7	-	-
591.35	11		A50	Ju,ro	Lower shoreface	Mudstone/Siltstone	33.0	-	6.7	0.3	-	3.0	-	7.3	5.0	tr	0.7	0.3	-	2.7	-	34.0	-	-
592.95	S 17			Ju/M,ro	Lower shoreface	Siltstone	51.0	0.7	7.3	-	-	2.3	-	9.3	3.3	tr	tr	-	-	2.0	-	?	tr	8.7
594.32	23			M,J,lp	Offshore	Claystone/Feldsp. Greywacke	14.3	-	2.7	-	-	0.3	-	2.3	2.0	tr	2.3	-	-	-	-	73.3	-	-
616.28	26			Jl,lp	Lower shoreface	Siltstone	45.0	0.3	13.0	-	2.3	3.3	0.3	11.0	1.7	tr	-	-	-	-	-	?	tr	7.7
628.46	75			M,J,mb	Offshore	Claystone	6.0	-	-	-	-	-	-	0.7	0.7	-	7.0	-	-	-	-	85.0	-	-
683.90	RSWS 2		A70																						
687.00	SWS 21				?Lower shoreface	Subarkose	46.3	2.3	9.3	0.7	-	-	0.7	3.0	10.0	-	-	-	0.3	-	1.3	-	-	1.7
826.00	SWS 16		A80		?Basin	Claystone	tr	-	-	-	-	-	-	-	tr	-	1.0	-	-	-	-	97.7	-	-
895.67	S 107			S1,dl	Sheet turbidites	Subarkose	39.0	1.3	10.7	-	-	-	0.7	5.7	4.3	tr	tr	-	1.0	-	1.0	6.0	-	4.7
897.03	113			M,J,lp	Sheet turbidites	Claystone	5.3	-	-	-	-	-	-	1.7	-	-	2.0	tr	-	-	-	90.0	-	-
907.15	153		D10	M,J,mb	Basin	Claystone	3.0	-	2.0	-	-	-	-	1.0	-	-	3.7	-	-	-	-	86.7	-	-
911.00	RSWS 11				?Turbidites																				
922.95	181			M,J,mb	Basin	Claystone	tr	-	-	-	-	-	-	-	-	-	0.3	-	-	-	-	98.0	-	-
940.22	236			M,J,mb	Basin	Claystone	1.3	-	-	-	-	-	-	tr	-	-	2.7	tr	-	-	-	95.3	-	-
951.87	278		D20	M,J,mb	Basin	Silty Claystone	8.3	-	-	0.3	-	-	-	3.3	1.0	tr	3.7	-	-	-	-	78.0	-	-
953.48	285			M,J,mb	Destratified turbidites	Silty Claystone/Arg. Siltstone	11.7	1.0	5.7	-	-	-	-	1.0	1.7	tr	4.0	tr	-	-	-	69.3	-	-
956.16	296			M,J,mb	Basin	Mudstone	19.7	0.7	3.0	-	-	0.7	-	4.0	1.3	-	1.0	tr	-	-	-	64.0	-	-
996.50	RSWS 4		D30		?Turbidites																				
1097.00	SWS 6		D40		?Turbidites	Feldspathic Greywacke	23.7	-	6.3	0.3	-	1.0	-	3.7	1.7	tr	tr	2.3	-	-	-	58.3	-	-
484-502 - 1	DST #5 No 19	Upper North Sea Gr.	A10																						
484-502 - 2	DST #5 No 20																								
484-502 - 3	DST #5 No 27																								
484-502 - 4	DST #5 No 28																								
679.5-686.5 - 1	DST Sample 2		A70																						
679.5-686.5 - 2	DST Sample 6																								
679.5-686.5 - 3	DST/SC 1 bottom																								
679.5-686.5 - 4	DST/SC middle																								
679.5-686.5 - 5	DST/SC 2 bottom																								

Abundance
tr = trace

Table G3 - Authigenic composition and porosity of sandstone, siltstone and claystone samples from the Upper North Sea Group, Well A15-3. From Panterra (1999).

Log Depth (m)	Plug Nº	Litho-stratigraphic Unit	Reservoir Unit	Litho-facies	Lithofacies Association	Rock Classification (Pettijohn, 1975)	Authigenic Minerals (%)						Visible Porosity (%)		Porosity (%)		Reservoir Properties	
							Ferroan Calcite	Siderite	?Gypsum	Sylvite	Hematite	Pyrite	Intergranular Porosity	Intraparticle Porosity	Macroporosity	Microporosity	Helium Porosity (%)	Horizontal Permeability (mD)
485.00	SWS 29	Upper North Sea Gr.	A10		?Lower shoreface	Subarkose	-	-	-	2.0	-	-	27.0	-	27.0	n.d.		
498.00	SWS 28				?Lower shoreface													
572.18	-		A40	Jl,M,lp	Offshore	Claystone/Siltstone	0.7	0.7	-	-	-	tr	3.3	-	3.3	n.d.		
572.92	5			M,J,lp	Offshore	Claystone	3.0	-	-	-	-	-	-	-	-	n.d.	n.m.	n.m.
581.35	11		A50	Ju,ro	Lower shoreface	Mudstone/Siltstone	-	-	-	-	-	-	7.0	-	7.0	26.0	33.0	10.2
582.95	S 17			Ju/M,ro	Lower shoreface	Siltstone	1.3	0.3	tr	-	-	-	13.7	-	13.7	n.d.	n.m.	n.m.
594.32	23			M,J,lp	Offshore	Claystone/Feldsp. Greywacke	-	-	-	-	-	-	2.7	-	2.7	n.d.	n.m.	n.m.
616.28	26			Jl,lp	Lower shoreface	Siltstone	-	-	-	-	-	-	15.3	-	15.3	23.3	38.6	38.6
628.46	75			M,J,mb	Offshore	Claystone	0.7	-	-	-	-	-	-	-	-	n.d.	n.m.	n.m.
663.90	RSWS 2		A70															
667.00	SWS 21				?Lower shoreface	Subarkose	-	-	-	-	-	-	24.3	-	24.3	n.d.		
826.00	SWS 16		A80		?Basin	Claystone	1.0	-	-	-	-	0.3	-	-	-	n.d.		
895.67	S 107			S1,dl	Sheet turbidites	Subarkose	-	-	tr	-	4.0	-	21.7	-	21.7	16.0	37.7	126
897.03	113			M,J,lp	Sheet turbidites	Claystone	0.3	0.3	-	-	-	0.3	-	-	-	n.d.	n.m.	n.m.
907.15	153		D10	M,J,mb	Basin	Claystone	0.7	?0.3	-	-	-	2.7	-	-	-	n.d.	n.m.	n.m.
911.00	RSWS 11				?Turbidites													
922.95	181			M,J,mb	Basin	Claystone	0.3	1.3	-	-	-	-	-	-	-	n.d.	n.m.	n.m.
940.22	236			M,J,mb	Basin	Claystone	0.7	-	-	-	?	tr	-	tr	0.0	n.d.	n.m.	n.m.
951.87	278		D20	M,J,mb	Basin	Silty Claystone	1.7	0.3	tr	-	-	3.0	0.3	-	0.3	n.d.	n.m.	n.m.
953.48	285			M,J,mb	Destratified turbidites	Silty Claystone/Arg. Siltstone	2.0	1.3	-	-	-	1.0	1.3	-	1.3	29.3	30.6	1.01
956.16	296			M,J,mb	Basin	Mudstone	2.3	-	-	-	-	2.7	0.7	-	0.7	n.d.	n.m.	n.m.
996.50	RSWS 4		D30		?Turbidites													
1097.00	SWS 6		D40		?Turbidites	Feldspathic Greywacke	-	-	-	-	-	2.0	0.3	0.3	0.7	n.d.		
484-502 - 1	DST #5 No 19	Upper North Sea Gr.	A10															
484-502 - 2	DST #5 No 20																	
484-502 - 3	DST #5 No 27																	
484-502 - 4	DST #5 No 28																	
679.5-686.5 - 1	DST Sample 2		A70															
679.5-686.5 - 2	DST Sample 6																	
679.5-686.5 - 3	DST/SC 1 bottom																	
679.5-686.5 - 4	DST/SC middle																	
679.5-686.5 - 5	DST/SC 2 bottom																	

Abundance
tr = trace

Core analysis
n.m. = not measured
n.d. = not determined

Appendix H – Repairing the sonic in A15-03

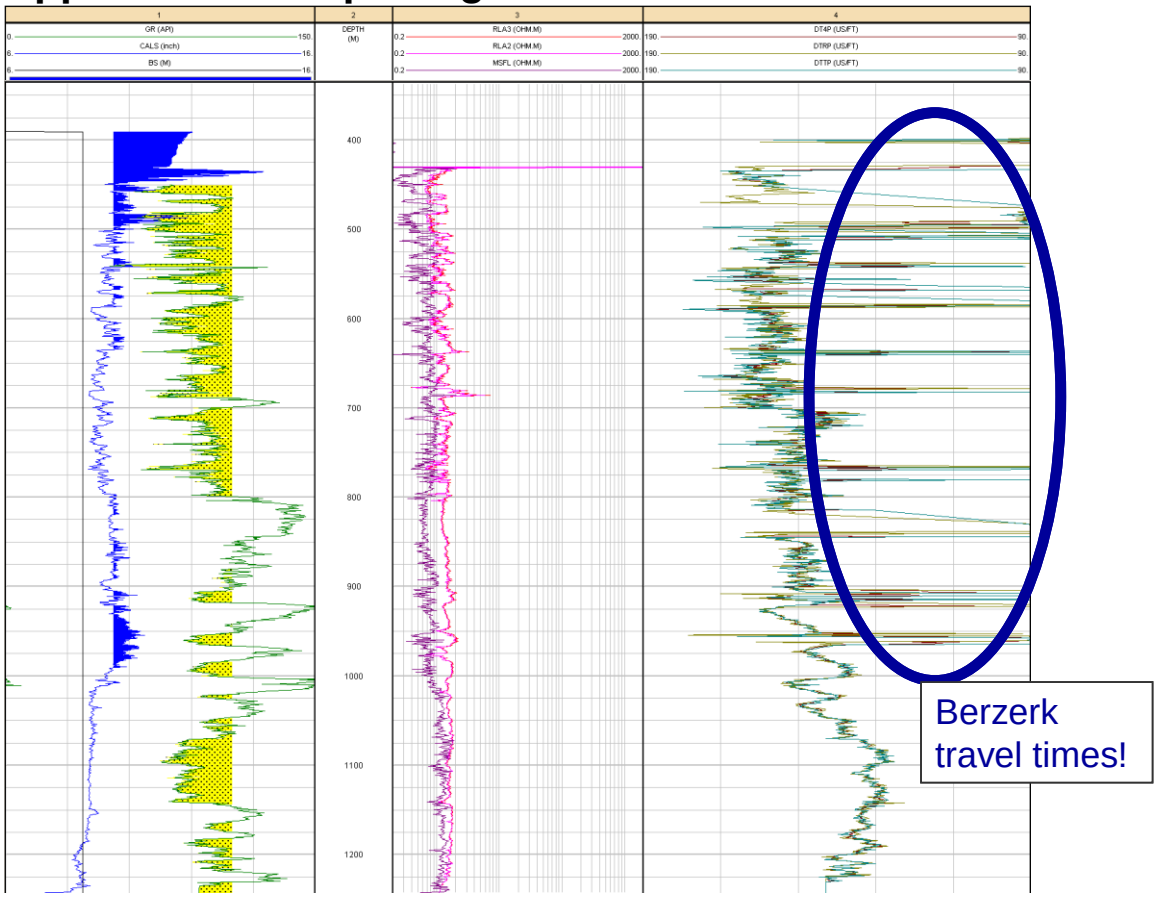

Figure H1 - Well A15-03 showing sonic logs from the DSI tool (track 4). Indicated are the very low travel times in several depth intervals.

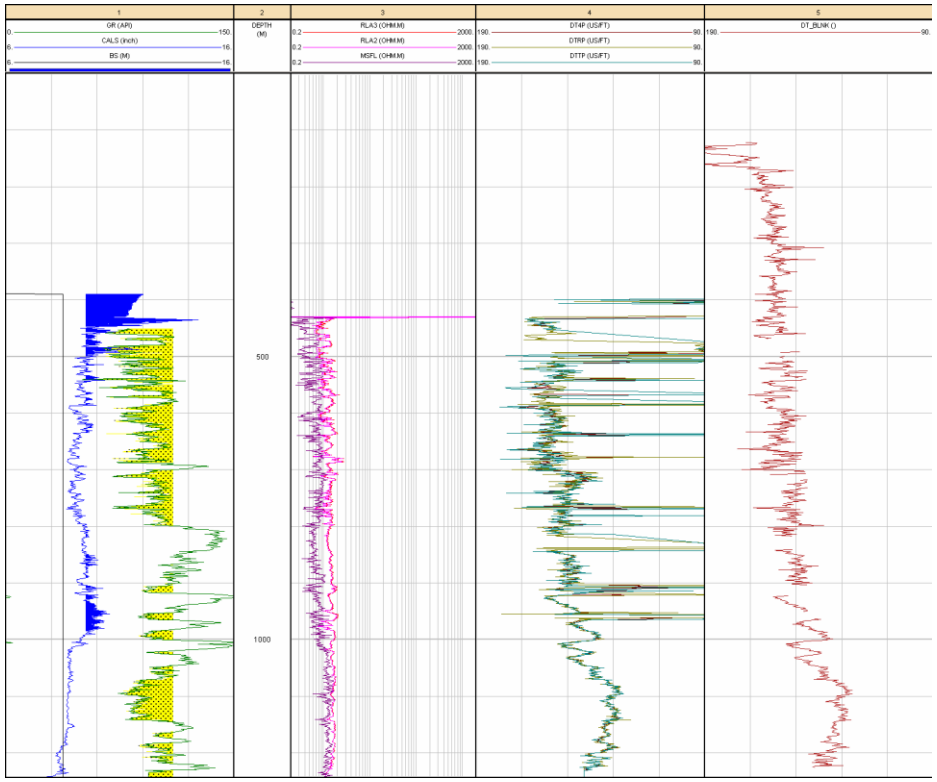

Figure H2 - Step 1: blank out faulty sections

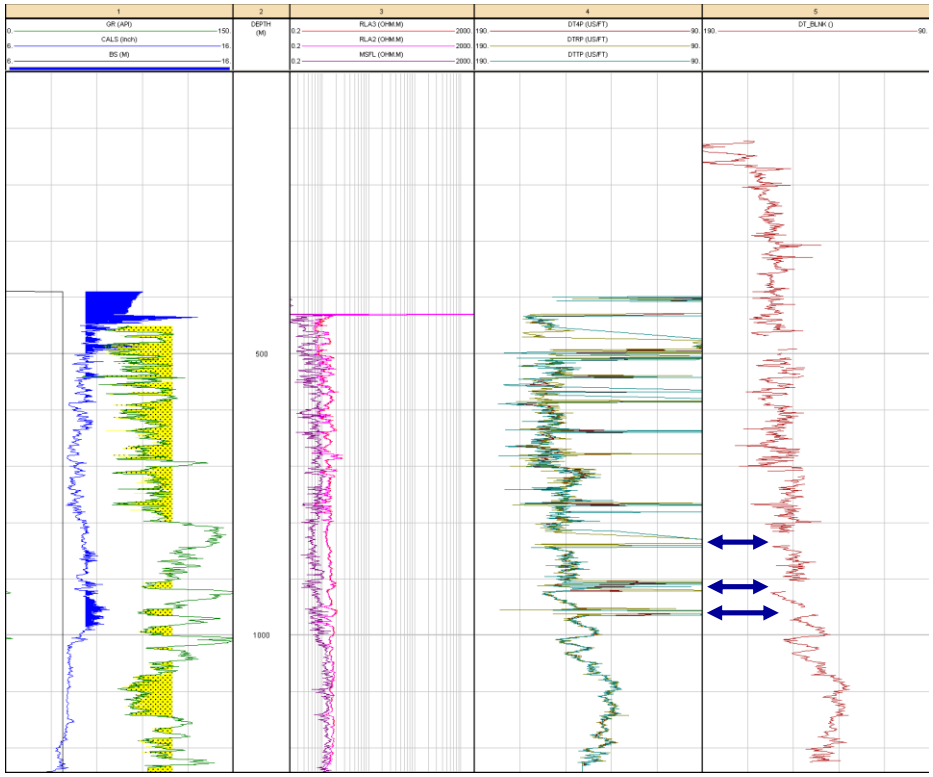

Figure H3 - Step 2: Intervals to repair in the turbiditic interval (notably D10 & D20)

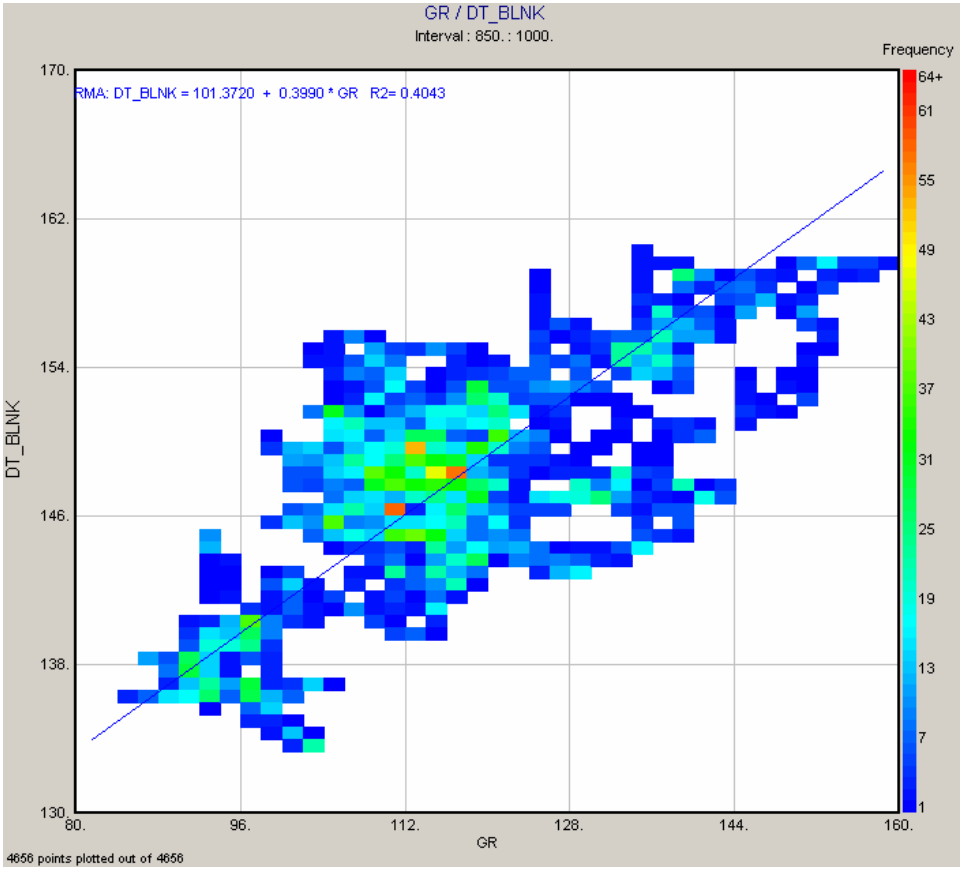

Figure H4 - Establish correlation between DT & GR in turbiditic interval, non-faulty sections

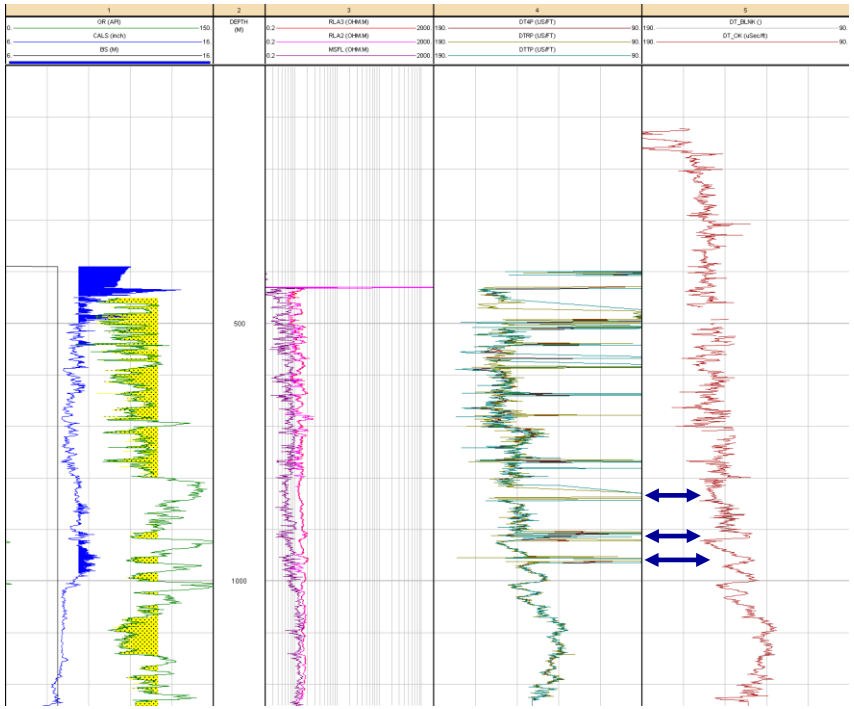

Figure H5 - DT-GR correlation applied in the turbiditic interval

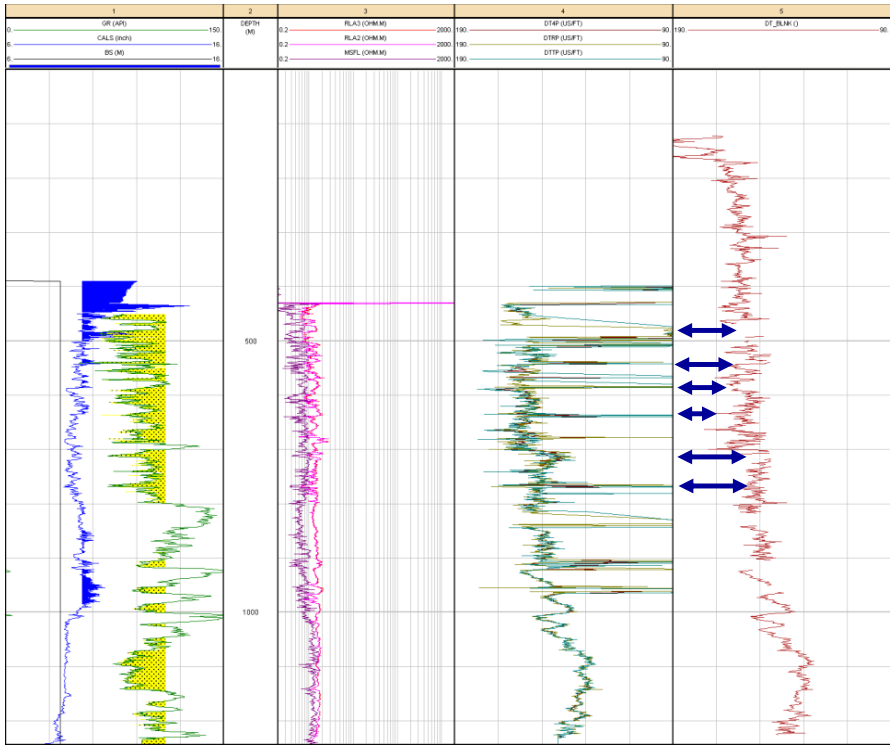

Figure H6 - Intervals to repair in the shallow marine interval (“A” sands)

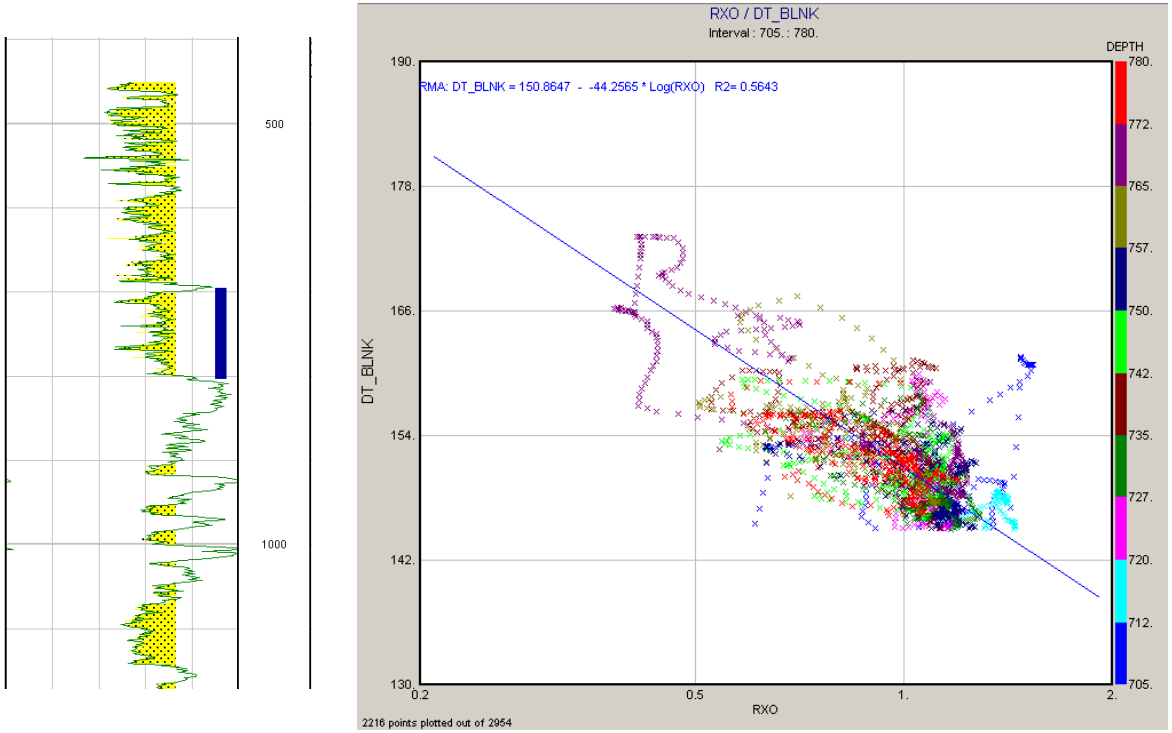

Figure H7 - Step 4: lowermost “A” sands: Correlation DT – RXO

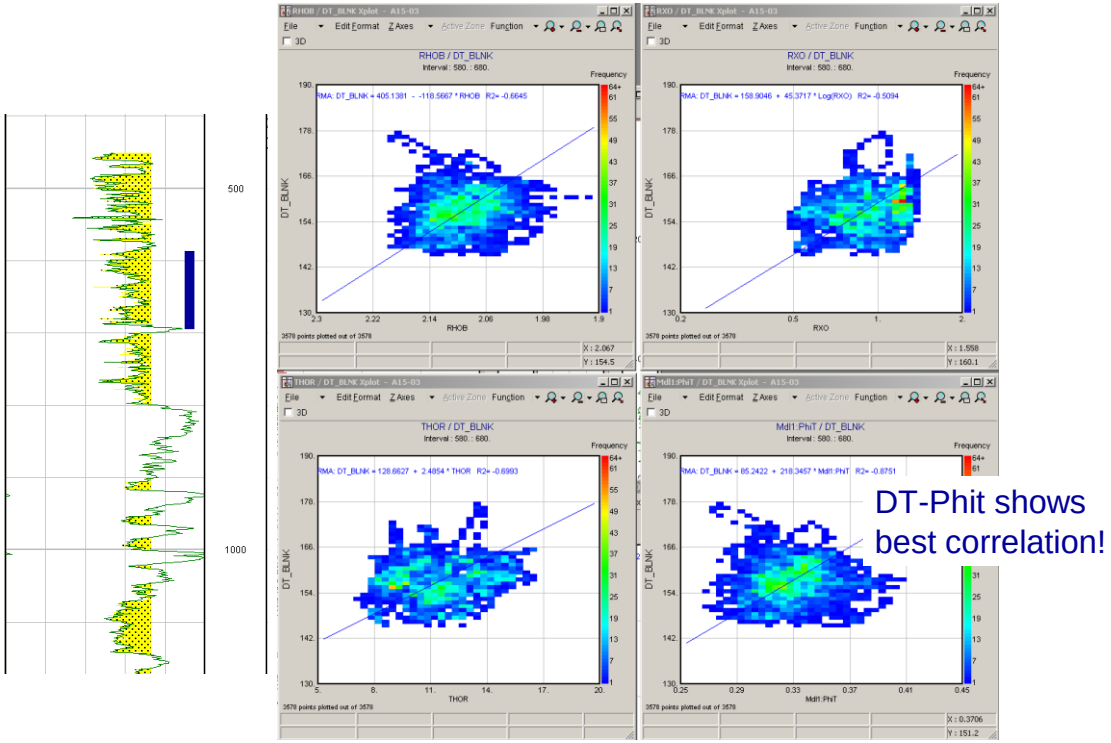

Figure H8 - Step 5: Middle “A” sands. Correlation DT – various logs (RHOB, RXO,THOR, PHIT). Dt vs. PHIT gives the best correlation.

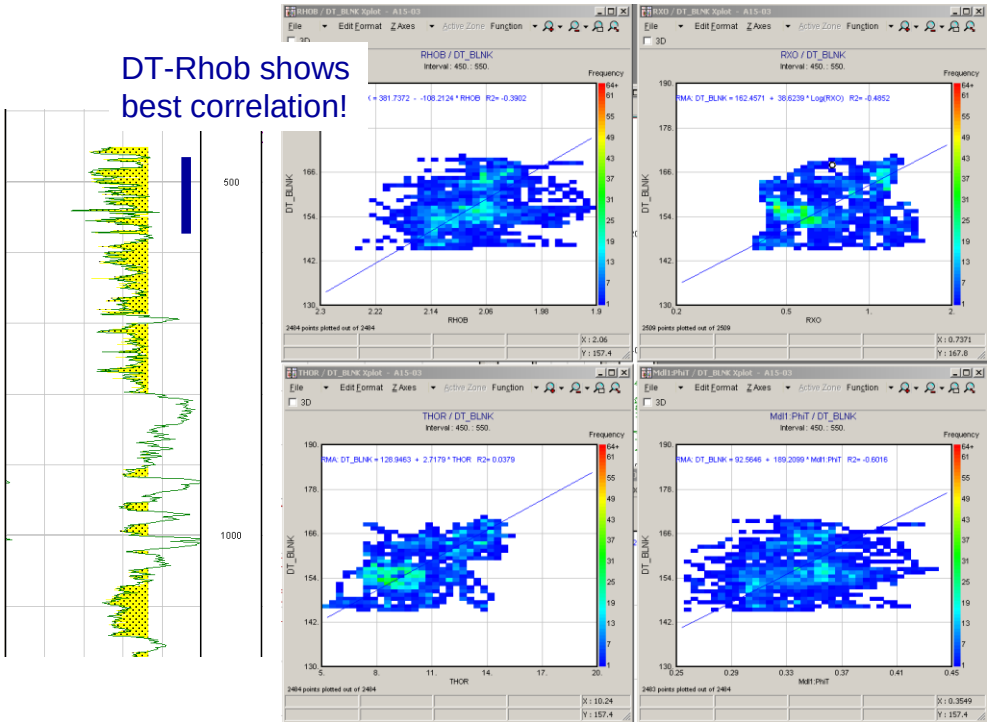

Figure H9 - Step 6: Upper “A” sands. Correlation DT – various logs (RHOB, RXO,THOR, PHIT). DT vs RHOB gives the best correlation.

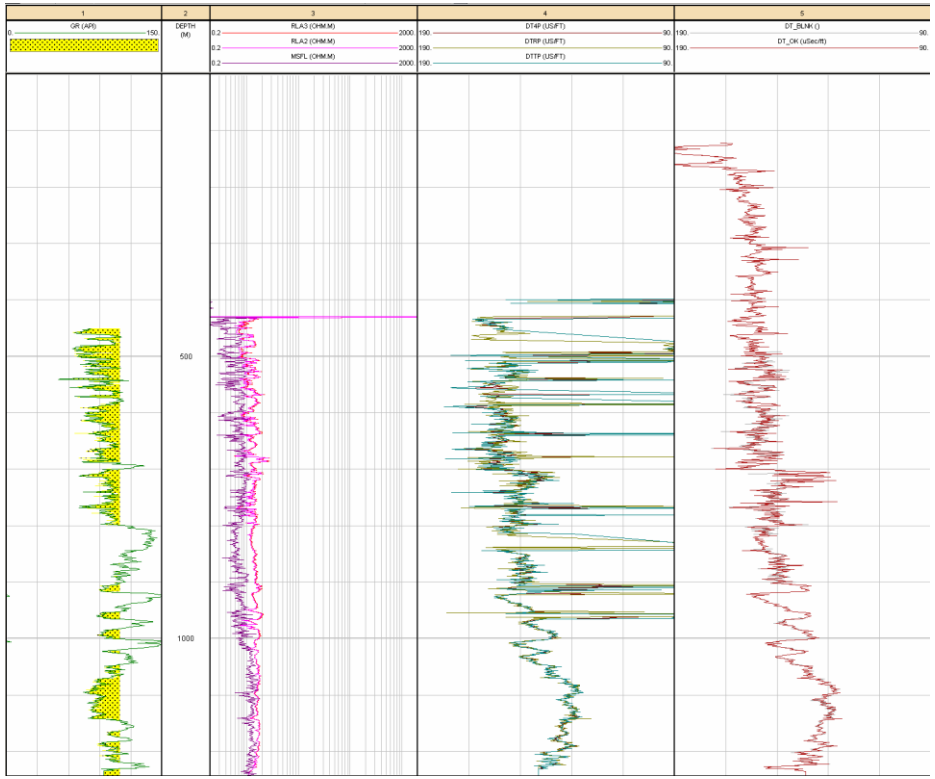

Figure H10 - End result of the repair process of the P-wave sonic log of well A15-03. Track 4 shows the recorded sonic log with many anomalously low travel times, Track 5 shows the repaired sonic.